University of Alberta

A novel group of zebrafish Class II ADP-ribosylation factors and their potential role in photoreceptor development

by

Navid Sharifi

A thesis submitted to the Faculty of Graduate Studies and Research
in partial fulfillment of the requirements for the degree of

Master of Science

Department of Cell Biology

Fall 2013
Edmonton, Alberta

Abstract

In this study we identified an unknown set of Class II Arf isoforms in zebrafish. Bioinformatics analyses grouped these paralogues into three distinct clades. Using antisense morpholino gene knockdown, we tested the effect of loss of each zebrafish Class II Arf on early development and photoreceptor organization. At 5 days post fertilization gross morphological defects in Arf II-A2 morphants was evident, while photoreceptor disorganization was seen in Arf II-C1 morphants. *In situ* hybridization experiments confirmed Arf II-C1 expression in regions of the brain and in the retina. We also found that zebrafish Arf II-C1 does not possess properties that are conserved in other Arfs. Most Class II Arfs examined in this study from different species localized to ERGIC-53 positive puncta in COS1 cells; while Arf II-C1 did not. Furthermore, in contrast to hArf4, Arf II-C1 quickly became cytosolic and dissociated from punctate structures in the presence of BFA.

Acknowledgments

First and foremost, I would like to thank my co-supervisor Dr. Paul Melançon for all his patience and love of teaching. Having Dr. Melançon as my supervisor truly made this experience a memorable one. I really could not have asked for a better mentor and teacher. I would like to thank my second co-supervisor, Dr. Ted Allison, for all the time he spent with me to ensure that my work measures up to the highest standards and quality. I would also like to thank Dr. Joel Dacks for all his invaluable input into my project. Besides my committee members, Drs. Paul Melançon, Ted Allison and Joel Dacks, I would also like to thank all the faculty and staff of the Department of Cell Biology at the University of Alberta. I would like to thank past and present members of the Melançon and Allison labs including Doug, Kelly, Victor, Fraser, Nathan, Michele, Trish, Aleah, Hao and Valarie.

I would like to thank my parents for always being there for me; none of this would have been possible without their guidance and help. I would like to thank my siblings Farid and Nasim and would like to dedicate this thesis to my daughter Kiana.

Table of Contents

List of Tables

List of Figures

Abbreviations

Arf	ADP-Ribosylation factor
ARNO	Arf-nucleotide binding site opener
BFA	brefeldin A
BRAG	Brefeldin resistant Arf GEF
CC	connecting cilium
Ce	Caenorhabditis elegans
COP	coatomer protein
Dm	*Drosophila melanogaster*
dpf	days post fertilization
ER	endoplasmic reticulum
ERES	ER exit sites
ERGIC	ER-Golgi intermediate compartment
FBS	fetal bovine serum
GAP	GTPase activating protein
GBF1	Golgi BFA resistant factor 1
GCL	ganglion cell layer
GDP	guanosine diphosphate
GEF	guanine nucleotide exchange factor
GFP	green fluorescent protein
GTP	guanine triphosphate
HA	Hemaggluttinin
IF	Immunofluorescence
IN	Inner Segment
INL	inner nuclear layer
MO	morpholino
NA	numerical aperture
ON	optic nerve
ONL	outer nuclear layer
OS	outer segment
PM	plasma membrane
PTU	phenthiourea
RPE	retinal pigment epithelium
SEM	Standard error of the mean
SB	splice blocking
SNARE	soluble N-ethylmaleimide-sensitive factor attachment protein receptors
TB	translation blocking
TGN	*trans*-Golgi network
VSVG	vesicular stomatitis viral G protein
VTC	vesiculo-tubular cluster

CHAPTER 1: INTRODUCTION

Overview

Trafficking of proteins to the correct cellular compartment, including for secretion, is regulated in part by trafficking of membranous intracellular vesicles. Control of this process is deeply conserved throughout eukaryotes and critical to cell function. The process is fundamentally driven by budding and fusion of vesicles to appropriate organelles, and trafficking of said vesicles in between organelles and to the appropriate cell compartments. These processes are regulated by a complex, conserved array of membrane-bound and cytosolic proteins with diverse functions. The members of this network of special interest for this thesis are the ADP-ribosylation factors (Arfs), members of the Ras superfamily of GTPase proteins. The exact role of some Arf isoforms in this process remains elusive, and refining this understanding is a goal of this work.

This thesis considers novel Arf proteins and their potential role in the secretory pathway; thus the cell biology of protein trafficking, especially cellular components wherein Arfs are known to play a role are discussed below.

1.1 Summary of the secretory pathway

Translation of the majority of mRNAs encoded by the nucleus is initiated on free ribosomes within the cytosol. When newly translated polypeptides include an ER signal sequence the nascent polypeptide-

ribosome complex is translocated to the rough endoplasmic reticulum (ER) where translation is completed. As polypeptide translation progresses in the ER, initial steps of post-translational modifications events take place (Palade, 1975). Secretory cargo exit the ER via ER Exit Sites (ERES) (**Figure 1.1**) where they are loaded into COP II transport vesicles for transport to vesicular-tubular clusters (VTCs), also known as the ER-Golgi intermediate compartment (ERGIC) (Bannykh *et al*., 1998; Appenzeller-Herzog and Hauri, 2006). The ERGIC functions as a cargo sorting station; shipment from the ERGIC can occur in an anterograde direction towards the Golgi complex, or back to the ER in a retrograde direction in a COPI-dependent manner (Appenzeller *et al.,* 1999). Once at the Golgi, proteins undergo further post-translational modifications as they advance from the *cis*- to the *trans*- side of the Golgi (Griffiths, 1983). At the Trans-Golgi Network (TGN), cargo is packaged in clathrin-coated vesicles and shipped to multiple different targets, including the extracellular environment, intracellular organelles and the plasma membrane (Stoorvogel *et al.,* 1996; Rémillard-Labrosse and Lippé, 2009) (**Figure 1.1**).

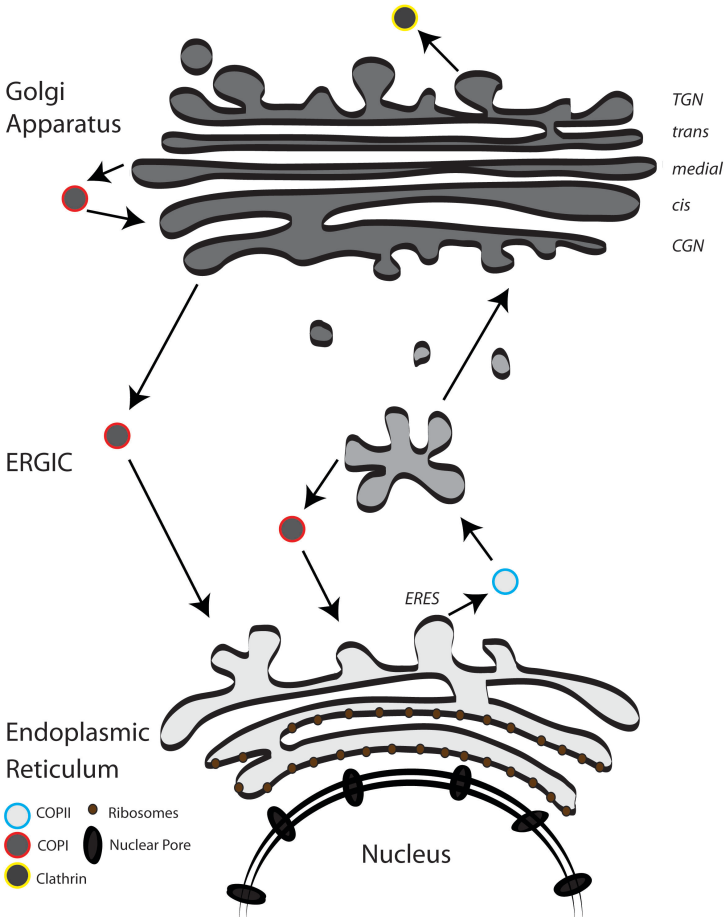

Figure 1.1: ER, ERGIC, and Golgi structures along with specific coat proteins play important roles at distinct steps of the secretory pathway. Secretory cargo leaves the ERES where it is packaged into COPII coated vesicles and is shipped towards ERGIC structures. At the ERGIC, cargo can travel in an anterograde direction towards the *cis*-Golgi or in a retrograde direction back towards the ER in a COPI coated vesicles. COPI coated vesicles also facilitate cargo traffic directly from Golgi back to the ER by bypassing the ERGIC. Clathrin-coated vesicles direct traffic away from the TGN towards other secretory organelles including the plasma membrane and lysosomes (not shown in this schematic).

1.2 COPII-coated vesicles mediate cargo trafficking away from the ER

Cargo trafficking requires vesicle budding; one of the coat complexes involved in vesicle formation early in the secretory pathway is the COP II complex. Components involved in COP II vesicle formation are essential for yeast survival and are conserved throughout eukaryotic evolution (Orci *et al*., 1991; Dacks and Field, 2004; Hebert and Molinari 2007, Strating and Martens, 2009). Most of the work involving the elucidation of COP II was done by genetic studies in the yeast *Saccharomyces cerevisiae*. Components of COP II vesicles include the small GTPase Sar1p, as well as the heterodimers Sec23/24p and Sec13/31p (Barlowe *et al*., 1994). Vesicle formation is initiated with the activation of the small GTPase Sar1p; the activation of Sar1p, like other GTPases, is achieved by having its GDP exchanged for GTP, a process mediated by Sec12p. The activated Sar1p-GTP initiates the recruitment of the Sec23/24p heterodimer, and subsequently of the Sec13/31p heterodimer complex, to induce membrane curvature. Sar1p together with Sec23/24p form the proximal layer of the coat adjacent to the membrane, while Sec13p•Sec31p forms the membrane-distal layer (Bonifacino and Glick, 2004). After vesicle budding, Sec23p acts on Sar1p a GTPase activating protein (GAP) prompting the dissociation of Sar1p and the uncoating of the vesicle. The GAP activity of Sec23 is enhanced 10 fold by the action of Sec13/31p (Antonny *et al*., 2001). Biochemical and X-ray

crystallography studies have shown the Sec13/31 proteins to be a heterotetramer consisting of two copies each of Sec13p and Sec31p while the Sec23/24p complex resembles a bow tie with one side corresponding to Sec23p and the other corresponding to Sec24p (Lederkremer *et al.,* 2001, Bi *et al.,* 2002). Sec23p makes direct contact with Sar1p•GTP (Bi *et al*., 2002), while Sec24p participates in cargo recognition (Bonifacino and Glick, 2004).

COPII interacts with cargo proteins in different ways, depending on the cargo protein's character. Cargo proteins include any protein that is to be loaded onto vesicles for transport. Loading of some cargo proteins out of the ER and into COPII vesicles occurs via direct interaction with COPII components. Alternatively, trans-membrane and soluble proteins bind indirectly to COPII by interacting with ER trans-membrane export receptors (Appenzeller *et al.,* 1999 Muñiz *et al.,* 2000; Powers and Barlowe, 2002). ER trans-membrane export receptors are recycled back to the ER once their cargo is unloaded at acceptor organelles. The specificity of cargo selection is accomplished by export signals found on cargo, or by export proteins that interact with cytosolic cargo. ER export signals include di-phenylalanine motifs (Appenzeller *et al.,* 1999, Nufer *et al.,* 2002), and di-acidic, Asp-X-Glu (D-X-E, where X is any amino acid) sorting signals that are found on ERGIC-53 and VSV-G proteins, respectively (Nishimura and Balch, 1997).

1.3 The ERGIC plays a central role in ER to Golgi trafficking

The ERGIC complex plays a central role in protein secretion by directing traffic to and from the ER and Golgi structure **(Figure 1.1).** The discovery of the ERGIC (Hauri *et al.,* 2000) was followed by the identification of a 53 kDa mannose lectin (ERGIC-53), (Saraste *et al.,* 1987; Schweizer *et al.,* 1988) which is localized predominantly at these structures and operates as cargo receptor aiding in the transport of glycoproteins from the ER to Golgi elements. ERGIC structures consist of juxtanuclear and peripheral punctate structures (Saraste and Kuismanen, 1984; Schweizer *et al.,* 1988; Hauri *et al.,* 2000). ERGIC marks the site at which anterograde trafficking from the ER to Golgi is blocked 15°C (Kuismanen and Saraste, 1989; Schweizer *et al.,* 1990; Lotti *et al.,* 1992; Blum *et al.,* 2000). The ERGIC was once thought to be a specialized domain of the ER or the *cis*-Golgi (Mellman and Simons, 1992; Sitia and Meldolesi, 1992). Further work using rat pancreatic acinar cells, however, led to the notion that the ERGIC constitutes a separate organelle, distinct from the ER and *cis*-Golgi (Mellman and Simons, 1992). Initially the transport complex model of the ERGIC was proposed; this model suggested ERGIC clusters to be transient and formed from the fusion of ER- derived COP II vesicles, which eventually form the *cis*-Golgi (Presley *et al.,* 1997; Bannykh *et al.,* 1998). Recent work using live imaging has questioned the transport complex model of the ERGIC and has put forth a static model of the ERGIC. These developments are based on

experiments involving ERGIC-53-GFP markers, which revealed these proteins to localize to long-lived stationary membrane compartments that showed no net movement towards the Golgi (Ben-Tekaya *et al.,* 2005). Later studies identified Surf4, member of the p24 family to play an important role in maintaining ERGIC structures (Mitrovic *et al.,* 2008).

It is generally agreed upon that COPII is involved in ER to ERGIC trafficking of cargo, whereas coatomer complex I (COPI)-coated vesicles control ERGIC to *cis*-Golgi traffic. COPI vesicles are also involved in retrograde trafficking of ER-resident proteins from ERGIC back to the ER (Figure 1.1) (Klumperman *et al.,* 1998). Rab1 and Rab 2 GTPases play important roles in tethering and COPI coat recruitment, respectively. COPI vesicle budding is propagated by members of Arf GTPases; different Arf isoforms are proposed to selectively play different roles in cargo sorting and selection (Goldberg, 2000; Appenzeller-Herzog and Hauri; 2006), reviewed below.

1.4 Arf generated COPI vesicles are important cargo carriers at Golgi structures

Although Sar1p/COPII coated vesicle trafficking is critical in the early stages of protein trafficking, Arf generated COPI coated vesicles play a central role in intra-Golgi transport and retrograde transport of cargo from the Golgi to the ER (Figure 1.1). The COPI complex is a heptameric structure consisting of α- β- β'-γ-δ-ε- and ζ coat subunits (Gaynor *et al.,*

1998; Duden, 2003). Arf1 and the seven-membered cytosolic COPI complex are necessary and sufficient to drive vesicle formation on the liposome (Orci *et al.,* 1993, Spang *et al.,* 1998). COPI coat unloading is achieved by the hydrolysis of GTP bound to Arf1; the bare bilayer vesicle can then fuse with the accepting membranes and unload their content (Rothman and Wieland, 1996). Besides its role in COPI assembly, Arf1 at the *trans*-Golgi network (TGN) also recruits heterotetrameric clathrin adaptor protein (AP) 1; AP-1 in turn, recruit specific clathrin coats generating clathrin coated vesicles (CCVs) which target cargo to endosomes and the plasma membrane (Bonifacino and Lippincott-Schwartz 2003). Two alternative models describe cargo transport through Golgi cisternae en route to their final destination. COPI was initially thought to play a role in both anterograde and retrograde traffic of cargo along Golgi structures (Waters *et al.,* 1991; Orci *et al.,* 1991). Recent observations question the role of the COPI machinery in anterograde trafficking and suggested an alternative model called cisternal maturation (Bonfanti *et al.,* 1998; Matsuura-Tokita *et al.,* 2006). This model describes how new cisterna “mature” as they move away from the *cis*- towards the *trans*-Golgi. Once at the *trans*-Golgi, the cisterna would disassemble by giving rise to budding vesicles containing secretory cargo. According to this model, COPI vesicles would not be required for anterograde movement of cargo; rather, they would only play a role in retrograde trafficking of Golgi resident enzymes from later cisternae to earlier ones

(Glick and Malhotra, 1998).

1.5 Arfs belong to the Ras superfamily of GTP-binding proteins

Arfs are small GTP-binding proteins (Pasqualato *et al.,* 2002) that were originally identified by their ability to support the AB5 cholera-toxin-catalyzed ADP-ribosylation of the α-subunit of the adenylyl cyclase activating G protein Gs (Khan and Gilman, 1986; Volpicelli-Daley *et al.,* 2005). Arfs are members of the Ras superfamily of proteins that also includes Ras, Rab, Rho and Ran families (Wennerberg *et al.,* 2005). The Arf family includes Arf, Arf-like (Arl) and Sar proteins that are all 21 kDa GTPases (Li *et al.,* 2004). Members of all the Arf family are highly conserved and found throughout eukaryotic evolution (Kahn *et al.,* 2006). In mammals, 22 members of the family are expressed including 6 Arf proteins, 2 Sar proteins and 14 Arls. Although mammals express six Arf isoforms, Arf1–6, Arf2 has been lost in humans and other primates (Donaldson, 2003). Arf isoforms have been grouped into three classes based on primary sequence and gene organization. Class I Arfs, Arf1–3 are 96% identical. Class II Arfs, Arf4 and Arf5, are 90% identical to one other and 81% identical to Arf1. Class III is comprised of only Arf6, the most divergent of the Arf proteins, e.g. human Arf6 only has 66–70% identity to the other human Arfs (Donaldson, 2003). Each class of Arf proteins has a distinct gene structure, including a conserved number of

exons and exon sizes. Similar to other members of the Ras Superfamily of GTPases, Arfs act as molecular switches that are considered active when bound to GTP and inactive when bound to GDP (Nuoffer and Balch1994; Kahn, 2009) (**Figure 1.2).** GTP loading onto Arf proteins is regulated by a family of Guanine nucleotide Exchange Factors (GEFs) which all share a conserved 200 amino-acid catalytic sec7 domain (Achstetter *et al.,* 1988; Mossessova *et al.,* 1998; Lowery *et* al., 2013;) GTP hydrolysis and inactivation of Arfs is enhanced by GTPase Activating Proteins (GAPs) (Cukierman *et al.,* 1995; Ding, 1996).

The distinguishing feature of the Arf proteins from other members of the Ras superfamily is their myristoylated N-terminal amphipathic helix that is necessary for binding to membranes (Donaldson and Jackson, 2011). Through their N-terminal helix, activated Arfs are able to form a stable interaction with membranes (Antonny *et al.,* 1997) **(Figure 1.2).** However, there is evidence showing that Arf1 binds weakly to membranes even without a myristoylated N-terminus; furthermore, Arf6 has been shown to interact with membranes in its inactive form (Franco *et al.,* 1993; Macia *et al.,* 2004). Work from our lab has shown human Arf4 also binds to ERGIC structures in its GDP bound state (Chun *et al.,* 2008).

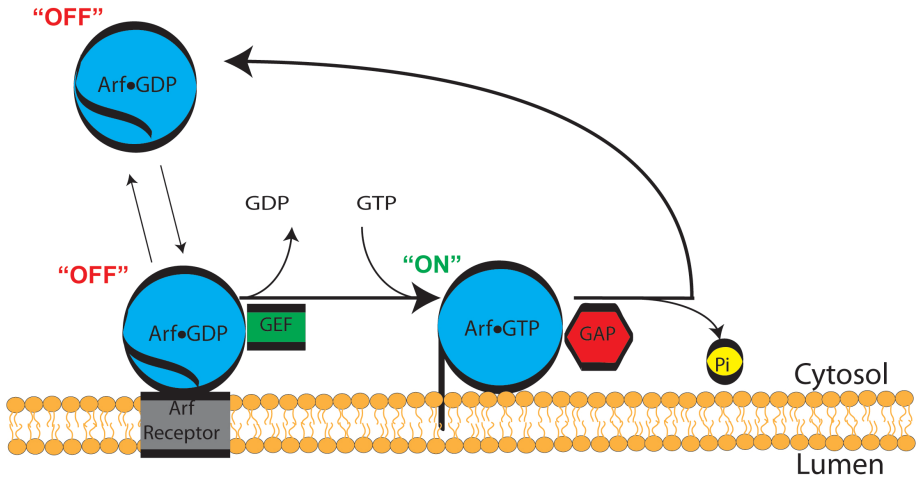

Figure 1.2: Specific GEFs and GAPs turn Arfs "ON" and "OFF", respectively. Cytosolic Arf□GDP binds loosely to membranes via an Arf□GDP receptor. Guanine nucleotide Exchange Factors (GEFs), activate, or turn Arfs "ON", by promoting the dissociation of GDP in exchange for GTP. GTP binding causes a conformational change in Arfs, that allows for tight binding onto membranes via their N-terminus tails. Arfs are inactivated, or turned "OFF", when GTPase Activating Proteins (GAPs) hydrolyze their bound GTP to GDP and Pi.

1.6 Arf GEFs aid in the exchange of GTP for GDP on Arfs, leading to Arf activation

As mentioned above, GTP loading onto Arf proteins (and thus the activation state of Arf proteins) is regulated by a family of Guanine nucleotide Exchange Factors (GEFs) which all share a conserved 200 amino-acid catalytic sec7 domain. A number of ArfGEF proteins have been identified in eukaryotes and can be classified based on structure and domain organization outside their Sec7 domain (Casanova, 2007). The ArfGEF, Golgi Brefeldin A (BFA) resistant factor 1 (GBF1), is a large GEF that localizes to early Golgi compartments and through the activation of Arfs recruits COPI coat subunits (Kawamoto *et al.,* 2002). GBF1 is sensitive to the fungal metabolite BFA at endogenously expressed levels, resulting in the collapse of the Golgi of treated cells. Overexpression of GBF1, however, leads to BFA resistance, allowing for normal Golgi morphology and cell growth in the presence of BFA. (Claude *et al,* 1999). Crystal structures (Renault *et al.*, 2003) have shown BFA to inhibit Arf activation by binding to a hydrophobic pocket created upon binding of Arf□GDP to the sec7 domain present on GEFs (Mossessova *et al.,* 2003; Niu *et al.,* 2005). Melançon and colleagues have shown GBF1 to act preferentially on Arf5 *in vitro*, while *in vivo* overexpression suggest that GBF1 acts on members of both Class I and II Arfs (Claude *et al.,* 1999; Zhao *et al.,* 2006). The BFA inhibited GEF1 and 2 (BIG1 and BIG2) share several domains with GBF1 outside of their sec7 domain. They are also

found on Golgi structures, but localize to the TGN where they interact with Arf3 (Zhao, *et al.,* 2002; Manolea *et al.,* 2010; Lowery *et al.,* 2013). As their name suggest, BIGs are also sensitive to BFA (Mansour *et al*., 1999).

Arf nucleotide binding site opener (ARNO)/cytohesins have been studied extensively and shown to be BFA resistant (Jackson and Casanova, 2000). Cytohesins are shown to localize to the cell periphery and plasma membrane, where they interact with Arf6, and this interaction is regulated by PI3K that serve to activate cytohesins (Klarlund *et al.,* 1997; Cohen *et al.,* 2007). The interaction of ARNO/ cytohesins with Arf6 at the plasma membrane was unanticipated because biochemical assays had shown ARNO to prefer Arf1 over Arf6 as a substrate (Cohen *et al.,* 2007).

Other ArfGEFs include exchange factor for Arf6 (EFA6), BFA resistant Arf GEF (BRAG) and F-Box only protein (FBX8) (Casanova, 2007). BRAGs are insensitive to BFA, and function mainly in neuronal tissue (Casanova, 2007), where mutations in BRAG1 have been identified in people with X-linked intellectual disability (Myers *et al.,* 2012). FBX8 contains an F-box motif, in addition to having a Sec7 domain. F-box motifs interact with E3 ligase to mediate the ubiquitination of Arf6 (Yano *et al.,* 2008). The sensitivity of specific Arf GEFs to BFA has been utilized to reveal differential behavior of Arf isoforms **(Discussed in Chapter 3)** (Chun *et al.,* 2008; Duijsings *et al.,* 2009).

1.7 ArfGAPs mediate Arf□GTP hydrolysis and inactivation.

ArfGAPs inactivate Arf proteins by hydrolyzing their bound GTP (Figure 1.2). ArfGAPs are a special class of GAPs that are associated with ARFs. Although Arfs are members of the GTPase family of proteins, their intrinsic namesake GTPase activity is very weak (Spang et al., 2010). Researchers discovered ArfGAPs on the basis that they strongly enhance the GTPase activity of Arfs (Randazzo and Kahn, 1994). There are 11 families of ArfGAP proteins and, like ArfGEFs, they localize preferentially to distinct regions of the cell. ArfGAP1, for instance, localizes mainly to Golgi structures (Cukierman *et al.,* 1995; Schlacht *et al.,* 2013). The ArfGAP domain consists of approximately 140 residues and contains the C-X_2-C-X_{16}−17-C-X_2-C-X_4-R motif (Gillingham and Munro, 2006). ArfGAP3 also localizes on Golgi structures and has been shown *in vitro* to work on Arf1□GTP (Poon *et al.,* 1999). The SMAP1, a member of the SMAP family, acts on Arf6 and is involved in clathrin-coat mediated endocytosis (Tanabe et al. 2005). Members of the ACAP family have been shown to localize to the cell periphery where they act as Arf6 GAP (Jackson et al. 2000). Although the Hrb family of GAPs proteins contains the GAP motif, their GTPase activating properties on Arfs remains unclear (Gillingham and Munro, 2006). The GIT family has been shown to act on all Arfs through their N-termini GAP motif (Nie *et al.,* 2003). Other GAP families include the centaurin-α family, centaurin-β family, centaurin-γ family, centaurin-δ family, the DDEF1 family and the ASAP family. Interesting for

this thesis, as discussed below, ASAPs have been implicated in opsin trafficking (Gillingham and Munro, 2006; Mazelova *et al.,* 2009).

1.8 Class I and III Arfs have important but distinct roles within the cell.

The roles of Class I and Class III Arfs have been studied extensively and much is known about their specific functions (Peters *et al.,* 1995; D'Souza-Schorey and Chavrier, 2006; Gillingham and Munro, 2007; Donaldson and Jackson, 2011). Class II Arfs, the focus of this thesis, remain poorly characterized and will be discussed separately in section 1.9 below.

Regarding Class I Arfs, work from several laboratories has shown Arf1 to be involved in the recruitment of COPI to budding transport vesicles that traffic cargo from the Golgi to the endoplasmic reticulum (ER) and between Golgi cisternae (Orci *et al.,* 2000). In addition to COPI recruitment, Arf1 also recruits adaptin complexes AP-1, AP-3 and AP-4 (Ooi *et al.,* 1998). All Arfs have a role in the recruitment and activation of enzymes that alter membrane lipid composition. For example, phospholipase D can generate phosphatidic acid by hydrolyzing phosphatidylcholine when activated by Arf1 (Hong *et al.,* 1998). Arf1 can also recruit and activate PI4 kinase to generate PI4P, an important membrane lipid for Golgi function (De Matteis and Godi, 2004).

Although the human Arf1 and Arf3 are nearly identical with only seven amino acid differences in their N termini they play distinct roles within the cell. For example, even though Arf1 is less abundant than Arf3 in bovine brain extracts, it was shown using GTPγs inhibition assays that Arf1 plays a much greater role in specific inhibitory activity than Arf3 (Taylor *et al.*, 1992). Our laboratory has previously shown Arf3 to localize preferentially to the TGN (Manolea *et al.,* 2010).

In contrast to above, the Class III Arf6 has been shown to regulate endosomal membrane trafficking, structural organization at the plasma membrane (D'Souza-Schorey and Chavrier, 2006; Chun *et al.,* 2008). Although Arf6 has been shown as the main Arf protein at the plasma membrane, it is not required for early embryonic development in mice (Suzuki *et al.,* 2006). This observation is based on Arf6-knockout experiments, where mice embryos developed normally in their early stages. However, Arf6 knockout mice die before birth and display abnormal liver development (Suzuki *et al.,* 2006). This likely results from the involvement of Arf6 in cell migration and wound healing.

1.9 Class II Arfs play a role at the ERGIC and TGN structures.

1.9.1 Role of Class II Arfs at ERGIC structures

In contrast to Class I and III Arfs, specific roles of Class II Arfs remain largely elusive. Previous work from our lab has shown human Class II

Arfs, in contrast to Class I Arfs, to remain on ERGIC in their GDP□bound state in the presence of BFA (Chun *et al.,* 2008). The differential membrane association dynamics seen by Melançon and colleagues (2008), were confirmed by another group (Duijsings *et al.,* 2009). This latter group also concluded that the difference in the behavior of Class I and II Arfs to BFA treatment comes from their differences at the N-terminus as well as a specific residue at position 62. By switching the Arf1 N-terminus and residue 62 by those corresponding to Arf4, they found the Arf1 to be insensitive to BFA treatment, as the distribution of this chimeric protein was indistinguishable from wild-type Arf4 in BFA challenge experiments (Duijsings *et al.,* 2009). The specific reason for the differential behavior of Class II Arfs at the ERGIC is not clearly understood.

1.9.2 Role of Class II Arfs at the TGN

Work from other laboratories has shown that Arf4 has a role in trafficking of ciliary proteins from the TGN (Deretic *et al.,* 2005; Mazelova *et al.,* 2009). Proteins of the primary cilia such as rhodopsin, polycystin-2, and the cyclic nucleotide-gated (CNG) channel CNGB1b subunit all possess a VxPx trafficking signal at their C-terminus. The VxPx motifs of rhodopsin and polycystin-2 have been shown to interact with Arf4 at the TGN where they are packaged and trafficked to the primary cilia (Deretic *et al.,* 2005; Mazelova *et al.,* 2009; Ward *et al.,* 2011).

In the case of opsin trafficking, cell-free experiments have suggested a direct interaction between the VxPx motif and Arf4's α3-helix

(Deretic *et al.,* 2005). Blocking the interaction site of Arf4 and rhodopsin C-terminus, by using specific antibodies against the α3-helix region of Arf4, led to a decrease in the number of Rhodopsin Transport Carriers (RTCs) budding from the Trans Golgi Network (TGN). RTC budding was also reduced when synthetic peptides corresponding to the α3-helix region of Arf4 were added to the reaction mix (Deretic *et al.,* 2005; Mazelova *et al.,* 2009). Later experiments identified other players to have a role in vesicle formation and trafficking of rhodopsin to the primary cilium; these include Rab11, the Arf GAP ASAP1 and FIP3; the latter being an effector of both Arf4 and Rab11 (Mazevola *et al.,* 2009). The exact role of each protein in vesicle formation and trafficking is not known (Donaldson, Jackson, 2011).

Class II Arfs have also been identified in the regulation of exocytosis of dense core vesicles from nerve terminals. Class II Arfs regulate dense core vesicles secretion by binding directly to calcium-dependent activator protein for secretion (CAPs) (Sadakata *et al.,* 2010). Interestingly Arf4/5 can only bind CAPs in their GDP and not GTP bound form (Sadakata *et al.,* 2010).

In addition to its role at ERGIC and TGN structures, Arf4 has also been shown to interact with the intracellular regions of the epidermal growth factor receptor (EGFR) to mediate EGF-dependent cellular activation of phospholipase D2 (PLD2), but not PLD1 (Kim *et al.,* 2003). Despite the unique roles for Class II Arfs, knockdown (KD) studies in tissue culture by Kahn and colleagues revealed that single KD of either

Arf4 or Arf5 had no effect on trafficking along the secretory pathway; rather, the authors showed that distinct pairs of Arfs may be required at each step of protein trafficking. For example, disruption of ER-to- Golgi traffic resulted only from double KD of Arf1 and Arf4 (Volpicelli-Daley *et al.,* 2005).

2.0 Zebrafish as model organism

Zebrafish (*Danio rerio*) have emerged as an excellent new model system during the last three decades to study the function of genes in vertebrate development (Streisinger *et al.,* 1981; Kettunen, 2012). Although other model organisms such as fruit flies (*Drosophila melanogaster*) and worms (*Caenorhabditis elegans*) have proven invaluable to researchers, they are not always representative for studying the differentiated genes and cell processes of vertebrates. For these reasons, researchers have turned to mice and chickens as their organism of choice; however development times of mice is usually around 21 days, whereas zebrafish develop from a single cell in a fertilized egg into an embryo in 24 hours. Furthermore, as discussed below, mice are nocturnal animals; they therefore, do not serve as a great model organism for those interested in studying day-vision specific cone photoreceptors (Watanabe *et al.,* 2010). Not only does the zebrafish provide a great model for studying cone photoreceptors, but the zebrafish retina is also anatomically and physiologically conserved with the human retina, and results from

zebrafish are thus more applicable to visual diseases in humans. Other attractive reasons for using zebrafish as a model organism include: 1) the ease with which zebrafish can be bred. Research facilities are able to maintain large numbers of aquariums with thousands of zebrafish; 2) A single female is able to spawn hundreds of embryos per mating session allowing for large-scale genetic screening; 3) The use of morpholino (MO) directed KD has allowed researchers to successfully study the function of genes in early stages of development zebrafish **(Discussed in Chapter 3)** (Bill *et al.,* 2009); 4) Also, since embryos develop externally, researchers are able to perform genetic manipulations such as MO injections without harming the mother; 5) Eggs are transparent, allowing for visual examination of early organ development. The use of 1-pheno2-thiourea (PTU), a tyrosinase inhibitor, prevents pigmentation of larvae, allowing embryo to stay transparent well after 5dpf **(Figure 1.3)** (Bohnsack *et al.,* 2011).

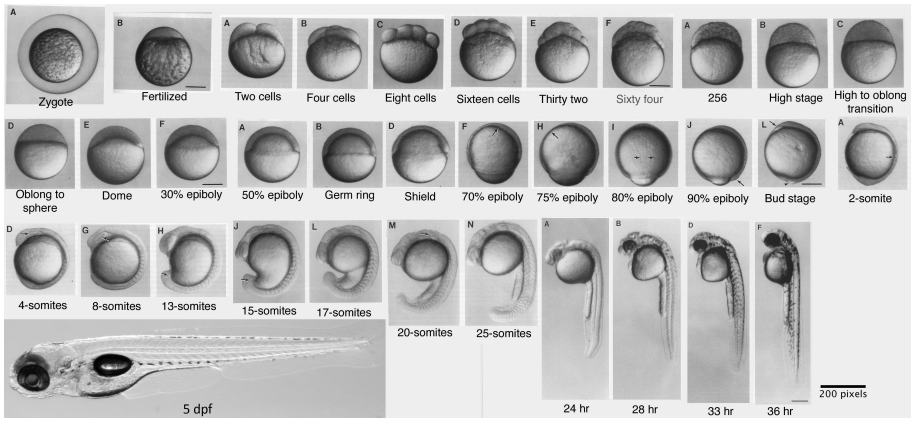

Figure 1.3 Early stages of zebrafish development. Images of zebrafish at selected early developmental points. Zebrafish embryos develop quickly and are transparent through most of their early development. Eye development of zebrafish larvae occurs approximately at the 24-48 hours post fertilization stage. Image is modified from Kimmel *et al.,* (1995) Stages of embryonic development of the zebrafish.

2.1 Zebrafish have been used as a model organism to gain insight into the role of Arf protein.

2.1.1 Bardet-Biedl Syndrome

Among other phenotypes, the pleiotropic disorder of Bardet-Biedl Syndrome (BBS) is associated with retinal degradation, renal abnormalities and obesity. Mutations in 16 genes, including BBS3, also known ADP-ribosylation factor-like 6 (Arl6), are known to cause BBS (Gascue *et al.,* 2012). Evidence shows that most phenotypes associated with BBS involve cilia dysfunction defined as ciliopathies (Bachmann-Gagescu *et al.,* 2011). Cilia are organelles that are present on the surface of most eukaryotic cells; in general, ciliopathies are defined as disorders that are a result of dysfunction of the microtubule-based primary cilium (Badano *et al.,* 2006). The vertebrate photoreceptor is composed of two segments; the photoreceptor Inner segments (IS) and the photoreceptor Outer Segment (OS). The IS and OS are connected via a specialized form of primary cilium named the connecting cilium (CC) (**Figure 1.4).** The IS houses the nucleolus, ER, Golgi and other organelles of the secretory pathway. Proteins synthesized in the IS are packaged into vesicles, and destined for the CC. Although there are topological differences between the outer segments of the rods and cones, initial steps of protein trafficking out of the TGN are likely the same due to the conserved C-terminus that are found on most opsin protein sub-types. A normal functioning connecting cilium is critical and necessary for the correct transport of

cargo into the OS **(Figure 1.4)**. Loss of the connecting cilium or associated intraflagellar proteins leads to abnormal photoreceptor and retinal development and causes cell death (Young, 1967; Pazour *et al.,* 2002; Krock and Perkins, 2008; Pretorius *et al.,* 2010-2011). Researchers have recently identified BBS3L, a longer transcript of BBS3, to be required for proper retinal organization in zebrafish (Pretorious *et al.,* 2010). To show the specific role of BB3L in the eye, they designed translation-blocking (TB) MOs to target both BBS3 and the BBS3L transcripts. Rescue experiments using human BBS3 RNA alone was sufficient to suppress most cardinal phenotypes associated with BBS, but did not rescue retinal defects in zebrafish. On the other hand, rescue experiments using human BBS3L reverted the defects seen in the retina, but were not able to rescue other BBS associated phenotypes in zebrafish (Pretorious *et al.,* 2010). Recently this same group identified an A89V mutation in the BBS3 and BBS3L sequences that leads to non-syndromic pigmentosa; in other words, patients harboring this mutation do not have other BBS related symptoms besides vision loss. Through rescue experiments, the group was able to show that the A89V mutation in BBS3L was still sufficient to suppress cardinal BBS phenotype of intracellular transport consistent with non-syndromic pigmentosa. On the other hand, they showed that rescue experiments using wild-type BB3L RNA but not A89V RNA was able to suppress retinal defects. Vision in rescue morphants was evaluated by using a natural escape response that measures larval

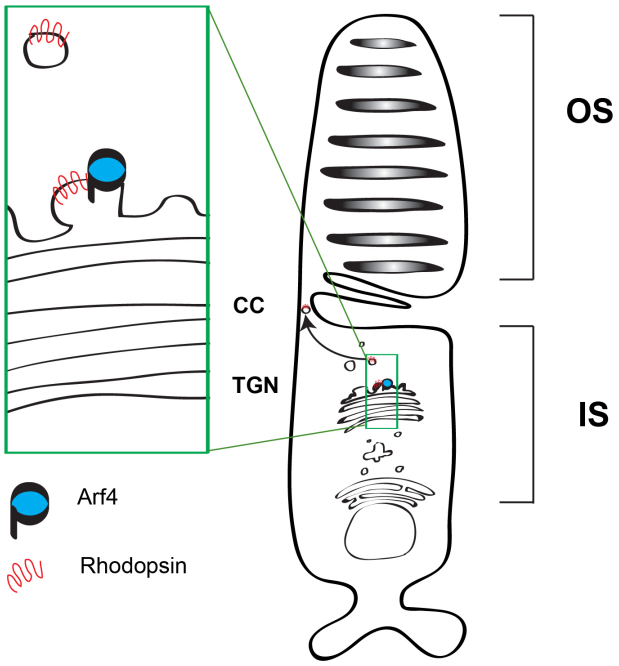

1.4 Schematic representation of Rhodopsin trafficking. Visual neurons including rods and cones are composed of the photoreceptor Inner Segments (IS) and a specialized form of the primary cilium called the photoreceptor Outer Segments (OS); OS and IS are connected via a Connecting Cilium (CC). Rhodopsin is packaged into Arf4-dependent vesicles at the Trans Golgi Network (TGN) and move vectorially to the CC where they fuse with the IS plasma membrane within the periciliary ridge complex.

reaction to rapid changes in light intensity. Quantification showed that injection of wild-type but not A89V RNA is able to restore normal reaction times (Pretorious *et al.,* 2011).

2.1.2 Arfs play a role in toxin resistance

Arf proteins were also examined in zebrafish with respect to their response to toxicants such as TMT. Organotins are comprised of tin with hydrocarbon substituents used as fungicides, as stabilizers in plastics, moluscicides, and miticides (Kimbrough, 1976). Trimethyltin (TMT) chloride is known as one of the most widely used organotins and environmental contaminants. TMT has been documented as an environmental contaminant, while TMT poisoning is thought to occur through ingestion of contaminated food or water (Chen *et al.,* 2012). The major symptom associated with TMT poisoning is neurotoxicity, and TMT has therefore been used widely as a tool to study central nervous system toxicity in model organisms (Zuo *et al.,* 2009). TMT, along with other organotins, have also been used in cancer treatment, as these compounds have been shown to act as apoptotic inducers (Alama *et al.,* 2009). In order to gain a better understanding of the applications of organotins' role as a tumor-suppressant, zebrafish were used a model organism to test the dosage-dependent effects of TMT on development. Phenotypic defects associated with TMT exposure include dose-dependent pericardial edema and aberrant vasculature development;

while at the molecular level, microarray studies and *in situ* hybridization experiments showed an increased level of Arf3 and Arf5 transcript expression. qRT-PCR revealed a 30- and 15-fold increase in the expression of Arf3 and Arf5 respectively, in treated larvae relative to control conditions (Note that based on the partial sequences provided by the authors, I could not define these Arfs according to our naming system; naming system will be discussed). In untreated larvae, *in situ* reactions revealed a low expression of Arf3 in the eye, fore- and mid-brain; while intense coloration was seen in the brain, trunk and tail regions in TMT treated larvae. In contrast to Arf3, Arf5 expression was little to none under control conditions; however, treatment with TMT led to the same expression pattern as seen for Arf3 in treated larvae. The authors show Arf3 expression to be is present in TMT treated and untreated larval eyes; however, they argue that Arf3 is expressed in the center of the eye under control conditions, while Arf3 expression is shifted to the eye-periphery of in TMT treated larva. Although this observation may be true, it is not possible to see the shift from the center of the eye to the periphery based on the images they have provided. Further experiments involving MO-directed KD of Arf5, protected against vasculature abnormalities associated with TMT poisoning. Although Arf3 was expressed 15 fold more than Arf5, The authors did not examine the effects of Arf3 KD on vasculature organization (Chen *et al*., 2012). This finding highlights the importance of Arf function in the brain, and points out their importance in

maintaining homeostasis.

2.1.3 Arfs play a role in lipid metabolism

A genetic screen for genes involved in lipid metabolism led to the isolation of a recessive lethal *fat-free (ffr)* mutant and associated gene in zebrafish (Ho *et al*., 2006). Mutations in *ffr* reduced phospholipid and cholesterol processing as indicated by fluorescently-tagged phospholipid analogs (Farber *et al.,* 2001). Electron microscopy revealed that the Golgi ultra structure is disrupted in the digestive tract of *ffr* mutants. The predicted Ffr protein contains a Dor-1 like domain that is typical of oligomeric Golgi complex (COG) (Ho *et al.,* 2006). The COG complex has been shown to aid in SNARE fusion at the Golgi complex (Laufman *et al.,* 2013). The presence of a Dor-1 like domain in Ffr hinted at a possible link between defects in the secretory pathway and disruptions in digestion (Liu *et al.,* 2010). Indeed, microanalysis showed that an EST corresponding to a region encoding zebrafish *Arf4* (renamed to *Arf II-C1* in this thesis, see Chapter 3) was upregulated significantly in in 4-5 day old *ffr* larvae. This observation came as no surprise because Arf proteins play a role in fat metabolism by altering membrane lipid composition through the activation of lipid modifying enzymes such as phospholipase D (PLD) (Cool *et al.,* 1999; Donaldson and Jackson, 2000; Deretic *et al.,* 2005; Gillingham and Munro, 2007). qRT-PCR and *in situ* hybridization experiments confirmed that higher transcript expression was also observed for *Arf1* (renamed to

Arf1b in this thesis, see Chapter 3) and *Arf6* (renamed to Arf6a in this thesis, see Chapter 3). Co-immunoprecipitation experiments showed that through a DPxxY motif present on the Ffr protein, Ffr can pull down GTP- but not GDP bound forms of Arf (Liu *et al.,* 2010). Subsequent experiments led the authors to the model the Ffr N-terminal region as an upstream activator of Arf□GTP; activation of Arf□GTP caused increase activity of its effector PLD, which resulted in increased phosphatidic production causing budding at the Golgi TGN. The C-terminus of Ffr was suggested to be responsible for the release of Arf□GDP, once vesicle fission is completed. In *ffr* mutants, the C-terminus of Ffr is missing, therefore, Arf□GTP remains on Golgi structures, (Liu *et al.,* 2010) causing aberrant budding leading to Golgi swelling as evidenced by EM micrographs (Ho *et al.,* 2006).

2.2 Zebrafish photoreceptor organization and eye anatomy

There are generally two groups of photoreceptors expressed in most vertebrate eyes (Lamb, 2013). Day vision is accomplished by multiple spectral-subtypes of cone photoreceptors, whereas night vision is accommodated by rod photoreceptors. Most of what we have learned about photoreceptor physiology, cell biology and disease comes from experiments involving rodents, nocturnal animals that have few cones compared to rods. Rods predominate the human retinal periphery; however, the macula, which is largely populated by cone photoreceptors,

is the most important region for day vision (reviewed in Raymond and Barthel, 2004). In the human macula, 3 spectral-subtypes of cones can be found that detect blue, green and red. Due to polymorphism, two versions of the red visual pigment exist with slightly different absorption maxima (Merbs and Nathans, 1992). In recent years zebrafish have become one of the best model organism for the study of cone cells. This is because in addition to expressing rod, zebrafish also express cone photoreceptors abundantly throughout their retinas (Raymond and Barthel, 2004; Fleisch, *et al.,* 2011). During the development of zebrafish, some of the photoreceptors express visual pigments by as early as 2dpf fertilization by 3dpf photoreceptors throughout the retina express photoreceptor specific genes (Liu *et al*., 2007). In zebrafish a total of 5 photoreceptors, including rod photoreceptors, are expressed. Zebrafish cone photoreceptors can be distinguished by their different morphologies along with differential expression of photoreceptor-specific genes. The four cones express visual pigments with maximum photon absorption corresponding to blue, green, red and ultraviolet (UV) wavelengths (Raymond and Barthel, 2004; Liu *et al.,* 2007; Allison *et al.,* 2010). Morphologically, the ultraviolet cones are the shortest followed by blue cones while the green and red cones are longest and are fused together to form double cone pairs. Many teleost fish species, including the adult zebrafish, express their photoreceptors in a defined mosaic pattern that consists of precise parallel rows of red and green double cone pairs that alternate with rows of blue and UV single

cones **(Figure 1.5)** (Branchek and BreMiller, 1984; Raymond and Barthel 2004; Allison *et al.,* 2004, 2010). In the adult retina, the ratio of red/green double cones to UV or blue cones is 2:1; where alternating UV and blue cones flank the red/green double cone on each side. Although photoreceptors in zebrafish larval retina are not organized in as precise mosaics as those described for the adult fish, larva cones also form a regular heterotypic mosaic that is statistically different from random (Allison *et al.,* 2010). As in other vertebrates, the zebrafish eye anatomy is composed of one glial and six neural cell types arranged in three nuclear layers and separated by two plexiform layers where synapse occurs (**Figure 1.6**). The outer nuclear layer (ONL) contains the cone and rod photoreceptors. The outer plexiform layer (OPL) where synaptic reactions occurs between cells of the ONL and the inner nuclear layer (INL), houses the somata of bipolar, horizontal, and amacrine interneurons **(Figure1.6)** (Gross and Perkins, 2008; Gestri *et al.,* 2012). Adjacent to the lens is the ganglion cell layer (GLC), which contains cell bodies of displaced amacrine and ganglion cells. The axons of the ganglion cells collectively converge to become the optic nerve (ON), which exit the eye to form the optic tract. The inner plexiform layer (IPL) is the synaptic region between cells of the INL and those of ganglion and amacrine cells (Gestri *et al.,* 2012).

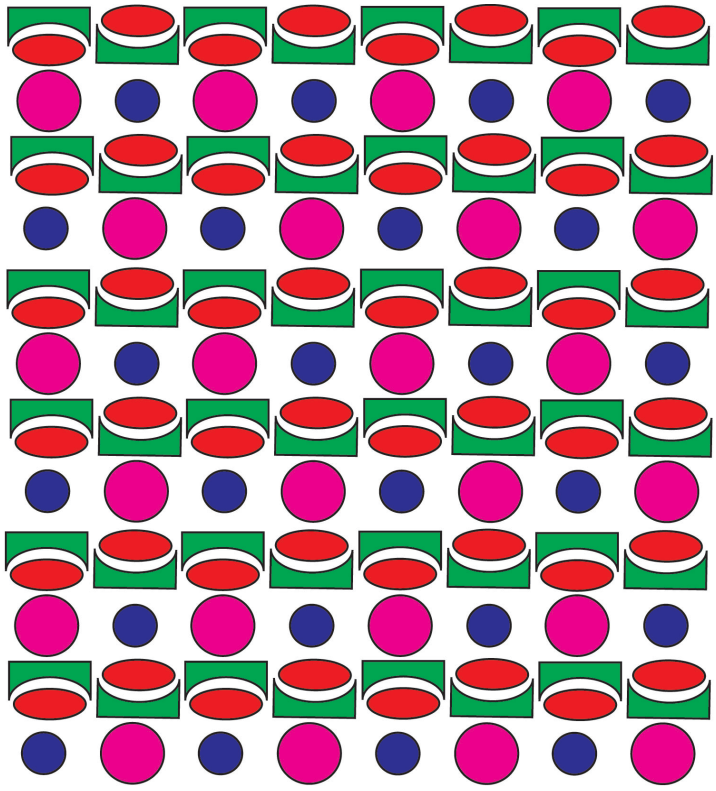

Figure 1.5 Schematic showing the cone mosaic of cone photoreceptors of the adult zebrafish. The four cone photoreceptor types present in the zebrafish eye include UV (shown as magenta), Blue and the Red and Green double cones. There are twice as many Red/Green cones as UV and Blue cones, and equal number of UV and Blue cones. Adult zebrafish express their photoreceptors in a defined mosaic pattern that consists of precise parallel rows of Red/Green double cone pairs that alternate with rows of Blue and UV single cones.

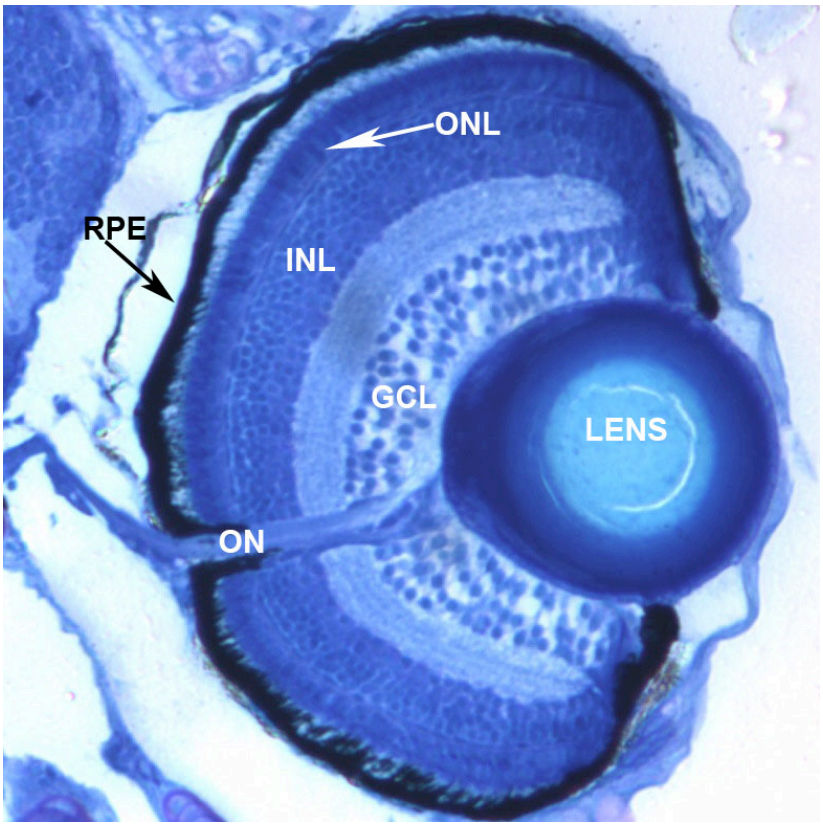

Figure 1.6 Retina morphology of 5 dpf larva. Histology of the different layers of the zebrafish eye includes: RPE, retinal pigment epithelium; ONL, outer nuclear layer; INL, inner nuclear layer; GCL, ganglion cell layer; ON, optic nerve. Image is used and modified with the permission of Dr. Steve Wilson, University College London.

Rationale for thesis

I sought to test the function of specific Class II Arf isoforms. We speculated that assays using cells grown in culture, or cell free assays, would not provide a sufficient range of processes to properly address my hypotheses. Therefore, I proposed to use zebrafish, including use of MO to deplete 1-2 celled embryos of Class II Arf isoforms and follow the embryos through their early development to understand the importance of Class II Arfs in embryogenesis. Specifically, we chose to focus on photoreceptor and retinal development because Class II Arfs have been shown to play a role in rhodopsin trafficking. We chose to use zebrafish as our model organism because, anatomically and physiologically, the zebrafish eye is very similar to, and highly conserved with, the mammalian eye. Furthermore, similar to mammals and in contrast to *D. melanogaster* and *C.elegans,* zebrafish express multiple class II Arfs. Cell-free assays, which showed a potential role for Class II Arfs in rhodopsin trafficking, were performed by other research groups using cytoplasmic retinal extracts isolated from *Xenopus* (Deretic *et al.,* 2005; Mazelova *et al.,* 2009).). Unlike humans and other mammals, *Xenopus* express only one Class II Arf isoform. Since there are multiple Class II Arfs expressed in both zebrafish and humans, and both species possess multiple spectral-subtypes of cone photoreceptors in their retinas, we reasoned we could also test for the existence of specific relationships between different Class II Arf isoforms and opsin sub-types.

The results of our bioinformatics along with time restrictions, however, swayed our attention away from our initial hypotheses. Instead we identified a total of seven Class II Arfs, which we were able to categorize into 3 distinct clades and found that the Arf II-C1 paralogue played a role in photoreceptor organization and number. Due to the lack of specific antibodies against this particular Arf, we were not able to localize intracellular localization pattern in the zebrafish retina; however, through *in situ* hybridization experiments we were able to confirm the expression of this Class II Arf paralogue in the zebrafish eye.

CHAPTER 2: MATERIALS & METHODS

2.1 Reagents

All reagents were used in accordance with procedures set out by the Environmental Health and Safety of the University of Alberta and Workplace Hazardous Materials Information System (WHMIS).

Table 2.1 Name and source of chemicals and reagents.

Reagent	Supplier
Acetic acid, glacial	Fisher Scientific
Acrylamide/bis (30%; 29:1)	Bio-rad
Agarose (UltraPure™)	Invitrogen
Ammonium chloride	Caledon
Ammonium persulfate	Bio-rad
Ampicillin	Novopharm
Bactotryptone	BD
Bacto-yeast	BD
Bovine serum albumin	Sigma
Brefeldin A	Sigma
Bromophenol blue	Sigma
Calcium chloride	BDH
CO_2-independent medium (- L-glutamine)	Gibco (Invitrogen)
Complete, EDTA-free protease inhibitor cocktail tablets	Roche
DTT (dithiothreitol)	Fisher Scientific
DMEM (Dulbecco's Modified Eagle Medium)	Gibco (Invitrogen)
DMSO (dimethyl sulfoxide)	Sigma
dNTP (deoxyribonucleotide triphosphate)	Invitrogen
EDTA (ethylenediamine-tetraacetic acid)	Sigma
Fermentas PageRuler™ Prestained Protein Ladder Plus	Fermentas
Fetal bovine serum (FBS)	Gemini Bio-Products
Fibronectin	Sigma
Gelatin	Fisher Scientific
GeneRuler 1 kb DNA Ladder	Fermentas

Glycerol	Fisher Scientific
Glycine	Roche
hydrochloric acid	Fisher Scientific
Isopropanol	Fisher Scientific
Kanamycin	Sigma
L-glutamine	Gibco
Magnesium chloride	BDH
Magnesium sulphate	Fisher Scientific
Methanol	Fisher Scientific
NBT/BCIP	Fisher Scientific
Opti-MEM	Gibco (Invitrogen)
Paraformaldehyde	Sigma
Penicillin/streptomycin	Gibco (Invitrogen)
PBS (phosphate buffered saline; Dulbecco's)	Gibco (Invitrogen)
Phosphate-free DMEM	Invitrogen
Platinum® Pfx DNA polymerase	Invitrogen
Potassium chloride	BDH
Prolong® Gold with DAPI antifade reagent	Molecular Probes (Invitrogen)
Restriction endonucleases	Invitrogen or NEB
RNAlater	Qiagen
Sodium bicarbonate	Caledon
Sodium chloride	Fisher Scientific
Sodium fluoride	Sigma
Sodium hydroxide	Fisher Scientific
Sucrose	Sigma
SYBR Safe DNA gel stain	Molecular probes (Invitrogen)
T4 DNA ligase	Invitrogen
TransIT-LTI transfection reagent	Mirus
Tris (tris-(hydroxymethyl)aminomethane)	Roche
Triton X-100	VWR
Trypsin-EDTA	Gibco (Invitrogen)
Tween 20 (Polysorbate 20)	Fisher Scientific

Table 2.2 Commercial Kits

Kit	Supplier
mMessage SP6 kit	Ambion
QIAGEN Plasmid Midi kit	Qiagen
QIAprep spin miniprep kit	Qiagen
QIAquick gel extraction kit	Qiagen
RNeasy	Qiagen

Table 2.3 Commonly used buffers and solutions

Solution	Composition
E3 media	34.8 g NaCl, 1.6 g KCl, 5.8 g $CaCl_2 \cdot 2H_2O$, 9.78 g $MgCl_2 \cdot 6H_2O$, 1% methylene blue, pH7.2
Luria-Bertani (LB) Broth	1% bactotryptone, 0.5% bacto-yeast extract, 1% (w/v) NaCl, pH 7.0
Paraformaldehyde (3%)	3% paraformaldehyde, 0.1 mM CaCl2, 0.1 mM MgCl2 (used to fix COS1 cells)
4%Paraformaldehyde/ PBS	4% paraformaldehyde/0.1M phosphate buffer pH 7.4 (Used to fix embryos)
Permeabilization buffer	0.1% (v/v) Triton X-100, 0.05% SDS in PBS
Phosphate buffered saline (PBS)	2.7 mM KCl, 1.5 mM KH2PO4, 137.9 mM NaCl, 8.1 mM Na2HPO4
PBS with Tween20 (PBST or PBT)	PBS,1% Tween, pH 7.4
Quench buffer	50 mM NH_4Cl in PBS
SOC medium	50 mM NH_4Cl in PBS
SOC medium	2% bactotryptone, 0.5% bacto-yeast extract, 10 mM NaCl, 2.5 mM KCl, 10 mM
Saline-sodium citrate (SSC) (20X)	3 M NaCl, 300 mM trisodium citrate, pH 7.0 with HCl
TAE (50X)	2 M Tris, 5.71% (v/v) glacial acetic acid, 50 mM EDTA, pH 8.0

2.2 Homology Searching

BLAST searches were conducted against protein and genomic databases for putative Arf homologues using Arf sequences from *Homo sapiens* as queries. See Table 3.1 for genomes/databases searched. Sequences retrieved with and e-value ≤ 0.05 were used in reciprocal BLAST experiments against the *H. sapiens* genome. Sequences that retrieved a human Arf with an e-value two orders of magnitude or greater than the next-best protein were validated as Arfs, and were kept for phylogenetic analysis. For genomic sequences, introns and non-coding regions were removed using Sequencher v4.9, as to maximized regions of homology to their human homologues. (This paragraph was contributed by Alex Schlacht)

2.3 Phylogenetic Analysis

Protein sequences were aligned using MUSCLE v3.6 (Edgar, 2004). Multiple alignments of the corresponding nucleotide sequences were carried out using the Pal2Nal web server (Suyama, *et al*., 2006, http://www.bork.embl.de/pal2nal/) to generate codon-based alignments. Alignments were masked and trimmed, using MacClade v4.08, retaining only unambiguously homologous regions for analysis. Model testing was carried out using jmodeltest v2.1.3 (Darriba, *et al*., 2012; Guindon and Gascuel, 2003), incorporating invariant sites and a Gamma rate distribution as required. Phylogenetic tree were constructed with MrBayes

v3.2.1 for Bayesian analysis with a minimum of 1,000,000 Markov Chain Monte Carlo generations, and the burn-in value determined graphically (Ronquist and Huelsenbeck, 2003). Maximum-Likelihood bootstrap values were determined with PhyML v3.0 (Guindon and Gascuel, 2003) and RAxML v7.0.3 (Stamatakis, 2006), each with 100 pseudoreplicates. Resulting phylogenetic trees were visualized using FigTree v1.4.0. (This paragraph was contributed by Alex Schlacht)

2.4 Zebrafish Husbandry

As juvenile and adults, zebrafish were maintained in aquaria system water using standard procedures as described by (Westerfield, 2000). Embryos and larvae were maintained in E3 media (Westerfield, 2000). To stop pigmentation, larvae were treated with PTU (1-phenol-2-thiourea). Fish were maintained at 28°C and were fed twice daily with brine shrimp and flaked food. All protocols were approved by the Animal Care and Use Committee: Biosciences at the University of Alberta with support of the Canadian Council on Animal Care.

2.5 Microinjection of anti-sense MO

Injection solutions were made using 1.0uL of 1M KCL, 2.5uL of 0.25% Phenol red, varying volumes of MO stock solutions that corresponded to sub-lethal doses and nuclease-free water filled to a total volume of 10uL (Table 2.4). All MOs were purchased from Gene Tools

(Philomath, OR, USA) and stock solutions of 25mg/ml were made. Injection volumes were calibrated to 1nl using an ocular micrometer immediately prior to injection. Morpholino cocktail solutions were then microinjected directly into the yolk of the embryos at 1-2 cell stage; embryos were spawned from a transgenic line of fish which express GFP and mCherry proteins throughout their UV and Blue photoreceptors, respectively. The transgenic line of fish is *Tg(−5.5opn1sw1: EGFP)kj9;Tg(−3.5opn1sw2: mCherry)ua3011* and used in (DuVal et al., 2013; Fraser et al., 2013). The microinjection apparatus included a pneumatic microinjector equipped with a micromanipulator with magnetic clamp stand. A 2% agarose plate was used to hold embryos for injection.

Table 2.4 MO antisense oligos used

Target Site	MO sequence	Sub-lethal dose
Arf II-A1	5'AGTTTCCTAATGTAATCTCACCTAT 3'	7ng
Arf II-A2	5' CAACAGTCCTGTCCTCTTACCTATT 3'	3ng
Arf II-B1	5' AGCAAGCACTTTCCAACTCACCCAT 3'	7ng
Arf II-B2	5' AGCAAGCACTTTCCAACTCACCCAT 3'	5ng
Arf II-C1	5'TAAAATGTCGTCGTCCTCACCCATA 3'	7ng
Arf II-C2	5' AAAGCAATACTCACACATAAGCAGC 3'	5ng
Arf II-C3	5' TGCATTCAATATTTACTCACCCATC 3'	5ng
Arf II-C1 (TB)	5' AGTGCAGTTAAAAGTGCTGTTCGCC 3'	3ng

2.6 Determination of sub-lethal doses of MO

Sub lethal doses of MO were determined as follow: the initial dose

of MO injection for all MO types started at 5ng. 6 hours after injection, each dish containing embryos were cleaned, E3 media was changed and PTU was added to each dish to prevent pigmentation. At 24 hours post injection (hpi), the media was changed and PTU was added; the number of live and dead embryos were counted and recorded. Counting of embryos and changing of media continued up until 5dpf. At 5dpf if greater than 50% of embryos had died from the 24hpi mark, then the MO dosage was decreased to 3ng. On the other hand, if greater than approximately 80% percent of embryos survived past 24hpi at the 5day mark, the MO dosage was increased to 7ng. The amount of effective MO dose is dependent on the amount of RNA that is expressed for each gene; therefore, I reasoned that an >80% survival rate may be indicative of too little MO concentration relative to RNA transcript amount. In the case of Arf II-C1 for example, increasing the dose to 7ng lowered the survival rate of embryos closer to 50%, hence a greater MO to RNA transcript ratio.

2.7 RT-PCR reaction

We confirmed the efficacy of our Arf II-C1 MO using RT-PCR on RNA extracts of uninjected and Arf II-C1 MO injected larvae at 2dpf. The primers used for this reaction were For: 5’ CCA CTC GAG ACC ATG GGC GTC TTC 3’ and Rev: For: 5’ CCA CTC GAG ACC ATG GGC GTC TTC 3’. The SB MO was designed to target the first exon/intron boundary of the Arf II-C1 transcript, so the primers were designed to amplify regions

encoded by exons 1 through 5 that span 426 base-pairs (bp). Since the length of intron 1 is 199 bp, a band of 625 bp would be indicative of the retention of this intron.

2.8 Cryosectioning

Retinal cryosections were prepared according to Barthel and Raymond (1990). In short, at 5dpf, larva were fixed in 4% paraformaldehyde/5% sucrose/0.1M phosphate buffer pH 7.4 overnight. 15-20 larvae were then washed three times with PBST and embedded in Tissue-Tek O.C.T. (Sakura Finetek). Cryostat section width was set at 10 µm. Sections from each sample were spread, and mounted in parallel, between 3-4 SuperFrost Plus glass slides. Slides were placed in a dark room for 2 hours to allow the tissue to air dry, then placed in -80°C for storage. Imaging of cryosections was performed as described in section *2.16* of this chapter.

2.9 mRNA rescue experiments

The plasmid ArfII-C1-pCS2+ was created by Hao Wang of the Allison Lab. To create this plasmid, Hao first created pME-Arf II-C1 using the primers listed in **Table 2.5.** He then moved the sequence to pCS2+ using a BP reaction Gateway System (Invitrogen). This plasmid was linearized with NOTI. hArf4 was amplified from hArf4-EGFP with the

introduction of XhoI and XbaI sites, cloned into pCS2+ and linearized by NOTI. Arf II-C1 and hArf4 mRNAs were generated with mMessage SP6 kit. All mRNAs were quantified using a GE NanoVue, electrophoresed on a 1% nuclease free agarose gel to check integrity and stored at -80 until use. mRNA was then dissolved in injection solution with the indicated dosage of MO for rescue experiments. Larvae were maintained in E3 media up to 5dpf at which point they were sacrificed and their eyes were analyzed.

2.10 Arf II-C1 riboprobe synthesis

20μg of full length (543 bps) Arf II-C1 in pCS2+ vector was linearized by digesting with BamHI, as BamH1 restriction site is upstream of the Arf II-C1 start codon. A 1.5μl sample of the restriction reaction solution was examined for linearization on an agarose gel. The remaining of the restriction reaction sample was purified using QIAquick gel extraction kit per manufacturers instructions. 1μg of the purified, linearized DNA was used in a 5X reaction to generate DIG-labeled probes using the DIG RNA Labeling Kit (SP6/T7) (Roche Molecular Biochemicals, Mannheim, Germany Product Id: 11175025910). Since the T7 promoter was downstream of the Arf II-C1 stop codon, the T7 polymerase was used to generate an antisense DIG-labeled Arf II-C1 probe. This reaction was allowed to proceed for 4 hours, and was stopped by adding 1/10v of 0.2M EDTA, pH 8.0. 70% ethanol was used to precipitate RNA overnight at -

20°C. RNA was then dissolved in 50μl of DEPC water, and a sample of this solution was run on RNase free 1% agarose gel to check for integrity. Riboprobe abundance was determined using a nanodrop spectrophotometer.

2.11 Whole-mount in-situ hybridization

Whole-mount in-situ hybridization was used to examine the spatial expression of Arf II-C1 at 5dpf. Larvae at 5dpf were fixed with 4% PFA/PBS solution at room temperature (RT) for 5 hours then washed with 1 x in 100% methanol for 10 min. Larvae were then stored overnight at -20°C in 100% methanol. The next day, larvae were rehydrated by washing with 1ml and 5 min per wash, with 75% methanol/25% PBST, 50%methanol/50% PBST, and 25%methanol/75% PBST washes. Next, the larvae were washed 5 x 5 min at RT in PBST (PBS/0.1% Tween-20). Embryos were permeabelized by treating with 10μg/ml Proteinase K in PBST for 20 min RT. The larvae were refixed all in 4% paraformaldehyde/ 10X PBS for 20 min at RT, rinsed 5 x 5 min each in PBST. Larvae were then pre-hybridized in 500μ mix (hyb mix) (50% formamide, 5 x SSC, 50 μg/ml heparin, 500 μg/ml tRNA, 0.1% Tween-20, sterile H_20, 0.092M citric acid adjusted to pH 6.0) for 1 hour at 65°C. The pre-hybridization mix was removed and larvae were incubated overnight at 65°C with a 200 x dilution of an Arf II-C1 riboprobe (300 μg/ml) into hybridization buffer solution. The next day larvae were washed for 5 min with 1 ml of each: 66% hyb mix (no

tRNA), 33% 2 x SSC at 65°C and 2 x SSC at 65°C. Larvae were further washed with 1 x 20 min in 0.2 x SSC +0.1% Tween-20 at 65°C, 2 x 20 min in 0.1 x SSC+0.1% Tween-20 at 65°C (high stringency), 5 min in 66% 0.2 x SSC, 33% PBST at RT, 5 min in 33% 0.2 x SSC, 66% PBST at RT and 5 min in PBST at RT. For the anti-digoxigenin-alkaline phosphatase binding reaction, larvae were incubated in blocking solution (PBST plus 2% sheep serum, 2 mg/ml BSA for 1 hour at RT. The anti-digoxigenin-AP antibody solution was prepared by diluting it 1/5000 in blocking solution (anti-fluorscein: 1/10,000). Larvae were incubated in the antibody solution on a shaker overnight at 4°C. The next day larvae were washed 5 x 15 min in PBST and readied for the coloration reaction. The coloration reaction consisted of 4 x 5 min washes in coloration buffer (100 mM Tris-HCl, pH9.5, 50 mM $MgCl_2$,100 mM NaCl, 0.1% Tween-20, sterile water. 45 µl of nitro-blue tetrazolium (NBT) stock was mixed with 10 ml coloration buffer, then 35 µl 5-bromo-4-chloro-3-indolyl phosphate (BCIP) stock was added (both available from Boehringer). 500 µl of this mix was added to larvae and incubated in the dark in the dark at 30°C for approximately 45 minutes until coloration reaction occurred. The reaction was stopped by quickly washing larvae 4 x 5 min in stop solution (PBST pH5.5).

2.12 Cell culture maintenance

COS1 cells were received from Dr. Stone (ATCC CRL-1650;

American Type Culture Collection) and maintained in Dulbecco's modified Eagle's medium (DMEM) with 4.5g/l D-glucose and L-glutamine supplemented with 10% fetal bovine serum (FBS) (Sigma-Aldrich), 100 g/ml penicillin, and 100 g/ml streptomycin (present at 1X concentration), at 37°C in a 5% CO_2 incubator. Transfection Media consisted of DMEM with 4.5g/l D-glucose and L-glutamine, supplemented with 10% FBS (Sigma-Aldrich).

2.13 Plating and transient transfection of cells

COS1 cells were plated onto glass coverslips that sterilized by ethanol and transferred to a sterile 6 well plates. Cells were grown to 40-60% confluency, at which point they were transfected with specified plasmid(s) using TransIT-2020 transfection reagent (Mirus, Madison, WI), as per manufacturer instructions with 1ml of Opti-MEM containing HEPES, 2.4g/L Sodium Bicarbonate and L-Glutamine. After 2 hours of transfection 1 ml of DMEM containing 200 µl FBS was added into each well. Cells were allowed to express proteins for approximately 16-18 hours before being examined.

2.14 Construction of plasmids for tagged Arfs

The plasmids used for Arf-GFP expression constructed by inserting Arf cDNAs between Xho1 and Kpn1 sites of the pEGFP-N1 vector (Clontech, Mountain View, CA). These specific Arf fragments were

obtained through PCR amplification from plasmids containing the Arf sequences of interest. Arf inserts were amplified through use of forward primers that introduced an Xho1 site immediately upstream of the ATG (start codon), and reverse primers that modified the stop codon to CGC and also introduced a Kpn1 site immediately downstream (Table 2.5). This procedure yielded in-frame translation of GFP after a 12-residue linker (AVPRARDPPVAT). The Arf PCR products were then digested with of XhoI and KpnI and then ligated into pEGFP-N1 vector digested with the same restriction enzymes as per manufacturer's instructions. The mCherry-tagged constructs were generated using a previously constructed pEGFP-N1 vector, where the EGFP coding fragments was substituted with a mCherry coding fragment through the use of BamHI and NotI restriction enzymes. Sources containing Arf sequences were *D. melanogaster*: Arf79F (Dm Class I Arf), in a pOT2 vector, Arf102F (Dm Class II Arf) in a pFLC-1 vector given to us by Dr. Andrew Simmonds from Berkley Drosophila Genome Project (BDGP) (www.fruitfly.org). *D.* rerio Arfs: Arf1b, obtained online through Thermoscientific (catalog #: MDR1734-7600133), Arf II-A2 and Arf II-B1 were obtained in a pMZ plasmid and Arf II-C1 was obtained in a pSC2+ plasmid constructed by Hao Wang. *C. elegans* Arfs: Arf1 (Ce Class I Arf) and Arf3 (Ce Class II Arf) cDNAs from EST clones in phagemid yk69a11.5 and yk319e2.5, respectively, were obtained from Dr. Kohara (National Institute of Genetics, Japan). All tagged forms of Arf1b, Ce Class I, Ce Class II, Dm Class I, Dm Class II, Arf II-A2 and Arf II-B1,

were all generated by Bahram (Victor) Foroutanpay.

Table 2.5 Primers used for molecular cloning

Primer Name	Sequence (5'—>3')	Construct name
Arf II-C1 For	GGG GAC AAG TTT GTA CAA AAA AGC AGG CTA CAT GG GCG TCTT CTT CTC TA-3	Arf II-C1-pCS2
Arf II-C1 Rev	GGG GAC CAC TTT GTA CAA GAA AGC TGG GTT TAT CGT TTG GAG AGT TGA TCT G	
Ce Class I For	CCA CTC GAG AGA ATG GGA AAC GTG TTC	Ce-Class I-GFP
Ce Class I Arf Rev	GCT CAA GAA TAG ATC TGC GGT ACC TGT G	
Ce Class II Arf For	CCA CTC GAG ACC ATG GGT TTA ACA ATC TCC TCC CTC	Ce-Class II-mCherry
Ce Class II Arf Rev	CAC AGG TAC CGC GGT CTT GGA AGG CTG GTT GGA TAG	
Dm Class I Arf For	CCACTCGAGGCCATG GGA AAC GTA TTC GCG AAC	Dm Class I-GFP
Dm Class I Arf Rev	CAC AGG TAC CGC GCG ATT AGC GTT CTT CAA TTG GTT G	

Dm Class II Arf For	CCA CTC GAG AAC ATG GGA CTA ACA ATA TCT AGT C	Dm Class II-mCherry
Dm Class II Arf Rev	CAC AGG TAC CGC TTT TTT AGC CAA TTC AGC TGA TAG	
Arf II-A2 For	CCA CTC GAG ACC ATG GGT CTG ACC ATC TCG TCG	Arf II-A2
Arf II-A2 Rev	CAC AGG TAC CGC GCG TTT GGA GAG CTC ATT TGA TAA CC	
Arf II-B1 For	CCA CTC GAG ACC ATG GGT TTG ACT ATT TCG AGC G	Arf II-B1-mCherry
Arf II-B1 Rev	CAC AGG TAC CGC GCG TTT GGA GAG CTG CTC GGA AAG	
Arf1b For	CCA CTC GAG AAG ATG GGA AAC ATA TTC GCA AAC C	Arf1b-GFP
Arf1b Rev	CAC AGG TAC CGC TTT CTG GTT TTT CAG CTG ATT GGA C	
Arf II-C1 For	CCA CTC GAG ACC ATG GGC GTC TTC	Arf II-C1-GFP
Arf II-C1 Rev	GTG TCC ATG GCG TCG TTT GGA GAG TTG ATC	
hArf4 For	CGT CT AGA TTA GCG CTT TGA CAG	hArf4-pCS2+

	CTG
hArf4 Rev	CGT CTA GAT TAG CGC TTT GAC AGC TG

2.15 Fixed cell imaging by confocal microscopy

Images used for figure 3.6, panels B, D and E were acquired with an LSM 510 scanning confocal microscope (Carl Zeiss) equipped with a 20X objective (NA=1.4). Images for figures 3.10 and 3.11 were also acquired with this microscope equipped with 63X objective. The GFP signal was excited with a 488 nm laser and collected with a 500-550 nm bandpass filter. The mCherry signal was excited with a 543 nm laser and collected with an Alexa >560 nm longpass filter as described by Zhao *et al.,* (2002). Signal from each channel was collected sequentially to avoid bleed-through.

2.16 Antibodies

The primary antibody used in our immuno-fluorescence experiments was a monoclonal mouse anti-ERGIC-53 (diluted to 1:1000 in PBS + 0.2% gelatin) (Enzo Life Sciences) and the secondary antibody was a donkey Alexa Fluor 647, anti-mouse IgG (H+L) (diluted to 1:600 in PBS + 0.2% gelatin) (Invitrogen).

2.17 Live cell imaging and BFA treatment

For live cell imaging, cells were grown on #1D round coverslips (Fisher Scientific, Ottawa, ON). Coverslips were then washed with 2 ml of PBS and secured into chambers. 250ul of CO_2 independent media (Gibco Laboratories, Grand Island, NY) supplemented with 10% FBS was added to each chamber and placed under the microscope. 1.5 µl of BFA from a 10µg/µl BFA stock solution was mixed with tubes containing 1.25ml of CO_2 independent media and placed in a water bath kept at 37ºC. At 1minute, the 1.25ml of BFA/CO_2 independent media was added into each chamber using a syringe. During imaging temperature of the microscopy room was set to 35ºC; a stage heater and a lens heater were used to maintain the temperature of cells close to physiological temperatures. Images were captured with a 9100-50 electron multiplier CCD digital camera and processed with Ultraview Image Suite.

2.18 Statistical analysis

Data are expressed as ± standard error of the mean (SEM). Student's t-test was used for comparisons between two variables and one-way ANOVA for more than two variables. When a significant effect ($p<0.05$) was detected, comparisons among multiple means were conducted by Student-Newman-Keuls (SNK) test. Statistical analyses were performed using SAS 9.0 for Windows (SAS Institute Inc., Cary, NC).

CHAPTER 3: RESULTS

3.1 Zebrafish express seven Class II Arf paralogues that cannot be distinguished as either Arf4 or Arf5

In order to uncover and categorize Arf isoforms within the *Danio rerio* (zebrafish) genome, we utilized BLASTp searches on the NCBI protein database. Using the amino acid sequences corresponding to human Arfs1, -3, -4, -5 and -6 and mouse Arf2 isoforms, we performed multiple protein BLASTp inquiries within the zebrafish protein database. Reciprocal protein BLASTp of zebrafish Arfs into human (and mouse) protein databases allowed us to compile and organize a list of zebrafish Arf proteins based on % identity to human and mouse Arf orthologues (**Table 3.1**). Note that several Class II Arf paralogues in this table were uncovered through the analysis of chromosome 11 within the region that is flanked by the genes 2-PE and FAM116A (discussed below). Arf paralogues discovered in this manner are labeled with their Ensembl ID as Accession Numbers are not available for these genes.

Most mammals harbor one gene for each Arf isoform in their genome. In contrast, with the exception of Arf2, multiple paralogues for each Arf protein are found in *zebrafish*. **Table 3.1** reveals that the maximum identity for most Arf homologues is in the >98% range. In the case of zebrafish Arf2, it is 96% identical to both human Arf1 and mouse Arf2. What is striking is the low amino acid percent identity between the seven zebrafish and human Class II Arfs that ranges from 94% to as low as 69%. More importantly, some zebrafish Class II Arf isoforms display

approximately equal percent identities to both human Class II and human Class I Arfs. We therefore chose to examine whether these seven divergent zebrafish isoforms were actually members of the Class II Arfs. Alex Schlacht performed bioinformatics analyses using amino acid and or/nucleotide sequences from multiple species databases and concluded that what we are calling zebrafish Class II Arfs are indeed members of the Class II Arfs, and not Class I or III. However, based on the sequence databases available today, Alex was not able to categorize the seven zebrafish Class II Arf into Arf4 and Arf5 sub-classes (**Figure 3.1).**

Interestingly, our studies showed that the seven zebrafish Class II Arfs categorize into three distinct clades (**Figure 3.2**). Because we could not phylogenetically group members of the three clades with either Arf4s or Arf5s, we proposed to label them simply as Arf IIs; the Roman numeral II denotes their inclusion with the Class II Arfs. However, because there are three distinct clades, we distinguished each clade by the letters A, B, C. The letter A was assigned to the clade with the highest percent identity to human Class II Arfs, while the letter C was given to the most divergent clade. We categorized members of the three clades as Arf II-A1, Arf II-A2, Arf II-B1, Arf II-B2 and Arf II-C1, Arf II-C2, Arf II-C1; the Arabic numerals reflect the different members within each clade. Members of clades A and C are also found in other species of bony fish. Interestingly, however, members of the zebrafish clade B are not found in any of the other fish species listed.

Table 3.1 Zebrafish express multiple paralogues of most Arf isoforms

Proposed Name (Accession number or Ensembl ID)	Chromo-some	A.A. length	% Identity to indicated Arf type					
			hArf1	mArf2	hArf3	hArf4	hArf5	hArf6
Arf1a (NP_958860)	2	180	**98%**	95%	96%	79%	80%	69%
Arf1b (NP_958888)	24	180	**98%**	95%	95%	80%	81%	69%
Arf2 (NP_958912)	3	181	**96%**	**96%**	95%	81%	81%	68%
Arf3a (NP_001003441)	23	181	**99%**	94%	**99%**	79%	78%	70%
Arf3b (NP_001012248)	6	181	96%	94%	**100%**	79%	79%	69%
Arf II-A1 (NP_954969)	18	180	84%	83%	82%	92%	**93%**	65%
Arf II-A2 (NP_956170)	18	180	84%	83%	82%	93%	**94%**	66%
Arf II-B1 (NP_001003590)	11	180	83%	81%	80%	91%	**92%**	67%
Arf II-B2 ENSDARG00000045989	11	181	79%	77%	76%	**86%**	**86%**	64%
Arf II-C1 (NP_001017707)	11	180	**74%**	73%	**74%**	73%	72%	66%
Arf II-C2 ENSDARG00000073876	11	180	**71%**	**71%**	70%	69%	69%	61%
Arf II-C3 ENSDARG00000074210	11	181	70%	70%	69%	**71%**	**71%**	59%
Arf6a (NP_956287)	20	175	67%	69%	69%	65%	66%	**99%**
Arf6b (NP_001154847)	17	175	67%	69%	69%	65%	66%	**99%**

Reciprocal Blastp inquiries on NCBI's database, along with Ensembl analysis of *D.rerio* chromosome 11 identified a total of 14 *D. rerio* Arf isoforms. Percent identity of each zebrafish Arf isoform to human and mouse Arf isoforms are indicated. Chromosome number and amino acid (A.A) lengths were identified using NCBI and Ensembl databases. Proposed names along with Accession Numbers are listed for each zebrafish Arf isoform. When Accession Numbers were unavailable, Ensembl IDs were used to identify each gene.

Although computational bioinformatics analysis is the most reliable tool available for phylogeneticists, exon/intron structure and organization can also be used as an inference for phylogenetic analysis (Fenn *et al.,* 2006). Based on this notion we decided to compare the genomic organization of human (mouse in the case of Arf2) Class I and II Arfs to their respective orthologues in zebrafish (Figure 3.3). Figure 3.3A clearly demonstrates that the genes for Class I and II Arfs possess very different exon structures. Genes for each of the Class I Arf isoforms examined in this figure are comprised of four exons, while Class II Arfs are encoded by five to seven exons. Human Arf1, -3, mouse Arf2, zebrafish Arf1a, -1b, -2, -3a, -3b all display identical exon structure length (with the exception of the first exons of zebrafish Arf1a and -1b, which are shorter by one codon relative to the other Class I Arfs listed). Arf II-A1, Arf II-A2, Arf II-B1 and Arf II-C1 paralogues have the same exact exon structure as their human Class II orthologues, whereas, Arf II-C2 and Arf II-C3 have lost an intron between exons 4 and 5, and Arf II-B2 has gained an intron within exon 3. It is worth noting that the length of Arf II-B2 and Arf I-C3 are one amino acid longer than the other Class II Arf isoforms listed. As discussed above, Liu *et al.* (2010) identified a section within the zebrafish chromosome 11 that is syntenic to a region on human chromosome 3p14 where human Arf4 is found. The authors identified what they called Arf 4 (called Arf II-C1 here) as the only zebrafish Class II Arf in this region. However, closer examination of this region by Dr. Ted Allison, led to the discovery of an

additional four Class II Arfs (Figure 3.3B). Therefore, of the seven identified zebrafish Class II Arfs, five of these genes are positioned in tandem on chromosome 11. The clades that occupy this region are the Arf II-Bs, Arf II-Cs, while the two members of the Arf II-A clade are positioned on chromosome 18 (Figure 3.3B). Note the opposite gene orientation of Arf II-C1 relative to its paralogues. Though there is evidence for the expression of Arf II-C1, and its complete coding region has been cloned from cDNA, the genomic regions past the fifth exon have not yet been sequenced; therefore, as illustrated in Figure 3.3B, the length of the last intron is not known. The number of exons that encode Arf II-C1 past the last intron also remain unknown.

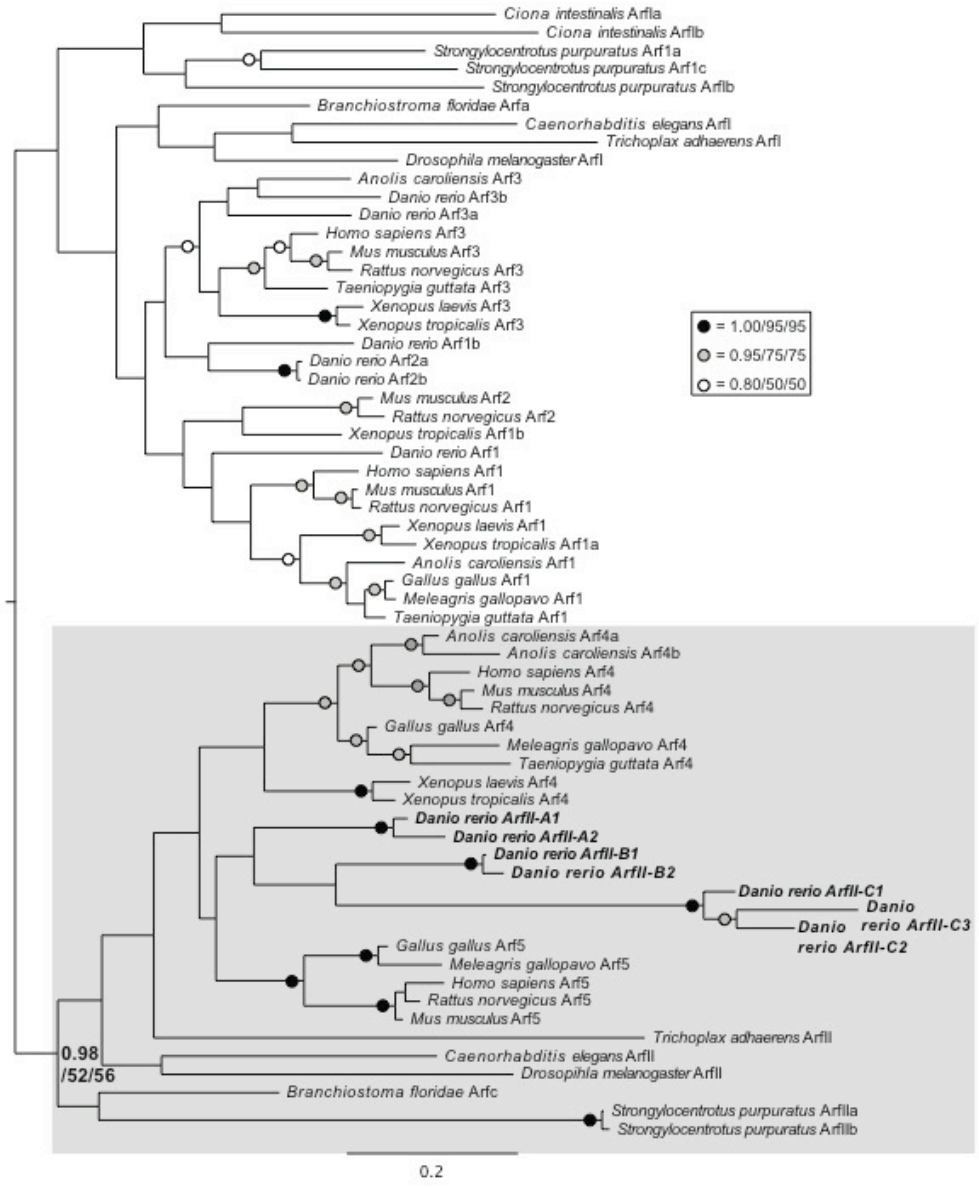

Figure 3.1: Phylogenetic analysis of Class I and Class II Arf proteins. Phylogenetic analysis of novel *Danio rerio* Arf paralogues demonstrates that they belong to Class II not Class I. The analysis identified three clades of class II *Danio rerio* Arf paralogues; however, it did not establish whether they belong to the Arf4s, Arf5s, or are pre-duplicates of the two former clades. Important nodes are shown in bold; support values indicate Bayesian posterior probabilities, and Maximum-Likelihood bootstrap values from PhyML and RAxML, respectively. Symbol legend is provided in inset.

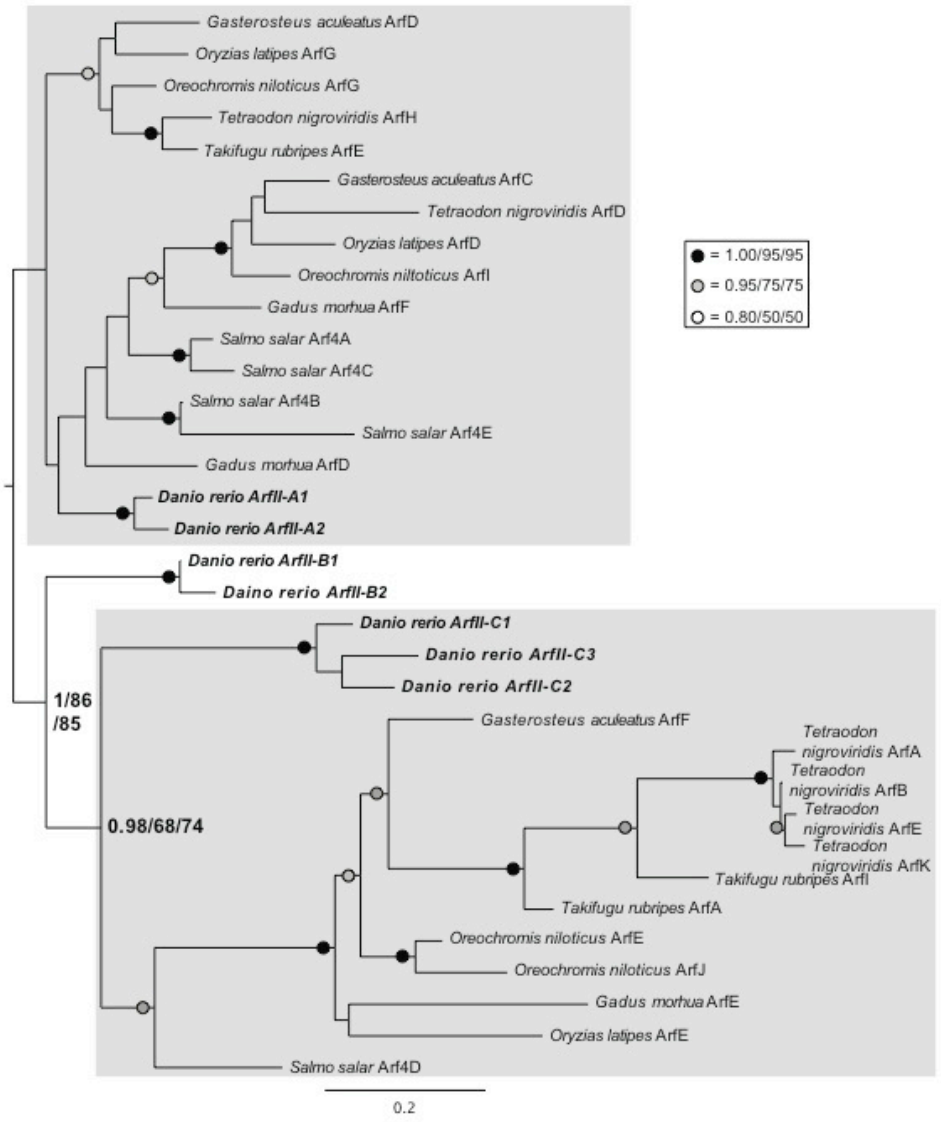

Figure 3.2: Phylogenetic analysis of actinopterygian Class II Arf proteins. Two distinct clades of Class II Arf proteins are present in bony fish, both of which contain paralogues identified in *Danio rerio*. Orthologues of the *D.rerio* ArfII-A (upper grey box) and ArfII-B (lower greybox) clades are also present in *Salmo salar, Oryzias latipes, Gadus morhua, Oreochromis niloticus Takfugu rubripes, Tetraodon nigroviridis, and Gasterosteus aculeatus* indicating that these additional Arfs are not a specific feature of *D. rerio*, but are found in other fish as well. Important node values are in bold; support values indicate Bayesian posterior probabilities, and Maximum-Likelihood bootstrap values from PhyML and RAxML, respectively. Symbol legend shown in inset.

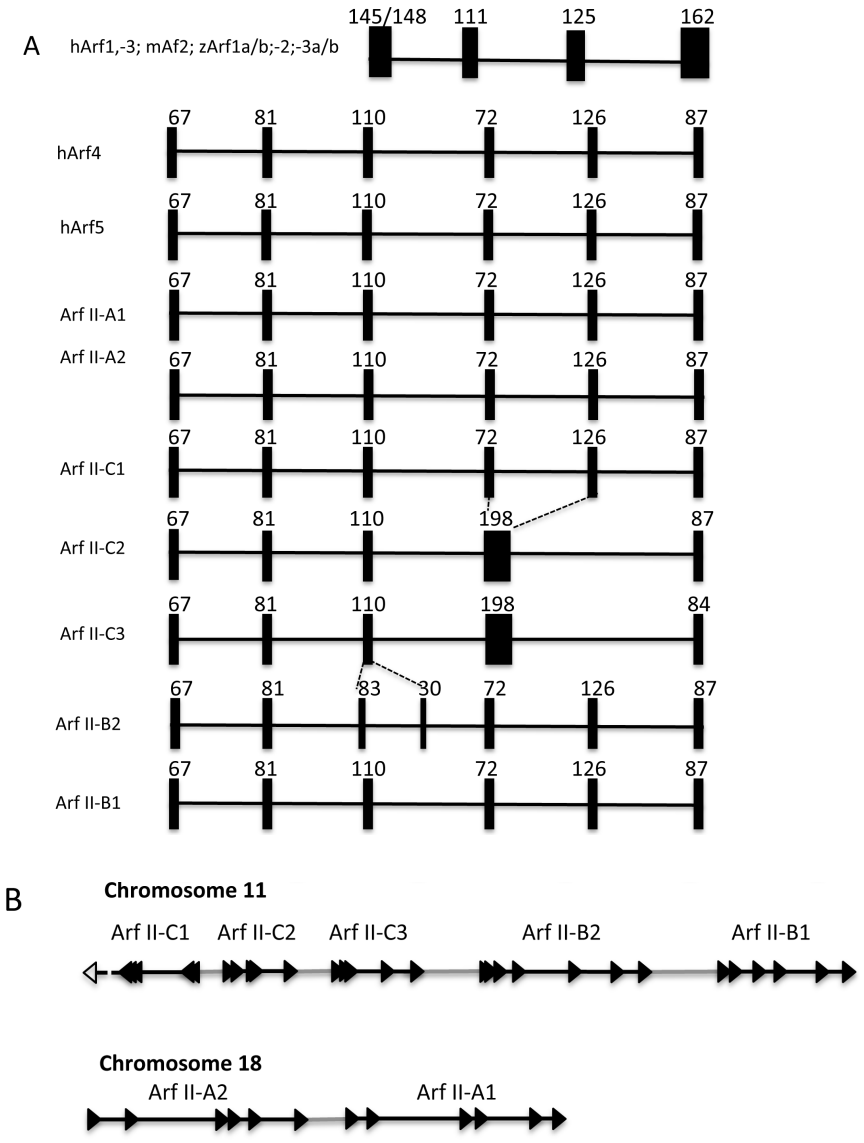

Figure 3.3: Gene structure and exon length of zebrafish and human Class I and II Arfs are nearly identical. A. The length and number of exons for both Class I and Class II Arf genes were obtained through Ensembl. Exons are shown to scale but intron lengths are drawn arbitrarily. Number above each exon refers to exon length in bp. **B.** (top) Schematic representation of a contig found on chromosome 11 that houses five of the seven zebrafish Class II Arfs. In the case of Arf II-C1, regions past the fifth exon are not sequenced as of now and the intron is represented by dashes; the number of exons that encode Arf II-C1 past the last intron also remain unknown. (bottom) The two remaining zebrafish Class II Arfs are found on chromosome 18 (lower).

3.2 MO-directed knockdown of Class II Arfs in zebrafish causes morphological defects in Arf II-A2 morphants

In order to address the role of Class II Arfs in zebrafish eye development, we took advantage of antisense MO oligomers. In general, there are two types of morpholinos: splice-blocking (SB) MOs and TB MOs. SB MOs block the expression of their target protein by impeding the correct splicing of zygotically coded RNA into mature RNA. TB MOs, on the other hand, block the translation of both zygotically expressed as well as maternal mRNA by binding to their 5'UTR and therefore hindering their interaction with the cell's translation machinery. The advantage of SB MOs over TB MOs is that the efficacy of SB MOs can be confirmed by RT-PCR. Based on this reasoning we designed SB MOs to block the zygotic expression of all zebrafish Class II Arfs **(Figure 3.4**). We also designed a TB MO against Arf II-C1 gene, reasons for which will become apparent in later sections of this chapter.

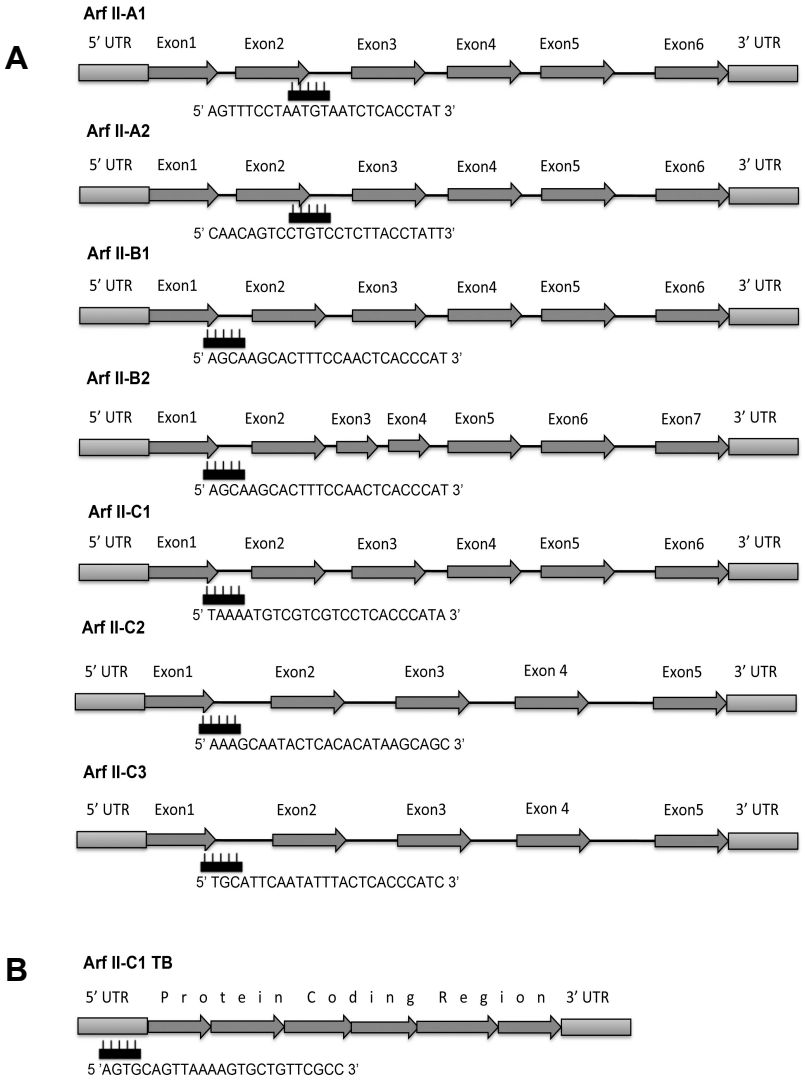

Figure 3.4: MO antisense oligos were designed to target specific regions of all seven zebrafish Class II Arfs. A. All seven zebrafish Class II Arfs are listed. Each arrow represents a single exon; exons are drawn to scale and numbered above each arrow. Black "combs" represent MOs placed at the targeted exon/intron boundary; MO sequences are provided under each gene. Arf II-B1 and Arf II-B2 have nearly identical nucleotide sequences and the MO we designed targets both mRNAs. **B** Translation-blocking MO against Arf II-C1 was designed to target the 5' region of both zygotically and maternally expressed Arf II-C1 RNA.

3.3 MO directed knockdown of Arf II-A2 but not any other Class II Arf isoform causes morphological defects in morphants at 5dpf

As described in Chapter 2, larvae at the 1-2 cell stage (see **Figure 1.3**) were injected with sub-lethal doses of specific SB MO or TB MO, where indicated. A sub-lethal dosage is defined as an experimentally determined dose of MO solution with ≅50% morphant survival rate at 5 days post-fertilization (dpf). Sub-lethal doses for each MO are listed in **Table 3.2**. After the injection of the specified doses of MO, we followed the development of each morphant type and imaged them under the same magnification, in groups of 5-9 larvae, to examine for gross morphological defects associated with the KD of the specified Class II Arfs (**Figure 3.5A).** At 5dpf, it became apparent that fish knocked down for Arf II-A2, but not any other morphant type or the control MO (Control MO) showed "bending" of their bodies. Upon closer examination of the Arf II-A2 morphant larvae, we noticed that body bending was present with varying degrees of severity, and that the body bending was not in a specific spatial orientation. This observation was quantified by measuring the percent of larvae displaying body bending per image (**Figure 3.5B**). Body bending was compared to that observed with Control MO morphants. Greater than 65% of Arf II-A2 morphants displayed some degree of body bending. Significant body deformities were not seen in any other morphant types (**Figure 3.5A**) and this was not quantitated.

Table 3.2: Sub-lethal doses of MO per injection

Gene Name	Sub-lethal Dosage
Arf II-A1	7ng
Arf II-A2	3ng
Arf II-B1	7ng
Arf II-B2	5ng
Arf II-C1	5ng
Arf II-C2	5ng
Arf II-C3	5ng
Arf II-C1 TB	3ng

Embryos at the 1-2 cell stage were injected with the indicated doses of splice-blocking MO, or translation-blocking MO where indicated. Experimentally determined sub-lethal doses are those that led to an approximately 50% survival rate of larvae at 5dpf.

(Figure on Next Page)

Figure 3.5: With the exception of Arf II-A2, knockdown of Class II Arfs by injection of sub-lethal doses of splice-blocking MOs, causes no gross morphological defects. A. Embryos were injected at the 1-2 cell stage (refer to Materials and Methods) with either sub-lethal doses of the indicated splice-blocking MO (and translation-blocking MO in the case of Arf II-C1), or with a non-sense control morpholino (Ctrl. MO) and imaged at 5dpf. Images were captured with different lighting parameters but all under the same magnification. Under these conditions, with the exception of Arf II-A2, most morphants display no obvious gross morphological deformities. **B.** Representative images seen in part A containing 5-9 larvae at 5dpf were examined and the percent of fish with bends in their body from each group were recorded. Body-bending observed in Arf II-C1 morphants was compared to that observed with Ctrl. MO morphants. Bars are presented as ±SEM from 3 different experiments. A total of 127 and 211 fish were examined for Ctrl. MO and Arf II-A2 morphants, respectively.

A

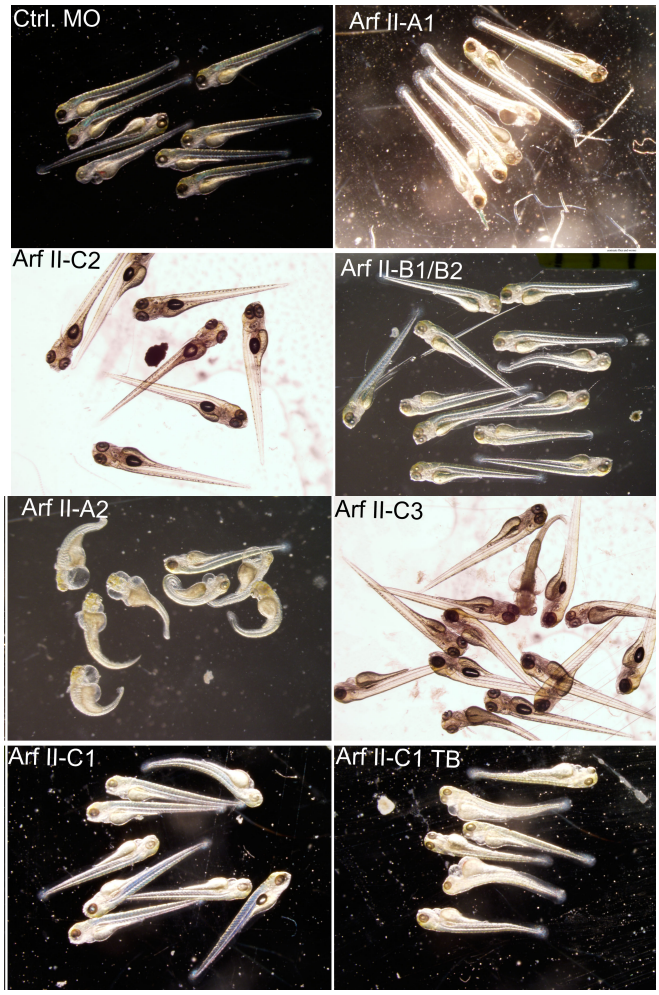
Ctrl. MO
Arf II-A1
Arf II-C2
Arf II-B1/B2
Arf II-A2
Arf II-C3
Arf II-C1
Arf II-C1 TB

B

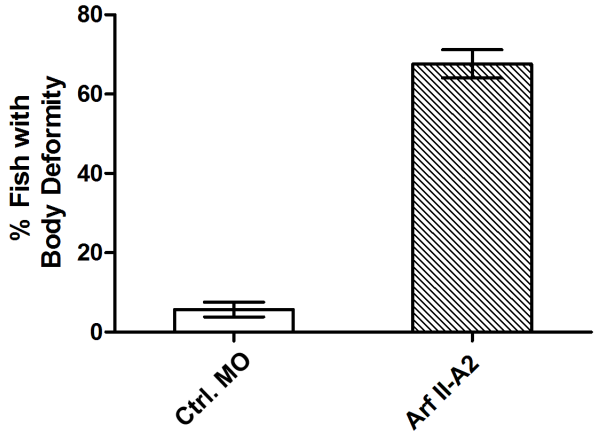
% Fish with Body Deformity
80
60
40
20
0
Ctrl. MO
Arf II-A2

3.4 Knockdown of Arf II-C1, causes disruption of UV and Blue photoreceptor number and organization

Zebrafish possess four spectral subtypes of cone photoreceptors, including: ultraviolet (UV)-, blue-, green-, and red-sensitive cones. Cone spectral subtypes in zebrafish larvae form a non-random, regular, mosaic pattern and predictable ratio of the number of cone spectral subtypes (Allison *et al.,* 2010). In order to readily observe morphological defects in zebrafish larval eyes upon MO-directed KD of specific Class II Arfs, we took advantage of a transgenic line of zebrafish that express GFP proteins throughout their UV cone photoreceptors and mCherry protein throughout their blue cone photoreceptors. Embryos at the 1-2 cell stage were injected with specific, sub-lethal, dosages of MOs corresponding to the gene of interest. At 5dpf, larval eyes were dissected and retinas were mounted on coverslips for observation (**Figure 3.6A)**. Retinal images were acquired by confocal microscopy and z-stacks were examined. Upon visual inspection of the confocal slices of each stack, it became apparent that the organization of the UV (green) and Blue (magenta) cones was clearly different in Arf II-C1 morphants compared to that observed in the Control MO or any of the other morphant types. The two striking features that stand out in the Arf II-C1 morphants are 1) the spatial organization of the UV photoreceptors relative to one another; 2) the decrease in Blue relative to UV cones.

To confirm the specificity of our Arf II-C1 SB MO, we also designed and injected Arf II-C1 TB MO into 1-2 celled embryos. As seen in Figure 3.6A (bottom right) injection of Arf II-C1 TB MO resulted in a phenotype similar to that observed with the Arf II-C1 SB MO. Single slice images acquired using a 20x objective allowed us to visualize the disorganization throughout the retina (**Figure 3.6B)**. To confirm the efficacy of our Arf II-C1SB MO, we utilized RT-PCR to establish whether the SB MO blocked splicing of the first intron (**Figure 3.6C)**. As illustrated in **Figure 3.4A,** the Arf II-C1 SB MO was designed to target the first exon/intron boundary; therefore, primers were designed to amplify a region upstream of the MO target site on exon 1 through exon 5 which span a total of 426 base-pairs (bp). Since the length of intron 1 is 199 bp, a band of 625 bp would indicate the retention of this intron. Results of the RT-PCR reaction indicated that a 625 bp band was indeed present in reactions performed with total RNA from Arf4 II-C1 morphant extracts, but not with extracts from Control MO morphants (**Figure 3.6C)**. Note that there are 2 bands present for the Arf II-C1 reaction; as alluded to above, SB MOs can only block the splicing of newly (or zygotically) coded RNA; therefore, the lower band likely reflects the presence of maternal mRNA which gets passed off to her progeny in its correctly spliced form. It is also likely that the lower band represents unaffected zygotic mRNA, which is consistent with the incomplete efficacy of most morpholino reagents. Sequencing of the two

bands generated from the RT-PCR reaction confirmed the presence of the 199 bp first intron in the upper, but not the lower band.

In order to better appreciate the changes in the organization and numbers of UV and Blue photoreceptors first detected in images of whole mount retinas, we set out to examine transverse cryosections of larval eyes at 5dpf (**Figure 3.6D).** Transverse cryosections of the eye reveal that the spacing between the UV photoreceptors has changed in the Arf II-C1 TB morphants relative to the control MO morphants. Also clear is the substantial decrease in the number of Blue cones in the Arf II-C1 morphants. Although there is a dramatic difference in photoreceptor organization and number, changes in the characteristic laminar cellular organization of the retina are not observed **(Figure 3.6E; see also Figure 1.6 in Chapter 1).**

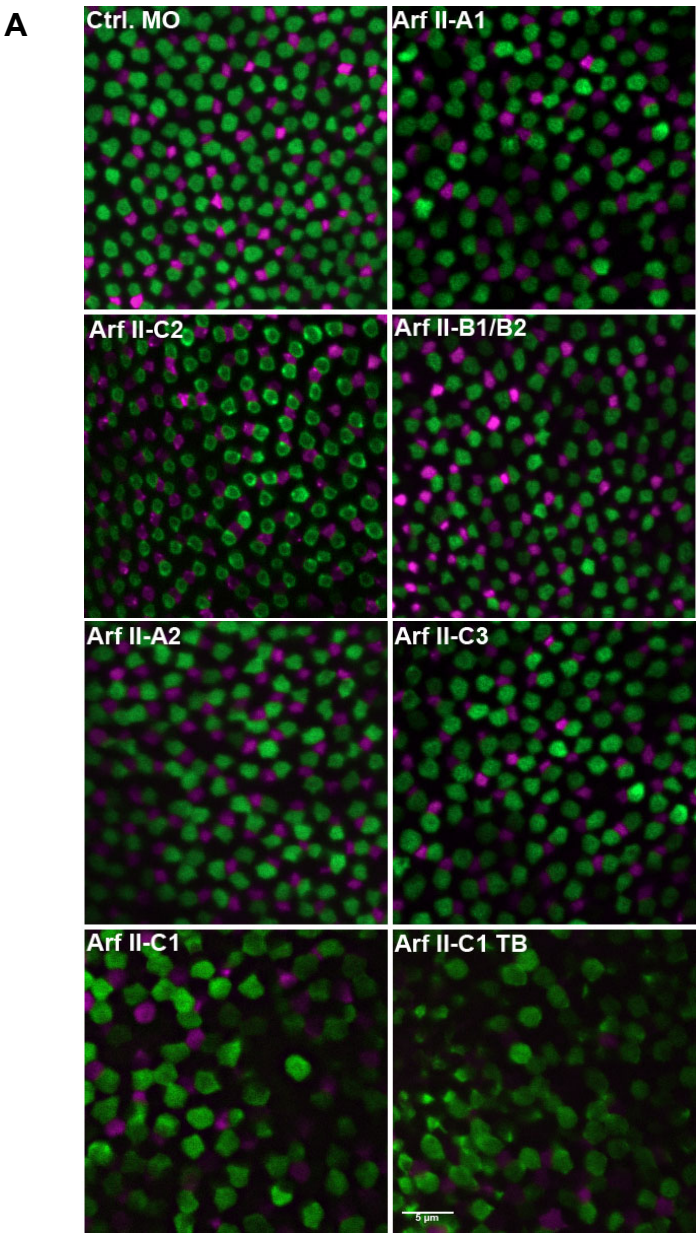

Figure 3.6: Knockdown of Arf II-C1, but not any other Class II Arf, causes disruption of UV and Blue photoreceptor number and organization. A. Whole-mounts of retinas recovered from various morphant types were imaged using a spinning disc confocal microscope equipped with a 40x lens. Morphants were derived from transgenic fish that express GFP (pseudo-colored green) in their UV photoreceptors and mCherry (pseudo-colored magenta) in their Blue photoreceptors. Shown are identically cropped sections of single slices from a z-stack. The nature of the MO injected is indicated on each panel. Arf II-C1 morphants display an apparent difference in the organization and size of UV and Blue photoreceptors. Injection of Arf II-C1 TB MO resulted in similar disorganization of UV and blue cones seen in Arf II-C1 morphants.

B

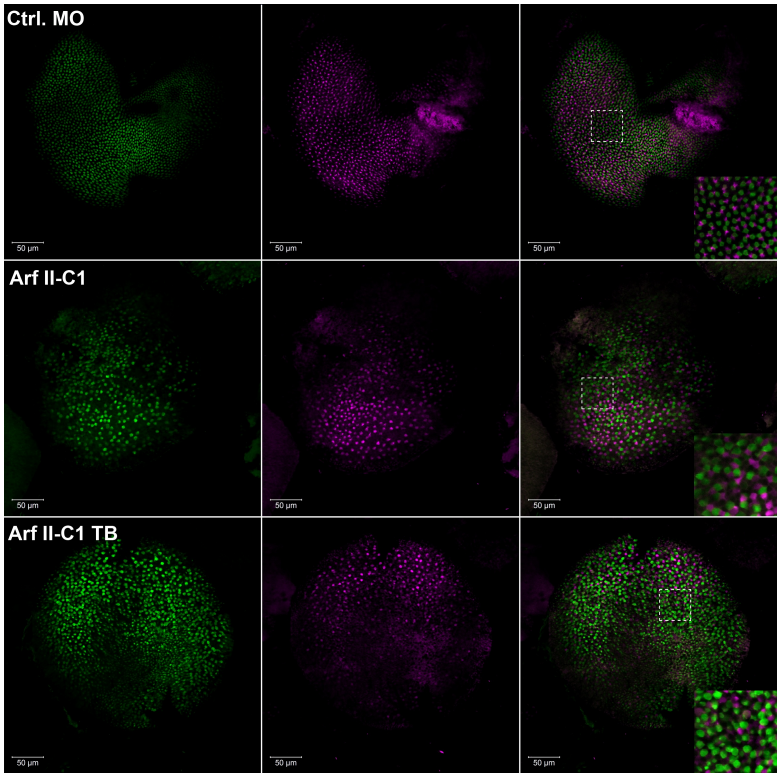

(Figure 3.6, continued) B. Slides were prepared as in panel A; single slice images were acquired with a scanning confocal microscope equipped with 20x objective to allow for the visualization of UV and Blue photoreceptors throughout the whole retina.

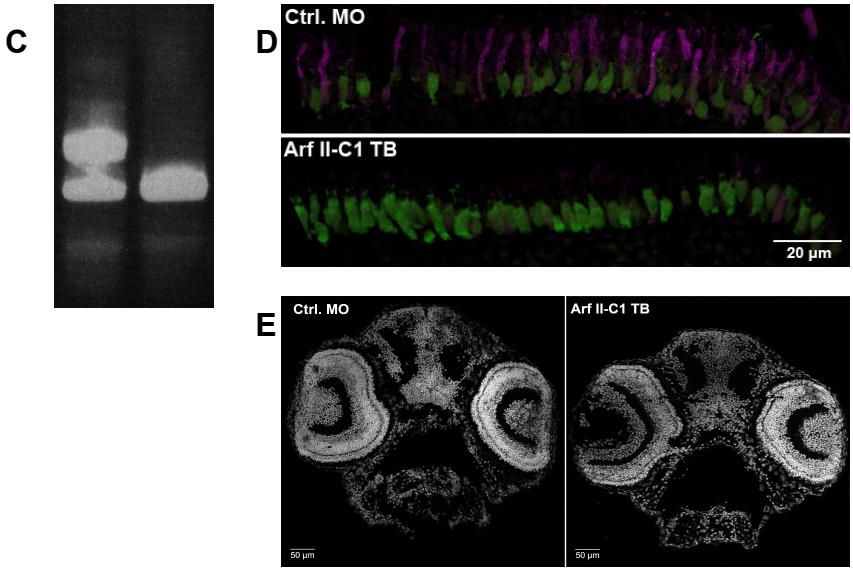

(Figure 3.6, continued) C. RT-PCR confirms the efficacy of Arf II-C1 splice-blocking MO. The splice-blocking MO was designed to target the first exon/intron boundary (see Figure 3.4); primers were designed to amplify regions encoded by exons 1 through 5 that span a total of 426 bp. A band of 625 bp would indicate the inclusion of the199 bp-long intron 1. RT-PCR indicated that a 625 bp band was present in reactions performed with total RNA from Arf II-C1 morphant extracts, but not with extracts from Ctrl. MO morphants**. D.** Transverse retinal cryosections of 5 dpf larval eyes display a dramatic decrease of Blue photoreceptors and apparent change in spacing of UV photoreceptors relative to each other in Arf II-C1 TB relative to Ctrl. MO morphants. The combination of these two events results in the disruption of UV and Blue photoreceptor number and organization that is seen in panel **A. E.** At 5dpf, cryosections of Arf II-C1 TB and Ctrl. MO morphants were stained with TO-PRO3. Arf II-C1 TB morphants display normal histology of eye layers compared to Ctrl. morphants.

3.5 Knockdown of Arf II-C1 reduces significantly the number of UV and Blue photoreceptors but affects the number of Blue cones more dramatically than that of UV Cones.

We set out to quantify the observations reported in **Results Section 3**.4 above by measuring the number of UV and Blue cones on 3 randomly selected 30X30 μm areas of whole-mounted retinal images per larval eye. UV and Blue photoreceptor number of Arf II-C1, Arf II-C1 TB as well as Arf II-A2 morphants were compared to Control MO. morphants. Even though we did not observe an apparent disorganization and decrease in the number of UV and Blue photoreceptors in Arf II-A2 morphant eyes, we decided to quantify their photoreceptor number to see if the gross morphological defects we saw earlier also affected UV and Blue photoreceptor number **(Figure 3.7A).** Statistical analysis shows that the number of UV and Blue photoreceptors in Arf II-C1 morphants were reduced dramatically compared to the Control MO morphants.

For our statistical analysis, we used one-way ANOVA to compare our variables. When a significant effect ($P < 0.05$) was detected, comparisons among multiple means were conducted by Student-Newman-Keuls (SNK) test. Based on the statistical criteria we put forth, we noted a statistically significant decrease in the number of Blue but not UV photoreceptors in Arf II-A2 morphants. During our quantification we noticed that the number of Blue photoreceptors had decreased more dramatically than UV

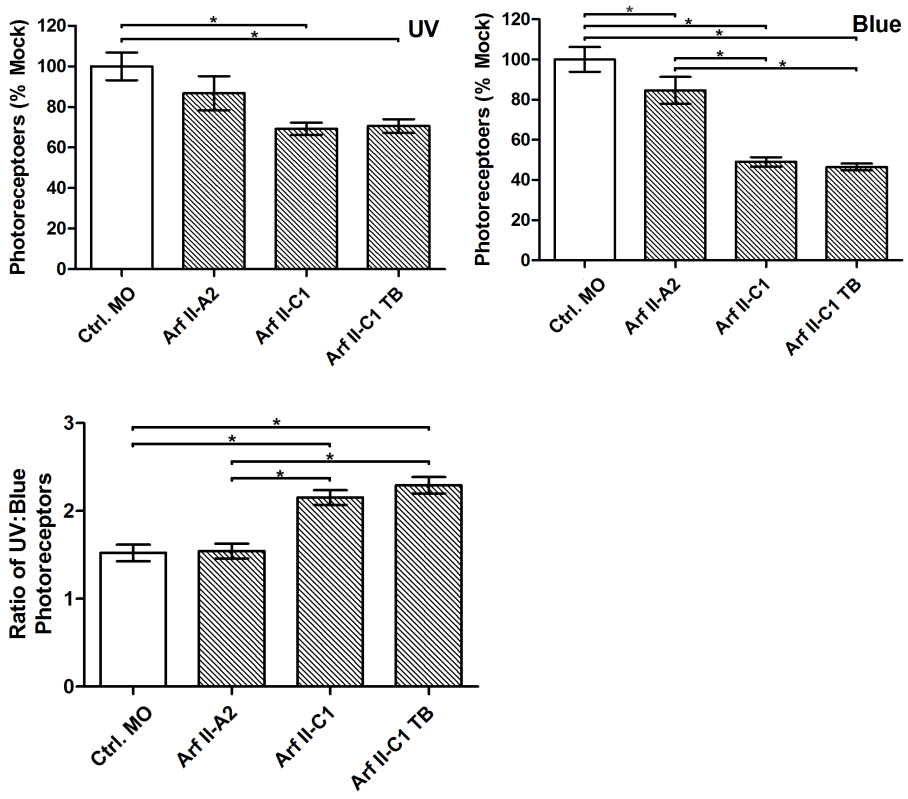

Figure 3.7: Knockdown of Arf II-C1 reduces significantly the number of UV and Blue photoreceptors. Images used for quantification were generated using spinning disc confocal microscopy. Photoreceptor numbers were counted from a minimum of three random 30X30 µm section areas of multiple confocal slices from one image for each 5dpf morphant. The number of UV and Blue photoreceptors measured in Ctrl. MO samples were set at 100%. For each experiment, photoreceptor numbers from other samples were normalized to the Ctrl. MO values. Quantitated images were obtained from two separate experiments for Arf II-A2 morphants and three separate experiments for Arf II-C1 morphants. Results are expressed ± SEM. The average ratio of UV to Blue photoreceptors were quantitated for each experiment shown in panels A and B. Symbol (*) denotes a statistically significant difference ($p < 0.05$) between samples as determined by one-way ANOVA analysis. **A.** The average number of UV and Blue photoreceptor cones decreased in the Arf II-C1 and Arf II-C1 TB morphants compared to the Ctrl. MO morphants. In Arf II-A2 morphants, a statistically significant decrease was seen only in Blue photoreceptors. **B.** The average ratio of UV to Blue photoreceptors in Arf II-C1 and Arf II-C1 TB morphants were statistically higher than the ratios seen in Ctrl. MO and Arf II-A2.

numbers in both Arf II-C1 and Arf II-C1 morphants; therefore, we decided to quantify this observation and report the ratio of UV to Blue photoreceptors in **Figure 3.7B.** As can be seen in the bar graph, there is a statistical increase in the ratio of UV to Blue photoreceptors in both Arf II morphants compared to Control MO morphants. A statistically significant increase in ratio was not seen for Arf II-A2 morphants.

3.6 In situ *hybridization confirms the expression of Arf IIC-1 in larval eyes*

The results presented in the previous two sections suggest that Arf II-C1 plays a critical role in retinal development or physiology. As a first step towards validating this result, we sought to confirm expression of this isoform in 5dpf larvae using DIG-labeled probes complementary to the Arf II-C1 transcript. Though we understand that the retinal morphology of Arf II-C1 morphants may be the result of silencing Arf II-C1 at various organs, we reasoned that expression of Arf II-C1 in the retina would be suggestive of a specific function of this Class II Arf in the retina and therefore photoreceptor organization.

Digoxigenin (DIG)-labeled RNA antisense probes against Arf II-C1 mRNA was generated *in vitro* as described in Chapter 2. Next, we separated zebrafish larvae siblings at 5dpf into two groups. One group was incubated with our DIG-labeled probe and the second group was incubated with no probe and used as control **(Figure 3.8).** At higher

magnification it becomes apparent that Arf II-C1 is expressed in certain regions of the head. Upon closer examination we noted that Arf II-C1 may also be expressed in the eye (arrow). However, due to the transparency of the PTU-treated larvae, we could not explicitly confirm that the reaction was specifically in the eye and not in the head region, directly behind the eye, where the reaction signal was very strong. Eyes were therefore dissected from several stained larvae and imaged separately. Images of dissected eyes at higher magnification proved positive for the nitro blue tetrazolium indicating the specific expression of Arf II-C1 in the eye.

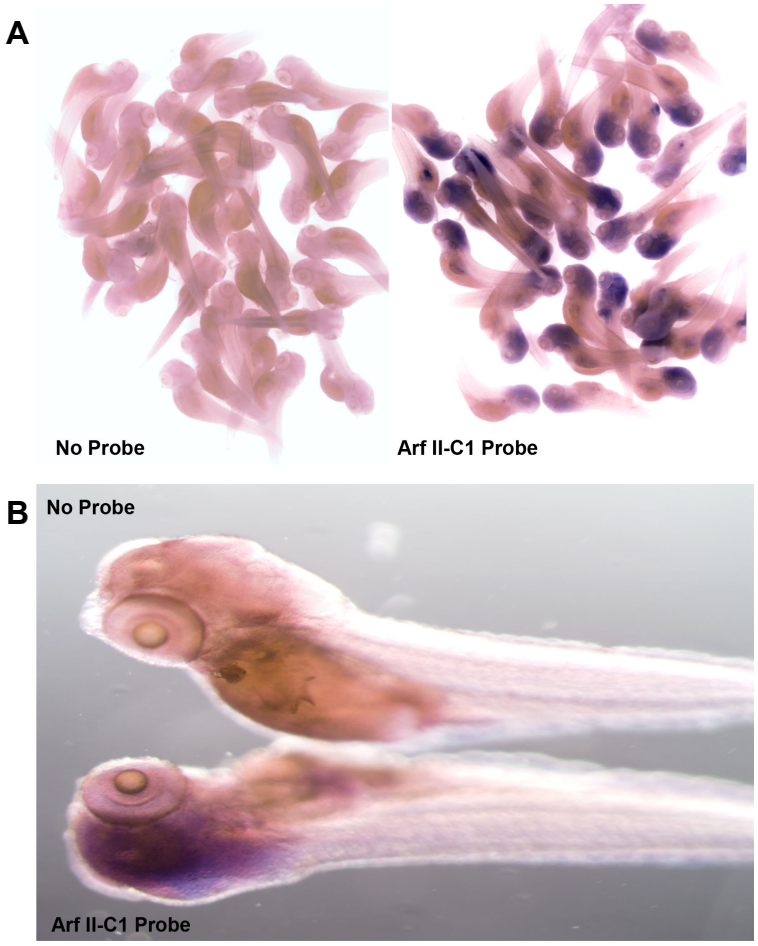

Figure 3.8: *In situ* hybridization confirms the expression of Arf II-C1 in larval retina. A, B. Whole mount *in situ* hybridization using a DIG-labeled antisense riboprobe was performed as described in Materials and Methods. Images from 5dpf larvae incubated with (Arf II-C1 probe) and without (No Probe) are shown at various magnifications.

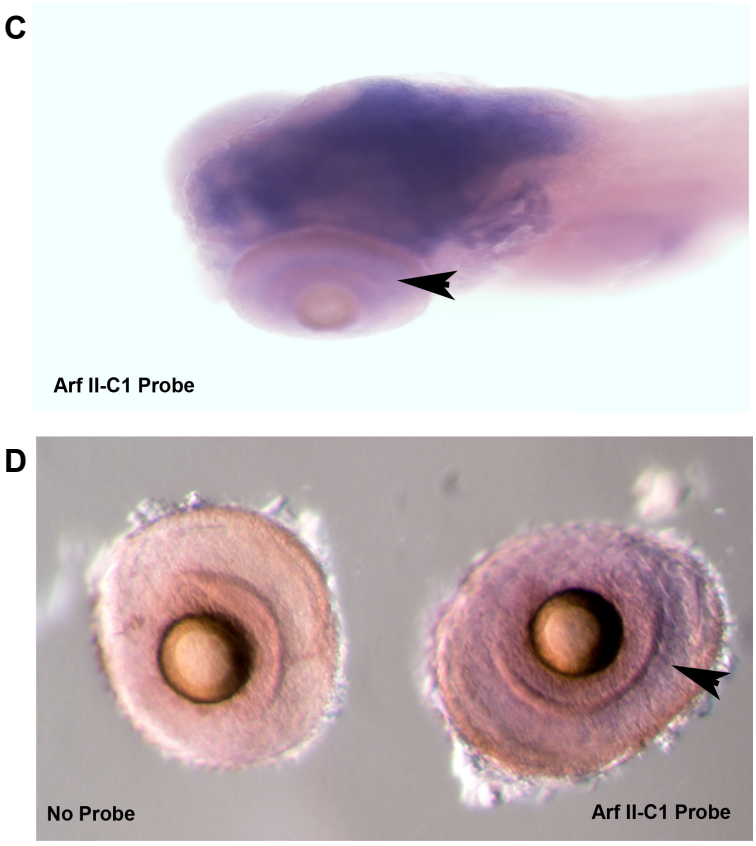

(Figure 3.8, continued) C. Arf II-C1 is expressed at 5dpf in specific regions of the head **D**. Eyes were dissected from morphants incubated with mock and Arf II-C1 DIG-probe and imaged as above. This image confirms the expression of Arf II-C1 in larval retina at 5dpf. Arrowheads point to regions in the eye where Arf II-C1 is expressed.

3.7 The disruption of photoreceptor observed in Arf II-C1 morphants can be rescued the co-injection of MO-resistant mRNA.

In order to confirm the effects seen on UV and Blue cone number and organization was due specifically to Arf II-C1 KD and not some off target event, we chose to rescue Arf II-C1 morphants by co-injection of Arf II-C1 RNA. The use of two separate MO types, that each target Arf II-C1 in an independent fashion, to KD Arf II-C1 in **Results Section 3.4** suggests strong specificity of our MOs for Arf II-C1; this conclusion is based on the fact that the use of both MOs resulted in similar phenotypes of photoreceptor disorganization. However, rescue by injection of MO resistant mRNA provides a powerful complementary test of the specificity of MO-knockdown experiments. As discussed before, TB MOs block protein translation by binding to mRNA at their 5' UTR; in doing so, they hinder the association of the RNA to the cell's translation machinery. The mRNA that was co-injected with the Arf II-C1 MO was insensitive to the Arf II-C1 TB MO because it was prepared to only contain the coding sequence beginning with the start codon and thus devoid of a 5' UTR . In the following experiment, we co-injected embryos at the 1-2 cell stage with a solution containing either Arf II-C1 TB alone or Arf II-C1 TB + Arf II-C1 mRNA; Control MO was used as control. At 5dpf, larval retinas of the various morphants were recovered and imaged as in **Figure 3.9A**. Co-injection of the Arf II-C1 mRNA with the Arf II-C1 TB MO led to an

observable and reproducible partial reversion of UV and Blue photoreceptor organization and number back to control MO conditions. This result provides strong evidence for the specificity of the Arf II-C1 MO. Rescue of zebrafish phenotypes by means of human orthologous mRNAs have become a common practice among researchers (Xhu *et al.* 2011; Kaiser *et al.* 2012). This type of rescue experiment termed Humanized Zebrafish Orthologous Rescue (HuZOR), highlights the high degree of conservation of genes between fish and humans (Tsetskhladze *et al.* 2012). Even though Arf II-C1 and human Arf4 share only 73% sequence identity at the amino acid level, the human orthologue was able to also rescue the phenotype observed in Arf II-C1 morphants to a great extent (**Figure 3.9A).**

We noted earlier that larvae knocked down for Arf II-C1 show a statistically significant increase in their UV to Blue photoreceptor ratios. Therefore, we argued that a reduction in the UV to Blue photoreceptor ratio should indicate successful rescue. Quantification of UV and Blue photoreceptor number as performed in **Results Section 3.4** indicated a ratio of UV to Blue photoreceptor that had decreased away from Arf II-C1 TB towards Control MO conditions. Rescue experiments involving Arf II-C1 TB hArf4 mRNA also shifted the UV to Blue ratio away from Arf II-C1 TB alone (**Figure 3.9B).**

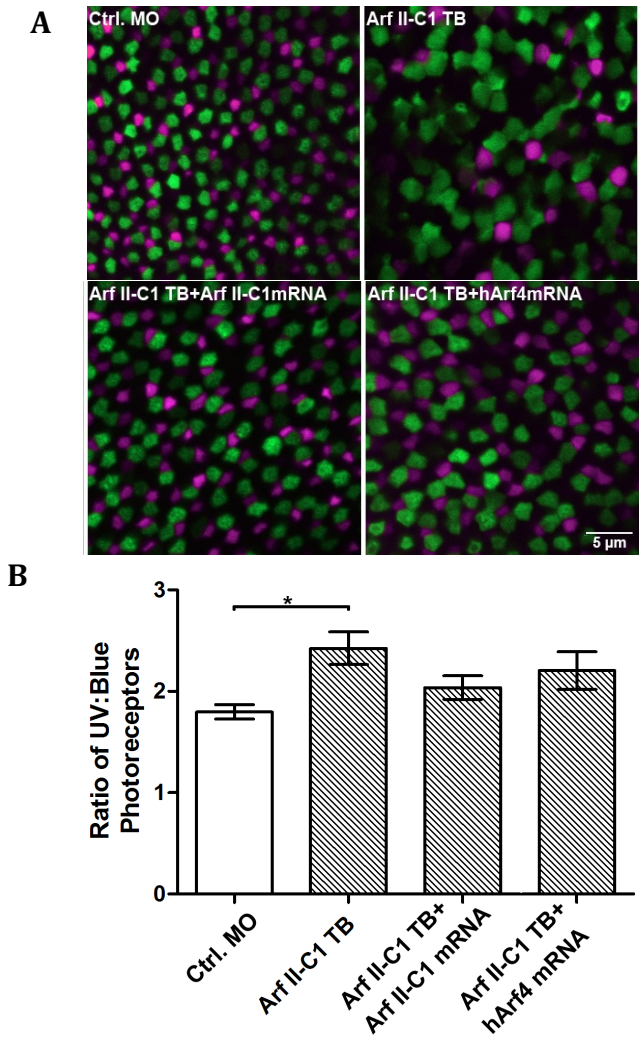

Figure 3.9: The disruption of photoreceptors observed in Arf II-C1 morphants can be rescued by expression of MO-resistant mRNA. A. 1-2 cell-stage embryos were injected with Arf II-C1 TB MO, or with Arf II-C1 TB MO in combination with either Arf II-C1 mRNA or hArf4 mRNA; larval eyes at 5dpf were prepared and imaged as described for Figure 3.6 panel A. The apparent disruption of photoreceptor UV and Blue organization and number were reverted back to normal when embryos were co-injected with Arf II-C1 mRNA and, to a lesser extent, hArf4 mRNA. **B.** The ratio of UV to Blue photoreceptor number from both rescue morphants displayed an increase towards Ctrl. MO conditions compared to Arf II-C1 TB morphants. Images used for quantification were generated using spinning disc confocal microscopy. Quantification was performed as described for **Figure 3.7**.

3.8 H. sapiens, D. melanogaster and C. elegans Class II Arfs localize almost exclusively with ERGIC-53 positive structure; while most, but not all, Class I Arfs co-localize with ERGIC-53 on peripheral puncta.

To better characterize the zebrafish Class II Arfs, in particular the clade C, we chose to first examine their localization pattern within mammalian cells. We base the following experiments on previous findings which show that ~80 % of human (h) Class II, and ~50% of Class I Arfs – positive puncta co-localize with peripheral ERGIC structures (Chun *et al.* 2008). Specifically, we examined whether the expression pattern reported for hClass I and II Arfs was a characteristic shared across multiple species. To answer that question, we determined the localization of *D. melanogaster* (Dm) and *C. elegans* (Ce) Class I and II Arfs in HeLa cells. We chose these organisms, because they express only one undifferentiated isoform of each Arf Class. We argued that the observation of similar cellular localization for Class I and II Arfs of human, worm and fly origin would establish properties that could be used to classify the new zebrafish Arfs.

We began by successfully replicating the experiments performed by Chun *et al.* (2009), by transfecting COS1 cells with hArf1 tagged with GFP (hArf1-GFP) and hArf4 tagged mCherry (hArf4-mCherry). Similar transfection experiments were then performed with DmClass I Arf□GFP and DmClass II mCherry constructs, or, C*e*Class I Arf□GFP and CeClass

II mCherry constructs. Cells were then fixed approximately 16 hours after transfection and stained with an ERGIC-53 antibody that marks peripheral as well as perinuclear ERGIC structures (Blum *et al.,* 2000) **(Figure 3.10A).** Samples were then imaged with a scanning confocal microscope equipped with a 63x objective. Merged images confirmed that 1) all Arfs tested were successfully expressed in COS1 cells; 2) Class I and II Arfs from all three species tested localized to both juxtanuclear regions and peripheral punctate structures as expected of Class I and II Arf localization. Consistent with previous results, for all three species the majority of Class II Arfs –positive puncta colocalized with ERGIC-53. In contrast, not all Class I Arfs-positive puncta colocalized with ERGIC-53. Although the majority of the signal from all Arf isoforms was strongest on Golgi structures, it is important to note that we only focused on peripheral puncta, for the purpose of this study, and not the Golgi structure. Arrowheads indicate structures that are only positive for Class I Arfs; arrows mark structures that are positive for both Class I and Class II Arfs as well as with ERGIC-53.

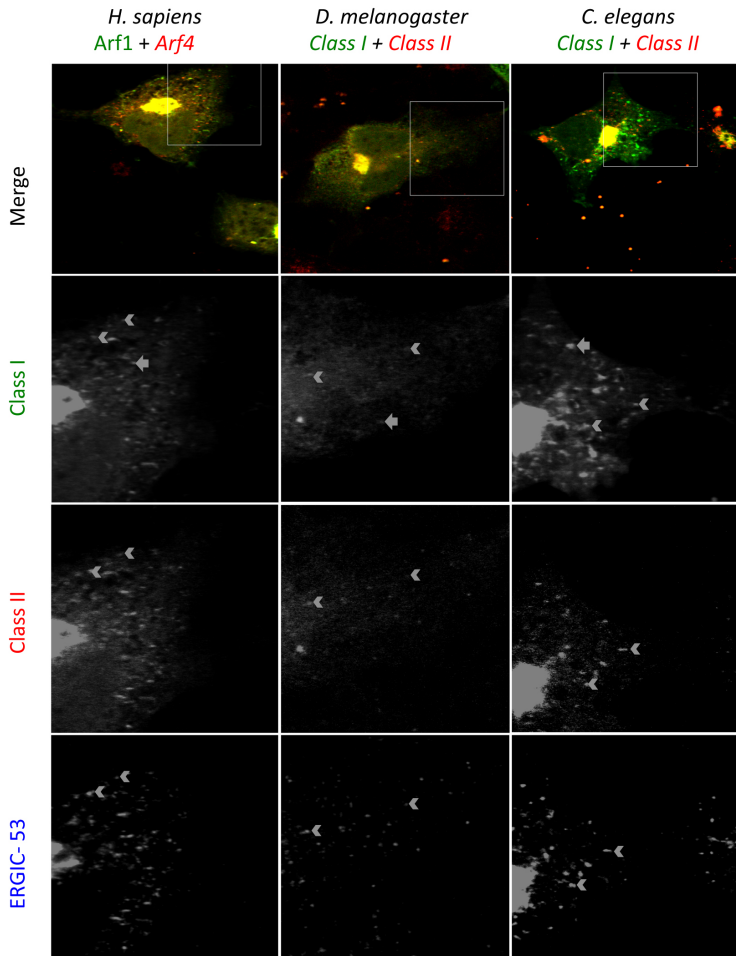

Figure 3.10: Most *H. sapiens, D. melanogaster* and *C. elegans* Class II but not all Class I Arfs on peripheral puncta colocalize with ERGIC-53. COS1 cells were co-transfected with constructs encoding Class I and Class II Arfs from the indicated species. Class I and Class II Arfs were tagged with -GFP and -mCherry, respectively. Transfectants were fixed and stained with anti-ERGIC-53 antibodies as described in Chapter 2. Class II Arfs of all three species tested behave similarly as they all localize primarily to ERGIC-53 positive puncta, while a significant fraction of Class I Arfs do not colocalize with ERGIC-53 structures. Arrowheads indicate puncta that are positive for all three signals; arrows indicate structures that are only positive for the indicated protein. Images are representative of three separate experiments.

3.9 In contrast to other Class II isoforms, Arf II-C1 does not localize to ERGIC structures and becomes cytosolic in the presence of BFA

Once we established the expected localization of Class I and Class II Arf across multiple vertebrate and invertebrate species, we repeated similar experiments using zebrafish Class I and Class II Arfs. As discussed above, zebrafish Class II Arfs group into three distinct clades. We chose one representative member from each clade for further testing. COS1 cells were co-transfected with zebrafish Arf1-GFP and mCherry-tagged forms of either Arf II-A2, Arf II-B1 or Arf II-C1. Cells were fixed, stained and imaged as described in **Results Section 3.7**. Based on the merge images, all four proteins were expressed in COS1 cells and localized to regions known to be occupied by Class I and Class II **(Figure 3.11).** Closer examination of transfected cells revealed that similar to other class I Arfs, Arf1 was found mostly on ERGIC-53 positive structure. The Class II Arf II-A2 and Arf II-B1 localized on ERGIC-53 positive puncta in a fashion similar to human, Dm and Ce Class II Arfs. To our surprise however, Arf II-C1 was completely excluded from ERGIC-53 puncta on all cells examined. The exclusion of Arf II-C1 at ERGIC structures suggests a differential role for Arf II-C1, and perhaps other members of the C clade, in cellular trafficking.

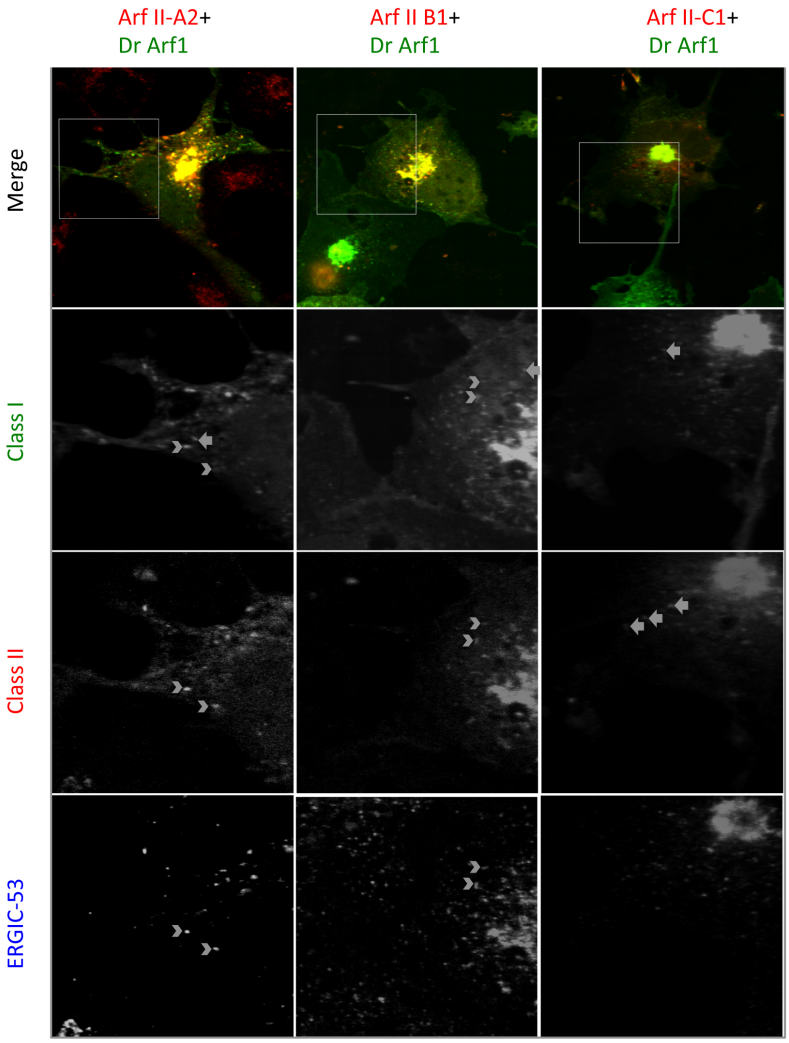

Figure 3.11: In contrast to other zebrafish Class II paralogues, Arf II-C1 does not localize to peripheral ERGIC-53 positive structures. COS1 cells were co-transfected with the indicated constructs encoding *D. rerio* Class II Arfs tagged with mCherry **and** *D.rerio* Arf1 tagged with GFP. Transfectants were then fixed and stained with anti-ERGIC-53 antibody as for Figure 3.10. Arrowheads indicate puncta that are positive for all three signals; arrows indicate structures that are only positive for the indicated protein. Arf II-C1 does not co-localize with peripheral ERGIC-53 positive structures.

3.10 Unlike other Class II Arfs, Arf II-C1 dissociates from punctate structures when cells are treated with BFA

In order to better understand the peculiar behavior of Arf II-C1, we took advantage of the fungal metabolite Brefeldin A (BFA). Our approach is based on previous work from our lab, which established that human Class I and Class II Arfs behave differently when challenged with BFA **(Figure 3.12A)**. As discussed Chapter 1, BFA prevents Arf activation by their Golgi-associated GEFs, and therefore keeps these Arfs in their inactive GDP-bound form. Surprisingly, Dr. Chun observed that BFA causes rapid dissociation of hArf1 from Golgi and ERGIC structures while hArf4 remained associated to peripheral ERGIC membranes (Chun *et al.,* 2008).

We know that in the presence of BFA hArf1 quickly dissociates from punctate structures, while hArf4 remains bound. We tested to see how Arf II-C1 would behave in the presence of BFA. We began our experimentation by first repeating Dr. Chun's experiments **(Figure 3.12A)**. BFA treatment of cells expressing hArf1-GFP and hArf4-mCherry led to rapid dissociation of both Classes of Arfs from juxtanuclear Golgi structures; however, hArf4 but not Arf1 remained on peripheral ERGIC structures. To characterize the behavior or Arf4 II-C1 in BFA treated cells with respect to the behavior of human Arf1 and Arf4, we transfected COS1 cells with plasmids encoding Arf II-C1-GFP and hArf4-mCherry. We noted that after the addition of BFA, both hArf4 and Arf II-C1 dissociated from

juxtanuclear Golgi structures; however, the hArf4-mCherry signal remained on ERGIC structures as expected, whereas the Arf4 II-C1-GFP signal did not **(Figure 3.12B).**

In summary, our cell-culture experimentation showed that unlike all other Class II Arfs tested across multiple species, Arf II-C1 does not localize to ERGIC-53 positive structures; furthermore, unlike hArf4, Arf II-C1 dissociates from punctate structures and becomes cytosolic when challenged with BFA.

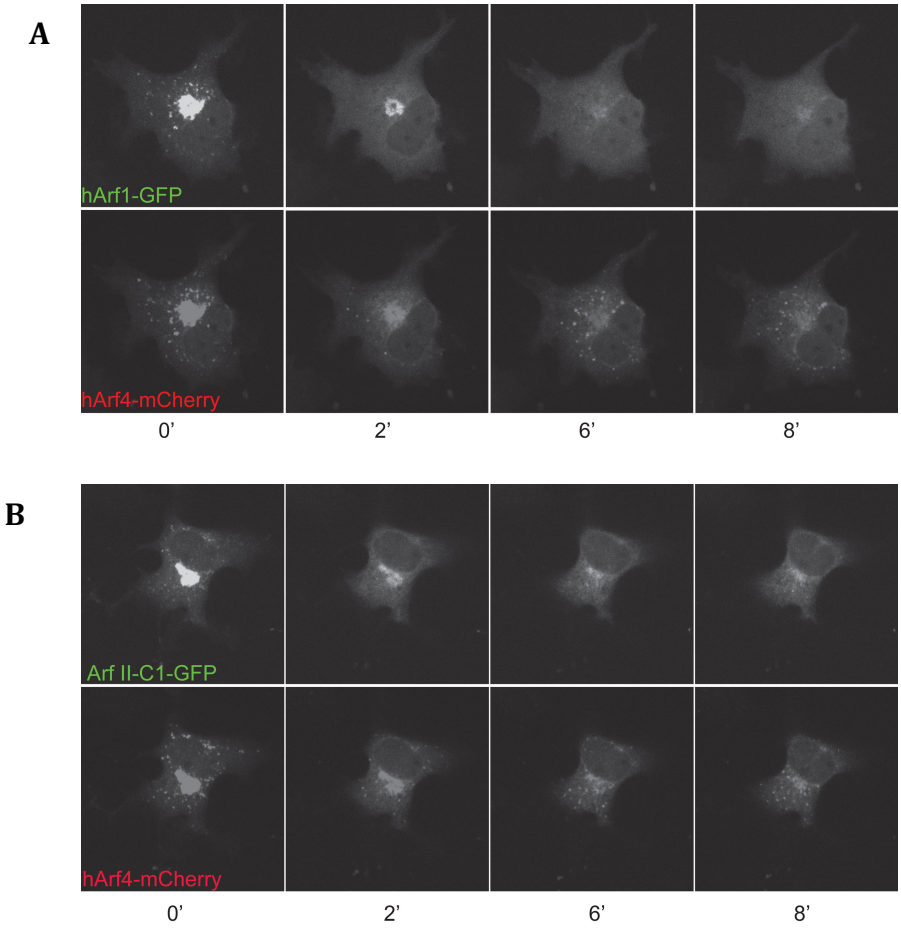

Figure 3.12: Human Class II Arf but not Arf II-C1, remains associated with peripheral puncta after BFA treatment. A. COS1 cells co-transfected with plasmids encoding human Arf1-GFP and Arf4-mCherry were imaged continuously for 1 min before drug addition and an additional 7 min after BFA addition (10 μg/ml). Panels show single channel images at the indicated times. After the addition of BFA, both hArf1 and hArf4 dissociate from the Golgi; however, Arf4 signal remains on punctate structures. **B.** COS1 cells were transfected with Arf II-C1-GFP and human Arf4-mCherry, treated and images as described in panel A. Unlike the human Class II Arf, Arf II-C1 dissociates from puncta structures.

CHAPTER 4: DISCUSSION

4.1 Summary of results

In this study we identified a previously unknown set of Class II Arf isoforms in zebrafish. Using MO-directed KD, we tested the role of each zebrafish Class II Arf paralogue on early development and photoreceptor organization. We defined specific sub-lethal MO doses that allowed at least 50% of morphants to survive up to 5dpf. We noted that KD of Arf II-A2 but not any of the other paralogues caused gross morphological defects in larvae; while, photoreceptor disorganization was only seen in Arf II-C1 morphants. The use of two sets of anti-sense MO oligos to target different regions of the Arf II-C1 transcript showed specificity of our MOs as they both resulted in similar phenotypes. Further confirmation of our MO specificity came from the use of synthetic RNA to rescue the effect of Arf II-C1 KD on photoreceptor organization. *In situ* hybridization experiments showed Arf II-C1 to be expressed in specific regions of the brain as well as the eye. In this study we established that except for Arf II-C1, all Class II and most Class I Arfs, we examined, from multiple species including *H. sapiens, D. melanogaster and C. elegans* localize to ERGIC-53 positive puncta. Furthermore, unlike hArf4, when COS1 cells expressing Arf II-C1 were treated with BFA, Arf II-C1 quickly became cytosolic and dissociated from punctate structures, whereas, hArf4 remained associated with punctate structures.

4.2 Classification of zebrafish Class II Arfs

In order to target Class II Arfs in zebrafish, we first had to identify these orthologues in the zebrafish genome. Our sequence alignment and bioinformatics analysis led to the identification of seven zebrafish Class II Arf paralogues. This finding was rather surprising because humans and most other model vertebrates such as *Xenopus laevis, Gallus gallus* or *Mus musculus* express only one to two Class II Arfs. What accounts for the presence of multiple orthologues in zebrafish is a whole genome duplication, which occurred in the ray-finned fish lineage approximately 230-400 million years ago (Karanth *et al.,* 2009). Gene duplication may account for the two Class II Arfs found on chromosome 18 which includes the A clade. In addition to gene duplication, the presence of five Class II paralogues on chromosome 11 may be due to a separate chromosomal duplication event on the region that houses the B and C clades.

Although a few of the zebrafish Class II paralogues share similar sequence identity with both Class I and Class II Arfs, Alex Schlacht's bioinformatics analyses concluded that the seven identified Arfs are not Class I and are indeed members of Class II Arfs; however, Alex's analyses were not able to place the zebrafish Class II Arfs into either Arf4 or Arf5 sub-classes. Furthermore, Alex's bioinformatics results grouped the seven zebrafish Class II Arfs into three distinct clades and showed that members of two of these clades are also found in other species of fish.

Looking specifically at Class I and III zebrafish Arfs isoforms in **Table 3.1**, we see that with the exception of Arf2, which shares 96% sequence identity with both hArf1 and mArf2, other Class I and III zebrafish isoforms are 98-99% identical to their human orthologues. On the other hand, the sequence identity of zebrafish Class II Arfs with their human counterparts range from 94% to as low as 69%. The large variance in the sequence identity may be lead back to the whole genome duplication event described above. After a duplication event, usually one gene copy becomes mutationally silenced and disappears over time and therefore leads to non-functionalization. In some cases however, a sub-functionalization of the duplicated gene occurs; this is a neutral process where the two copies partition the ancestral function. In yet another scenario, both duplicated copies may be preserved if beneficial mutations occur in one or both copies that allow the evolution of new functions, a process known as neo-functionalization (Karanth *et al.,* 2009; Rastogi and Liberles, 2005). Based on my project, it is not possible to decipher which evolutionary path the seven Class II Arfs took after the zebrafish gene duplication event; however, we do know that they are still present in the zebrafish genome. Therefore, a non-functionalization event can be disregarded. Also, we do not have evidence establishing whether all seven genes are actually expressed.

4.3 MO-KD of Class II Arfs

Once we identified Class II Arf paralogues our next task was to knock them down using antisense MO oligos in order to study their role in early zebrafish ontogeny. As described above, SB MOs can be used to silence zygotically expressed transcripts; TB MOs, on the other hand, can be used to KD both zygotically and maternally expressed transcripts. The advantage of the use of SB MO over TB MO comes from the fact that RT-PCR reactions can be used to detect the efficacy of SB MO. In contrast, the efficacy of TB MOs can only be detected through western blots with the use of specific antibodies against the translated protein. Due to the lack of commercially available antibodies against the seven Class II zebrafish Arfs, we chose to use SB MOs for our KD experiments. Once sub-lethal doses of each MO oligo against each class II Arfs were determined experimentally, we injected SB MOs into embryos at the 1-2 cell stage and followed their development up to 5dpf. The reason for examining our morphants at the 5dpf mark was twofold. MOs are generally only effective for 3-5 days post injection before becoming diluted and ineffective in the growing larvae (Renninger *et al.,* 2010). More importantly, by 5dpf zebrafish photoreceptors will have differentiated into their spectral subtypes (Raymond *et al.,* 1995). We found that knocking down Arf II-A2, but not any other Class II Arf, resulted in gross morphological defects of the larvae at 5dpf. Compared to the control, greater than 65% of Arf II-A2 morphants displayed bends in their bodies.

As discussed in **Chapter 1**, previous research has shown Class II Arfs to have a role in the initial steps of opsin trafficking out of the TGN. Since mis-localization of opsin proteins is associated with photoreceptor cell death, (Deretic *et al.,* 2005; Nakao *et al.,* 2012), then the absence or decrease of photoreceptors in Class II Arf morphant retinas could be indicative of a role for Class II Arfs in opsin trafficking. Therefore, we used a transgenic line of fish, which expressed GFP and mCherry reporter proteins throughout their UV and Blue photoreceptors, respectively. The use of this transgenic line allowed for quick monitoring of retinal defects associated with Class II Arf KD. At 5dpf, retinas from each morphant type were prepared for microscopy and imaged at various magnifications. We noted that knocking down Arf II-C1 with both SB and TB MOs led to similar disorganization and reduction of UV and Blue photoreceptors. An observable reduction in photoreceptor number and organization was not seen with the KD of any other Class II Arf paralogue or the Control.

We quantified the observable reduction in UV and Blue photoreceptor numbers associated with Arf II-C1 KD. Quantification revealed a statistically significance decrease in both UV and Blue photoreceptor numbers relative to the Control. Furthermore, we noted that Blue photoreceptor numbers were reduced more dramatically relative to UV photoreceptors. This is because the ratio of UV to Blue photoreceptors had increased significantly in the Arf II-C1 morphants relative to the Control.

Zebrafish possess four spectral subtypes of cone photoreceptors; however, due to the nature of the transgenic line of fish available to this study, we focused only on UV and Blue cones. It is possible that the organization and number of the Red/Green double cones may have also been affected in Arf II-C1 morphants. In this study we did not look at the Red/Green double cones due to a lack of antibodies against these photoreceptors that were available to us.

The studies conducted by Deretic *et al.* (2005), focused on the trafficking relationship between the night vision specific rod opsin and Arf4. We successfully labeled rod opsin proteins in zebrafish using the antibody Zpr-3 (Vihtelic *et al.,* 1998; Jurisch-Yaksi *et al.,* 2013); however, in our hands, knocking down Arf II-C1 did not cause an observable staining pattern that was different from the Control morphants at 5dpf.

With the exception of Arf II-A2 and Arf II-C1, KD experiments involving any of the other Class II Arfs did not lead to any observable defects of larvae at, and up to, 5dpf. It may be that the MOs designed against these paralogues were not effective, as we could not confirm the efficacy of our SB MOs using RT-PCR, or it could be due to redundancy of Arf function (Volpicelli-Daley *et al.,* 2005). Based on RNA interference studies in HeLa Cells, no single Arf isoform is required for proper Golgi morphology; instead, Arfs function in pairs at specific steps of cellular trafficking. For example, singly knocking down hArf4 or hArf5, has no effects on Golgi trafficking; however, knocking down hArf4 and hArf5

together blocks retrograde trafficking from the *cis*-Golgi to ERGIC structures, suggesting a redundant role of Class II Arfs at these steps. In the same study, the authors showed that Class I and Class II Arfs also play redundant roles, as knocking down hArf1 and hArf4 together, but not singly, led to a disruption in Golgi morphology (Volpicelli-Daley *et al.,* 2005). Therefore, any feasible understanding of the role of Class II Arfs in early zebrafish ontogeny may be better achieved with double MO KD experiments. Zebrafish, however, express a total of 14 Arf isoforms, making a comprehensive double KD experiments in this organism impractical. However, more limited studies involving only the two Arf1s, or the two Arf3s may be more practical and could prove to be very informative.

4.4 Arf II-C1 RNA can rescue photoreceptor disorganization.

In situ hybridization experiments confirmed expression of Arf II-C1 in larval eyes, a result that is suggestive of a direct role of Arf II-C1 in retinal development and physiology. In order to show that the photoreceptor disorganization was specifically due to the KD of Arf II-C1 and not some off-target effect, we performed RNA rescue experiments. Co-injection of Arf II-C1 RNA with Arf II-C1 TB MO led to a noticeable reversion of the disorganization of UV and Blue photoreceptor organization and number seen with the injection of Arf II-C1 TB MO alone.

Co-injection of hArf4 RNA with Arf II-C1 TB MO also greatly reverted the effects seen with Arf II-C1 TB MO alone. Our rescue experiments were performed using synthetic RNAs encoding only the coding sequence of the mature RNAs. Although the reversion of photoreceptor organization and number is highly suggestive of the successful expression of our synthetically prepared RNAs, we could not explicitly confirm their expression. A powerful approach would have been the use of RNAs encoding our proteins of interest linked to the RNA of a reporter protein such as GFP. In this way the expression of our synthetically prepared RNAs could be monitored with the expression of GFP proteins by fluorescence microscopy. Although tagged versions of Arf proteins have been used extensively in our field with much success, rescue experiments using GFP-tagged versions of Arf, would assure that having the relatively large GFP protein, tagged to the smaller Arf, does not interfere with the normal functioning of Arf proteins.

At the amino acid level, Arf II-C1 shares 73% and 74% sequence identity to hArf4 and hArf1, respectively (**Refer to Table 3.1**). We argued that if we could partially rescue the retinal phenotypes associated with Arf II-C1 KD using hArf4 RNA, partial rescue should also be achieved using hArf1 RNA. To our surprise, not only did the co-injection of hArf1 with Arf II-C1 TB MO not rescue Arf II-C1 morphants, but it also caused total ablation of UV and Blue photoreceptors (data not shown). Based on our experimental conditions, it cannot be determined whether UV and Blue

photoreceptor ablation was caused specifically by hArf1 expression, or whether hArf1 expression in combination with Arf II-C1 KD led to these results. Also, we did not examine for the presence of other photoreceptor sub-types in this experiment, nor did we examine the correct layering retinal layering. Future experiments using hArf1 injection alone can shed more light on this observation. The results of this experiment hint at the possibility that even though Arf II-C1 shares approximately the same amino acid sequence identity with both hArf4 and hArf1, there may be a specific domain or peptide shared between hArf4 and Arf II-C1 and absent on hArf1, that is essential for UV and Blue organization and number.

4.5 Unlike other Class II Arfs across multiple species, Arf II-C1 does not colocalize with ERGIC-53 positive structures and becomes cytosolic in the presence of BFA

In this project we established that in in COS1 cells, Class II Arfs across multiple species including human*, Dm and Ce* localize exclusively on ERGIC-53 positive structures. We also established that the majority, but not all, Class I Arfs across the aforementioned species also localize to ERGIC-53 positive puncta in the same cell line. Based on these results, we examined the localization pattern of our seven zebrafish Class II Arfs. As discussed in **Chapter 3**, the seven zebrafish Class II Arfs, group into three distinct clades **(Refer to Figure 3.2).** We chose a representative

member from each clade and expressed them in COS1 cells. We noted that Arf II-A2 and Arf II-B1 members of the A and B clade, respectively, had similar intracellular localization pattern to other tested Class II Arfs, as they localized exclusively with ERGIC-53 structures. In contrast to Arf II-A2 and Arf II-B1 localization patterns, Arf II-C1 did not localize with ERGIC-53 positive puncta and was totally excluded from these structures. To further study the peculiar behavior of Arf II-C1, we took advantage of a BFA test that had been used by previously in our lab. In this test, Chun *et al.* (2005), had noticed that when cells co-expressing hArf1 and hArf4 were treated with BFA, hArf1 quickly dissociated with ERGIC structures, whereas hArf4 remained on ERGIC structures long (>10 min) after BFA addition.

We had already established that Arf II-C1 does not localize with ERGIC-53 positive structures in our immunocytochemical experiments. However, we asked whether Arf II-C1, like the human Class II Arf, hArf4 would remain puncta-bound when cells expressing Arf II-C1 were challenged with BFA. We noted that unlike hArf4, and similar to hArf1, Arf II-C1 quickly dissociated from punctate structures and become cytosolic.

4.6 Future research

As alluded to above, future experiments should be performed to address the effects caused by the injection of hArf1 on UV and Blue photoreceptor ablation. Based on our findings, human and zebrafish Arf1

orthologues are nearly identical (Refer to Table 3.1); therefore, the reason for such dramatic effects on UV and Blue photoreceptor numbers is not immediately obvious. It could be that overexpression of Arf1 in general is lethal to photoreceptors. In this case, overexpression in fish embryos of Arf1 from any species, even *D. rerio*, would lead to the same result.

Since our rescue experiments were repeated 3 separate times, on three different days using embryos from different parents and injected with freshly prepared RNA/MO cocktails, experimental error may be ruled out as the cause of this result. It would be interesting to see whether zebrafish Arf1 paralogues cause the same effect on UV and Blue cone numbers when they are overexpressed in the embryos.

The MO-directed KD of Arf II-A2 caused clear morphological defects in the developing embryos. Although we did not see effects of Arf II-A2 KD on the ratio of UV:Blue photoreceptor numbers; it would be interesting to see whether Arf II-A2 KD has effects on other organs of the body separate from eye. It is clear that Arf II-A2 plays some important role in early skeletal development; therefore, it may be of interest for researchers following bone development to look into the function of Arf II-A2 more closely.

Future research should also examine the role of the B clade to see why they are specifically expressed in zebrafish and not any of the other bony fish whose genomes we analyzed. In our hands, KD of Arf II-B1 and Arf II-B2 using SB or TB (not shown) MOs had no effect on zebrafish

morphology or photoreceptor number/organization. This observation cannot result from functional redundancy of the B clade Arfs since the single MO targets expression of both of the nearly identical Arf II-B1 and Arf II-B2. It may be that members of the B clade have a role in later stages of the zebrafish development.

Our *in situ* hybridization confirmed the expression of Arf II-C1 in the larval retina at 5dpf. Based on our results we know that Arf II-C1 plays a role in photoreceptor development; what we do not know however, is the exact role of Arf II-C1 in photoreceptor development. Histo-immunochemical studies should shed some light on the exact localization of this protein within the photoreceptor cell or other regions of the retina once antibodies against Arf II-C1 become available.

Further cyto-immunochemical experiments should also shed light on the identity of the punctate organelles that Arf II-C1 colocalizes with in COS1 cells. It would be interesting to see whether Arf II-C1 has the same localization pattern in cell cultures derived from zebrafish; it would also be interesting to test the behavior of Arf II-C1 in zebrafish cells when treated with BFA. It may be possible that the differential behavior seen with Arf II-C1 in BFA treated COS1 cells could be purely because of the cell line that it is expressed in.

It is important to note that for my ERGIC-53 colocalization experiments, I focused only on peripheral puncta. From my observation of peripheral puncta, I concluded that Arf II-C1 did not colocalize with

structures that were positive for the ERGIC-53 signal. Looking at Figure 3.11, it becomes clear that Arf II-C1 localizes greatly to Golgi structures; it is not clear however, which compartments of the Golgi, Arf II-C1 localizes to. p115 and TGN 46 antibodies, which stain the *cis*- and the *trans*-Golgi, respectively, can be used to examine the relative localization of Arf II-C1 within sub-compartments of the Golgi.

BIBLIOGRAPHY

Achstetter T, Franzusoff A, Field C, Schekman R. SEC7 encodes an unusual, high molecular weight protein required for membrane traffic from the yeast Golgi apparatus. J Biol Chem. 1988 Aug 25;263(24):11711-7. PubMed PMID: 3042778.

Alama A, Tasso B, Novelli F, Sparatore F. Organometallic compounds in oncology: implications of novel organotins as antitumor agents. Drug Discov Today. 2009 May;14(9-10):500-8. doi: 10.1016/j.drudis.2009.02.002. Epub 2009 Feb 11. Review. PubMed PMID: 19429510.

Allison WT, Barthel LK, Skebo KM, Takechi M, Kawamura S, Raymond PA.Ontogeny of cone photoreceptor mosaics in zebrafish. J Comp Neurol. 2010 Oct 15;518(20):4182-95. doi: 10.1002/cne.22447. PubMed PMID: 20878782; PubMed Central PMCID: PMC3376642.

Allison WT, Haimberger TJ, Hawryshyn CW, Temple SE. Visual pigment composition in zebrafish: Evidence for a rhodopsin-porphyropsin interchange system. Vis Neurosci. 2004 Nov-Dec;21(6):945-52. Erratum in: Vis Neurosci. 2005 Mar-Apr;22(2):249. PubMed PMID: 15733349.

Antonny B, Madden D, Hamamoto S, Orci L, Schekman R. Dynamics of the COPII coat with GTP and stable analogues. Nat Cell Biol. 2001 Jun;3(6):531-7. PubMed PMID: 11389436.

Antonny B, Beraud-Dufour S, Chardin P, Chabre M. N-terminal hydrophobic residues of the G-protein ADP-ribosylation factor-1 insert into membrane phospholipids upon GDP to GTP exchange. Biochemistry. 1997 Apr 15;36(15):4675-84. PubMed PMID: 9109679.

Appenzeller C, Andersson H, Kappeler F, Hauri HP. The lectin ERGIC-53 is a cargo transport receptor for glycoproteins. Nat Cell Biol. 1999 Oct;1(6):330-4. PubMed PMID: 10559958.

Appenzeller-Herzog C, Hauri HP. The ER-Golgi intermediate compartment (ERGIC): in search of its identity and function. J Cell Sci. 2006 Jun 1;119(Pt 11):2173-83. Review. PubMed PMID: 16723730.

Bachmann-Gagescu R, Phelps IG, Stearns G, Link BA, Brockerhoff SE, Moens CB, Doherty D. The ciliopathy gene cc2d2a controls zebrafish photoreceptor outer segment development through a role in Rab8-dependent vesicle trafficking. Hum Mol Genet. 2011 Oct 15;20(20):4041-55. doi: 10.1093/hmg/ddr332. Epub 2011 Aug 4. PubMed PMID: 21816947; PubMed Central PMCID: PMC3177654.

Badano JL, Mitsuma N, Beales PL, Katsanis N. The ciliopathies: an emerging class of human genetic disorders. Annu Rev Genomics Hum Genet. 2006;7:125-48. Review. PubMed PMID: 16722803.

Bannykh SI, Nishimura N, Balch WE. Getting into the Golgi. Trends Cell Biol. 1998 Jan;8(1):21-5. Review. PubMed PMID: 9695803.

Barlowe C, Orci L, Yeung T, Hosobuchi M, Hamamoto S, Salama N, Rexach MF, Ravazzola M, Amherdt M, Schekman R. COPII: a membrane coat formed by Sec proteins that drive vesicle budding from the endoplasmic reticulum. Cell. 1994 Jun 17;77(6):895-907. PubMed PMID: 8004676.

Barlowe C, Schekman R. Expression, purification, and assay of Sec12p: a Sar1p-specific GDP dissociation stimulator. Methods Enzymol. 1995;257:98-106. PubMed PMID: 8583945.

Barthel LK, Raymond PA. Improved method for obtaining 3-microns cryosections for immunocytochemistry. J Histochem Cytochem. 1990 Sep;38(9):1383-8. PubMed PMID: 2201738.

Ben-Tekaya H, Miura K, Pepperkok R, Hauri HP. Live imaging of bidirectional traffic from the ERGIC. J Cell Sci. 2005 Jan 15;118(Pt 2):357-67. Epub 2005 Jan 4. PubMed PMID: 15632110.

Bi X, Corpina RA, Goldberg J. Structure of the Sec23/24-Sar1 pre-budding complex of the COPII vesicle coat. Nature. 2002 Sep 19;419(6904):271-7. PubMed PMID: 12239560.

Bill BR, Petzold AM, Clark KJ, Schimmenti LA, Ekker SC. A primer for morpholino use in zebrafish. Zebrafish. 2009 Mar;6(1):69-77. doi: 10.1089/zeb.2008.0555. Review. PubMed PMID: 19374550; PubMed Central PMCID: PMC2776066.

Blum R, Stephens DJ, Schulz I. Lumenal targeted GFP, used as a marker of soluble cargo, visualises rapid ERGIC to Golgi traffic by a tubulo-vesicular network. J Cell Sci. 2000 Sep;113 (Pt 18):3151-9. PubMed PMID: 10954414.

Bohnsack BL, Gallina D, Kahana A. Phenothiourea sensitizes zebrafish cranial neural crest and extraocular muscle development to changes in retinoic acid and IGF signaling. PLoS One. 2011;6(8):e22991. doi: 10.1371/journal.pone.0022991. Epub 2011 Aug 19. PubMed PMID: 21886774; PubMed Central PMCID: PMC3158757.

Bonfanti L, Mironov AA Jr, Martínez-Menárguez JA, Martella O, Fusella A, Baldassarre M, Buccione R, Geuze HJ, Mironov AA, Luini A. Procollagen traverses the Golgi stack without leaving the lumen of cisternae: evidence for cisternal maturation. Cell. 1998 Dec 23;95(7):993-1003. PubMed PMID: 9875853.

Bonifacino JS, Glick BS. The mechanisms of vesicle budding and fusion. Cell. 2004 Jan 23;116(2):153-66. Review. PubMed PMID: 14744428.

Bonifacino JS, Lippincott-Schwartz J. Coat proteins: shaping membrane transport. Nat Rev Mol Cell Biol. 2003 May;4(5):409-14. Review. PubMed PMID: 12728274.

Branchek T, Bremiller R. The development of photoreceptors in the zebrafish, Brachydanio rerio. I. Structure. J Comp Neurol. 1984 Mar 20;224(1):107-15. PubMed PMID: 6715574.

Casanova JE. Regulation of Arf activation: the Sec7 family of guanine nucleotide exchange factors. Traffic. 2007 Nov;8(11):1476-85. Epub 2007 Sep 10. Review. PubMed PMID: 17850229.

Chen J, Huang C, Truong L, La Du J, Tilton SC, Waters KM, Lin K, Tanguay RL, Dong Q. Early life stage trimethyltin exposure induces ADP-ribosylation factor expression and perturbs the vascular system in zebrafish. Toxicology. 2012 Dec 16;302(2-3):129-39. doi: 10.1016/j.tox.2012.09.004. Epub 2012 Sep 21. PubMed PMID: 23000284; PubMed Central PMCID: PMC3511642.

Chun J, Shapovalova Z, Dejgaard SY, Presley JF, Melançon P. Characterization of class I and II ADP-ribosylation factors (Arfs) in live cells: GDP-bound class II Arfs associate with the ER-Golgi intermediate compartment independently of GBF1. Mol Biol Cell. 2008 Aug;19(8):3488-500. doi: 10.1091/mbc.E08-04-0373. Epub 2008 Jun 4. PubMed PMID: 18524849; PubMed Central PMCID: PMC2488303.

Claude A, Zhao BP, Kuziemsky CE, Dahan S, Berger SJ, Yan JP, Armold AD, Sullivan EM, Melançon P. GBF1: A novel Golgi-associated BFA-resistant guanine nucleotide exchange factor that displays specificity for ADP-ribosylation factor 5. J Cell Biol. 1999 Jul 12;146(1):71-84. PubMed PMID: 10402461; PubMed Central PMCID: PMC2199737.

Cohen LA, Honda A, Varnai P, Brown FD, Balla T, Donaldson JG. Active Arf6 recruits ARNO/cytohesin GEFs to the PM by binding their PH domains. Mol Biol Cell. 2007 Jun;18(6):2244-53. Epub 2007 Apr 4. PubMed PMID: 17409355; PubMed Central PMCID: PMC1877112.

Cool RH, Schmidt G, Lenzen CU, Prinz H, Vogt D, Wittinghofer A. The Ras mutant D119N is both dominant negative and activated. Mol Cell Biol. 1999 Sep;19(9):6297-305. PubMed PMID: 10454576; PubMed Central PMCID: PMC84598.

Cukierman E, Huber I, Rotman M, Cassel D. The ARF1 GTPase-activating protein: zinc finger motif and Golgi complex localization. Science. 1995 Dec 22;270(5244):1999-2002. PubMed PMID: 8533093.

D'Souza-Schorey C, Li G, Colombo MI, Stahl PD. A regulatory role for ARF6 in receptor-mediated endocytosis. Science. 1995 Feb 24;267(5201):1175-8. PubMed PMID: 7855600.

D'Souza-Schorey C, Chavrier P. ARF proteins: roles in membrane traffic and beyond. Nat Rev Mol Cell Biol. 2006 May;7(5):347-58. Review. PubMed PMID: 16633337.

Dacks, J. B. and Field, M. C. (2004). Eukaryotic cell evolution from a genomic perspective: the endomembrane system. In Organelles, Genomes and Eukaryote Phylogeny: An Evolutionary Synthesis in the Age of Genomics (ed. R. P. Hirt and D. S. Horner), pp. 309-334. London: CRC Press.

Dancourt J, Barlowe C. Protein sorting receptors in the early secretory pathway. Annu Rev Biochem. 2010;79:777-802. doi: 10.1146/annurev-biochem-061608-091319. Review. PubMed PMID: 20533886.

Darriba, D., Taboada, G. L., Doallo, R., and Posada, D. 2012. jModelTest 2: more models, new heuristics and parallel computing. *Nature Methods* 9:772.

De Matteis MA, Godi A. Protein-lipid interactions in membrane trafficking at the Golgi complex. Biochim Biophys Acta. 2004 Nov 3;1666(1-2):264-74. Review. PubMed PMID: 15519320.

Deretic D, Williams AH, Ransom N, Morel V, Hargrave PA, Arendt A. Rhodopsin C terminus, the site of mutations causing retinal disease, regulates trafficking by binding to ADP-ribosylation factor 4 (ARF4). Proc Natl Acad Sci U S A. 2005 Mar 1;102(9):3301-6. Epub 2005 Feb 22. PubMed PMID: 15728366; PubMed Central PMCID: PMC552909.

Ding M, Vitale N, Tsai SC, Adamik R, Moss J, Vaughan M. Characterization of a GTPase-activating protein that stimulates GTP hydrolysis by both ADP-ribosylation factor (ARF) and ARF-like proteins. Comparison to the ARD1 gap domain. J Biol Chem. 1996 Sep 27;271(39):24005-9. PubMed PMID: 8798635.

Donaldson JG, Jackson CL. Regulators and effectors of the ARF GTPases. Curr Opin Cell Biol. 2000 Aug;12(4):475-82. Review. PubMed PMID: 10873831.

Donaldson JG, Jackson CL. ARF family G proteins and their regulators: roles in membrane transport, development and disease. Nat Rev Mol Cell Biol. 2011 Jun;12(6):362-75. doi: 10.1038/nrm3117. Epub 2011 May 18. Review. Erratum in: Nat Rev Mol Cell Biol. 2011;12(8):533. PubMed PMID: 21587297; PubMed Central PMCID: PMC3245550.

Donaldson JG. Multiple roles for Arf6: sorting, structuring, and signaling at the plasma membrane. J Biol Chem. 2003 Oct 24;278(43):41573-6. Epub 2003 Aug 11. Review. PubMed PMID: 12912991.

Duden R. ER-to-Golgi transport: COP I and COP II function (Review). Mol Membr Biol. 2003 Jul-Sep;20(3):197-207. Review. PubMed PMID: 12893528.

Duijsings D, Lanke KH, van Dooren SH, van Dommelen MM, Wetzels R, de Mattia F, Wessels E, van Kuppeveld FJ. Differential membrane association properties and regulation of class I and class II Arfs. Traffic. 2009 Mar;10(3):316-23. doi: 10.1111/j.1600-0854.2008.00868.x. Epub 2008 Jan 5. PubMed PMID: 19170981.

Duval MG, Chung H, Lehmann OJ, Allison WT. Longitudinal fluorescent observation of retinal degeneration and regeneration in zebrafish using fundus lens imaging. Mol Vis. 2013 May 23;19:1082-95. Print 2013. PubMed PMID: 23734077; PubMed Central PMCID: PMC3668685.

Edgar RC. MUSCLE: a multiple sequence alignment method with reduced time and space complexity. BMC Bioinformatics. 2004 Aug 19;5:113. PubMed PMID: 15318951; PubMed Central PMCID: PMC517706.

Farber SA, Pack M, Ho SY, Johnson ID, Wagner DS, Dosch R, Mullins MC, Hendrickson HS, Hendrickson EK, Halpern ME. Genetic analysis of digestive physiology using fluorescent phospholipid reporters. Science. 2001 May 18;292(5520):1385-8. PubMed PMID: 11359013.

Fleisch VC, Fraser B, Allison WT. Investigating regeneration and functional integration of CNS neurons: lessons from zebrafish genetics and other fish species. Biochim Biophys Acta. 2011 Mar;1812(3):364-80. doi: 10.1016/j.bbadis.2010.10.012. Epub 2010 Oct 28. Review. PubMed PMID: 21044883.

Franco M, Chardin P, Chabre M, Paris S. Myristoylation is not required for GTP-dependent binding of ADP-ribosylation factor ARF1 to phospholipids. J Biol Chem. 1993 Nov 25;268(33):24531-4. PubMed PMID: 8227008.

Fraser B, DuVal MG, Wang H, Allison WT. Regeneration of cone photoreceptors when cell ablation is primarily restricted to a particular cone subtype. PLoS One. 2013;8(1):e55410. doi: 10.1371/journal.pone.0055410. Epub 2013 Jan 30. PubMed PMID: 23383182; PubMed Central PMCID: PMC3559598.

Gabernet-Castello C, O'Reilly AJ, Dacks JB, Field MC. Evolution of Tre-2/Bub2/Cdc16 (TBC) Rab GTPase-activating proteins. Mol Biol Cell. 2013 May;24(10):1574-83. doi: 10.1091/mbc.E12-07-0557. Epub 2013 Mar 13. PubMed PMID: 23485563; PubMed Central PMCID: PMC3655817.

Gascue C, Tan PL, Cardenas-Rodriguez M, Libisch G, Fernandez-Calero T, Liu YP, Astrada S, Robello C, Naya H, Katsanis N, Badano JL. Direct role of Bardet-Biedl syndrome proteins in transcriptional regulation. J Cell Sci. 2012 Jan 15;125(Pt 2):362-75. doi: 10.1242/jcs.089375. Epub 2012 Feb 2. PubMed PMID: 22302990; PubMed Central PMCID: PMC3283873.

Gaynor EC, Graham TR, Emr SD. COPI in ER/Golgi and intra-Golgi transport: do yeast COPI mutants point the way? Biochim Biophys Acta. 1998 Aug 14;1404(1-2):33-51. Review. PubMed PMID: 9714721.

Gestri G, Link BA, Neuhauss SC. The visual system of zebrafish and its use to model human ocular diseases. Dev Neurobiol. 2012 Mar;72(3):302-27. doi: 10.1002/dneu.20919. Review. PubMed PMID: 21595048; PubMed Central PMCID: PMC3202066.

Gillingham AK, Munro S. The small G proteins of the Arf family and their regulators. Annu Rev Cell Dev Biol. 2007;23:579-611. Review. PubMed PMID: 17506703.

Glick BS, Malhotra V. The curious status of the Golgi apparatus. Cell. 1998 Dec 23;95(7):883-9. PubMed PMID: 9875843.

Goldberg J. Decoding of sorting signals by coatomer through a GTPase switch in the COPI coat complex. Cell. 2000 Mar 17;100(6):671-9. PubMed PMID: 10761932.

G, Quinn P, Warren G. Dissection of the Golgi complex. I. Monensin inhibits the transport of viral membrane proteins from medial to trans Golgi cisternae in baby hamster kidney cells infected with Semliki Forest virus. J Cell Biol. 1983 Mar;96(3):835-50. PubMed PMID: 6682112; PubMed Central PMCID: PMC2112386.

Gross JM, Perkins BD. Zebrafish mutants as models for congenital ocular disorders in humans. Mol Reprod Dev. 2008 Mar;75(3):547-55. Review. PubMed PMID: 18058918.

Guindon, S., and Gascuel, O. 2003. A simple, fast and accurate method to estimate large phylogenies by maximum-likelihood. *Systematic Biology* 52: 696-704.

Hauri H, Appenzeller C, Kuhn F, Nufer O. Lectins and traffic in the secretory pathway. FEBS Lett. 2000 Jun 30;476(1-2):32-7. Review. PubMed PMID: 10878245.

Hebert DN, Molinari M. In and out of the ER: protein folding, quality control, degradation, and related human diseases. Physiol Rev. 2007 Oct;87(4):1377-408. Review. PubMed PMID: 17928587.

Ho SY, Lorent K, Pack M, Farber SA. Zebrafish fat-free is required for intestinal lipid absorption and Golgi apparatus structure. Cell Metab. 2006 Apr;3(4):289-300. PubMed PMID: 16581006; PubMed Central PMCID: PMC2247414.

Hong JX, Lee FJ, Patton WA, Lin CY, Moss J, Vaughan M. Phospholipid- and GTP-dependent activation of cholera toxin and phospholipase D by human ADP-ribosylation factor-like protein 1 (HARL1). J Biol Chem. 1998 Jun 19;273(25):15872-6. PubMed PMID: 9624189.

Jackson CL, Casanova JE. Turning on ARF: the Sec7 family of guanine-nucleotide-exchange factors. Trends Cell Biol. 2000 Feb;10(2):60-7. Review. PubMed PMID: 10652516.

Jackson TR, Brown FD, Nie Z, Miura K, Foroni L, Sun J, Hsu VW, Donaldson JG, Randazzo PA. ACAPs are arf6 GTPase-activating proteins that function in the cell periphery. J Cell Biol. 2000 Oct 30;151(3):627-38. PubMed PMID: 11062263; PubMed Central PMCID: PMC2185579.

Jurisch-Yaksi N, Rose AJ, Lu H, Raemaekers T, Munck S, Baatsen P, Baert V, Vermeire W, Scales SJ, Verleyen D, Vandepoel R, Tylzanowski P, Yaksi E, de Ravel T, Yost HJ, Froyen G, Arrington CB, Annaert W. Rer1p maintains ciliary length and signaling by regulating γ-secretase activity and Foxj1a levels. J Cell Biol. 2013 Mar 18;200(6):709-20. doi: 10.1083/jcb.201208175. Epub 2013 Mar 11. PubMed PMID: 23479743; PubMed Central PMCID: PMC3601348.

Kahn RA, Cherfils J, Elias M, Lovering RC, Munro S, Schurmann A. Nomenclature for the human Arf family of GTP-binding proteins: ARF, ARL, and SAR proteins. J Cell Biol. 2006 Feb 27;172(5):645-50. Review. PubMed PMID: 16505163; PubMed Central PMCID: PMC2063696.

Kahn RA, Gilman AG. The protein cofactor necessary for ADP-ribosylation of Gs by cholera toxin is itself a GTP binding protein. J Biol Chem. 1986 Jun 15;261(17):7906-11. PubMed PMID: 3086320.

Kahn RA. Toward a model for Arf GTPases as regulators of traffic at the Golgi. FEBS Lett. 2009 Dec 3;583(23):3872-9. doi: 10.1016/j.febslet.2009.10.066. Epub 2009 Oct 29. Review. PubMed PMID: 19879269; PubMed Central PMCID: PMC2787837.

Kaiser DM, Acharya M, Leighton PL, Wang H, Daude N, Wohlgemuth S, Shi B, Allison WT. Amyloid beta precursor protein and prion protein have a conserved interaction affecting cell adhesion and CNS development. PLoS One. 2012;7(12):e51305. doi: 10.1371/journal.pone.0051305. Epub 2012 Dec 7. PubMed PMID: 23236467; PubMed Central PMCID: PMC3517466.

Karanth S, Lall SP, Denovan-Wright EM, Wright JM. Differential transcriptional modulation of duplicated fatty acid-binding protein genes by dietary fatty acids in zebrafish (Danio rerio): evidence for subfunctionalization or neofunctionalization of duplicated genes. BMC Evol Biol. 2009 Sep 2;9:219. doi: 10.1186/1471-2148-9-219. PubMed PMID: 19725974; PubMed Central PMCID: PMC2754478.

Kawamoto K, Yoshida Y, Tamaki H, Torii S, Shinotsuka C, Yamashina S, Nakayama K. GBF1, a guanine nucleotide exchange factor for ADP-ribosylation factors, is localized to the cis-Golgi and involved in membrane association of the COPI coat. Traffic. 2002 Jul;3(7):483-95. PubMed PMID: 12047556.

Kettunen P. Calcium imaging in the zebrafish. Adv Exp Med Biol. 2012;740:1039-71. doi: 10.1007/978-94-007-2888-2_48. Review. PubMed PMID: 22453983.

Kim SW, Hayashi M, Lo JF, Yang Y, Yoo JS, Lee JD. ADP-ribosylation factor 4 small GTPase mediates epidermal growth factor receptor-dependent phospholipase D2 activation. J Biol Chem. 2003 Jan 24;278(4):2661-8. Epub 2002 Nov 21. PubMed PMID: 12446727.

Kimbrough RD. Toxicity and health effects of selected organotin compounds: a review. Environ Health Perspect. 1976 Apr;14:51-6. Review. PubMed PMID: 789069; PubMed Central PMCID: PMC1475111.

Klarlund JK, Guilherme A, Holik JJ, Virbasius JV, Chawla A, Czech MP. Signaling by phosphoinositide-3,4,5-trisphosphate through proteins containing pleckstrin and Sec7 homology domains. Science. 1997 Mar 28;275(5308):1927-30. PubMed PMID: 9072969.

Klumperman J, Schweizer A, Clausen H, Tang BL, Hong W, Oorschot V, Hauri HP. The recycling pathway of protein ERGIC-53 and dynamics of the ER-Golgi intermediate compartment. J Cell Sci. 1998 Nov;111 (Pt 22):3411-25. PubMed PMID: 9788882.

Krock BL, Perkins BD. The intraflagellar transport protein IFT57 is required for cilia maintenance and regulates IFT-particle-kinesin-II dissociation in vertebrate photoreceptors. J Cell Sci. 2008 Jun 1;121(Pt 11):1907-15. doi: 10.1242/jcs.029397. PubMed PMID: 18492793; PubMed Central PMCID: PMC2637114.

Kuismanen E, Saraste J. Low temperature-induced transport blocks as tools to manipulate membrane traffic. Methods Cell Biol. 1989;32:257-74. Review. PubMed PMID: 2691852.

Lamb TD. Evolution of phototransduction, vertebrate photoreceptors and retina. Prog Retin Eye Res. 2013 Jun 19. doi:pii: S1350-9462(13)00040-2. 10.1016/j.preteyeres.2013.06.001. [Epub ahead of print] PubMed PMID: 23792002.

Laufman O, Hong W, Lev S. The COG complex interacts with multiple Golgi SNAREs and enhances fusogenic assembly of SNARE complexes. J Cell Sci. 2013 Mar 15;126(Pt 6):1506-16. doi: 10.1242/jcs.122101. Epub 2013 Feb 1. PubMed PMID: 23378023.

Lederkremer GZ, Cheng Y, Petre BM, Vogan E, Springer S, Schekman R, Walz T, Kirchhausen T. Structure of the Sec23p/24p and Sec13p/31p complexes of COPII. Proc Natl Acad Sci U S A. 2001 Sep 11;98(19):10704-9. Epub 2001 Sep 4. PubMed PMID: 11535824; PubMed Central PMCID: PMC58530.

Li Y, Kelly WG, Logsdon JM Jr, Schurko AM, Harfe BD, Hill-Harfe KL, Kahn RA. Functional genomic analysis of the ADP-ribosylation factor family of GTPases: phylogeny among diverse eukaryotes and function in C. elegans. FASEB J. 2004 Dec;18(15):1834-50. PubMed PMID: 15576487.

Liu HY, Lee N, Tsai TY, Ho SY. Zebrafish fat-free, a novel Arf effector, regulates phospholipase D to mediate lipid and glucose metabolism. Biochim Biophys Acta. 2010 Dec;1801(12):1330-40. doi: 10.1016/j.bbalip.2010.08.012. Epub 2010 Sep 8. PubMed PMID: 20816853.

Liu Q, Frey RA, Babb-Clendenon SG, Liu B, Francl J, Wilson AL, Marrs JA, Stenkamp DL. Differential expression of photoreceptor-specific genes in the retina of a zebrafish cadherin2 mutant glass onion and zebrafish cadherin4 morphants. Exp Eye Res. 2007 Jan;84(1):163-75. Epub 2006 Oct 30. PubMed PMID: 17070801; PubMed Central PMCID: PMC1853368.

Lotti LV, Torrisi MR, Pascale MC, Bonatti S. Immunocytochemical analysis of the transfer of vesicular stomatitis virus G glycoprotein from the intermediate compartment to the Golgi complex. J Cell Biol. 1992 Jul;118(1):43-50. PubMed PMID: 1320035; PubMed Central PMCID: PMC2289513.

Lowery J, Szul T, Styers M, Holloway Z, Oorschot V, Klumperman J, Sztul E. The Sec7 guanine nucleotide exchange factor GBF1 regulates membrane recruitment of BIG1 and BIG2 guanine nucleotide exchange factors to the trans-Golgi network (TGN). J Biol Chem. 2013 Apr 19;288(16):11532-45. doi: 10.1074/jbc.M112.438481. Epub 2013 Feb 5. PubMed PMID: 23386609; PubMed Central PMCID: PMC3630886.

Macia E, Luton F, Partisani M, Cherfils J, Chardin P, Franco M. The GDP-bound form of Arf6 is located at the plasma membrane. J Cell Sci. 2004 May 1;117(Pt 11):2389-98. PubMed PMID: 15126638.

Manolea F, Chun J, Chen DW, Clarke I, Summerfeldt N, Dacks JB, Melançon P. Arf3 is activated uniquely at the trans-Golgi network by brefeldin A-inhibited guanine nucleotide exchange factors. Mol Biol Cell. 2010 Jun 1;21(11):1836-49. doi: 10.1091/mbc.E10-01-0016. Epub 2010 Mar 31. PubMed PMID: 20357002; PubMed Central PMCID: PMC2877642.

Mansour SJ, Herbrick JA, Scherer SW, Melançon P. Human GBF1 is a ubiquitously expressed gene of the sec7 domain family mapping to 10q24. Genomics. 1998 Dec 1;54(2):323-7. PubMed PMID: 9828135.

Matsuoka K, Orci L, Amherdt M, Bednarek SY, Hamamoto S, Schekman R, Yeung T. COPII-coated vesicle formation reconstituted with purified coat proteins and chemically defined liposomes. Cell. 1998 Apr 17;93(2):263-75. PubMed PMID: 9568718.

Matsuura-Tokita K, Takeuchi M, Ichihara A, Mikuriya K, Nakano A. Live imaging of yeast Golgi cisternal maturation. Nature. 2006 Jun 22;441(7096):1007-10. Epub 2006 May 14. PubMed PMID: 16699523.

Mazelova J, Astuto-Gribble L, Inoue H, Tam BM, Schonteich E, Prekeris R, Moritz OL, Randazzo PA, Deretic D. Ciliary targeting motif VxPx directs assembly of a trafficking module through Arf4. EMBO J. 2009 Feb 4;28(3):183-92. doi: 10.1038/emboj.2008.267. Epub 2009 Jan 15. PubMed PMID: 19153612; PubMed Central PMCID: PMC2637330.

Mellman I, Simons K. The Golgi complex: in vitro veritas? Cell. 1992 Mar 6;68(5):829-40. Review. PubMed PMID: 1547485.

Merbs SL, Nathans J. Absorption spectra of human cone pigments. Nature. 1992 Apr 2;356(6368):433-5. PubMed PMID: 1557124.

Mossessova E, Gulbis JM, Goldberg J. Structure of the guanine nucleotide exchange factor Sec7 domain of human arno and analysis of the interaction with ARF GTPase. Cell. 1998 Feb 6;92(3):415-23. PubMed PMID: 9476900.

Mossessova E, Corpina RA, Goldberg J. Crystal structure of ARF1*Sec7 complexed with Brefeldin A and its implications for the guanine nucleotide exchange mechanism. Mol Cell. 2003 Dec;12(6):1403-11. PubMed PMID: 14690595.

Muñiz M, Nuoffer C, Hauri HP, Riezman H. The Emp24 complex recruits a specific cargo molecule into endoplasmic reticulum-derived vesicles. J Cell Biol. 2000 Mar 6;148(5):925-30. PubMed PMID: 10704443; PubMed Central PMCID: PMC2174538.

Myers KR, Wang G, Sheng Y, Conger KK, Casanova JE, Zhu JJ. Arf6-GEF BRAG1 regulates JNK-mediated synaptic removal of GluA1-containing AMPA receptors: a new mechanism for nonsyndromic X-linked mental disorder. J Neurosci. 2012 Aug 22;32(34):11716-26. doi: 10.1523/JNEUROSCI.1942-12.2012. PubMed PMID: 22915114; PubMed Central PMCID: PMC3459061.

Nie Z, Hirsch DS, Randazzo PA. Arf and its many interactors. Curr Opin Cell Biol. 2003 Aug;15(4):396-404. Review. PubMed PMID: 12892779.

Nishimura N, Balch WE. A di-acidic signal required for selective export from the endoplasmic reticulum. Science. 1997 Jul 25;277(5325):556-8. PubMed PMID: 9228004.

Niu TK, Pfeifer AC, Lippincott-Schwartz J, Jackson CL. Dynamics of GBF1, a Brefeldin A-sensitive Arf1 exchange factor at the Golgi. Mol Biol Cell. 2005 Mar;16(3):1213-22. Epub 2004 Dec 22. PubMed PMID: 15616190; PubMed Central PMCID: PMC551486.

Nufer O, Guldbrandsen S, Degen M, Kappeler F, Paccaud JP, Tani K, Hauri HP. Role of cytoplasmic C-terminal amino acids of membrane proteins in ER export. J Cell Sci. 2002 Feb 1;115(Pt 3):619-28. PubMed PMID: 11861768.

Nuoffer C, Balch WE. GTPases: multifunctional molecular switches regulating vesicular traffic. Annu Rev Biochem. 1994;63:949-90. Review. PubMed PMID: 7979258.

Oates AC, Bruce AE, Ho RK. Too much interference: injection of double-stranded RNA has nonspecific effects in the zebrafish embryo. Dev Biol. 2000 Aug 1;224(1):20-8. PubMed PMID: 10898958.

Ooi CE, Dell'Angelica EC, Bonifacino JS. ADP-Ribosylation factor 1 (ARF1) regulates recruitment of the AP-3 adaptor complex to membranes. J Cell Biol. 1998 Jul 27;142(2):391-402. PubMed PMID: 9679139; PubMed Central PMCID: PMC2133064.

Orci L, Ravazzola M, Meda P, Holcomb C, Moore HP, Hicke L, Schekman R. Mammalian Sec23p homologue is restricted to the endoplasmic reticulum transitional cytoplasm. Proc Natl Acad Sci U S A. 1991 Oct 1;88(19):8611-5. PubMed PMID: 1924322; PubMed Central PMCID: PMC52559.

Orci L, Ravazzola M, Volchuk A, Engel T, Gmachl M, Amherdt M, Perrelet A, Sollner TH, Rothman JE. Anterograde flow of cargo across the golgi stack potentially mediated via bidirectional "percolating" COPI vesicles. Proc Natl Acad Sci U S A. 2000 Sep 12;97(19):10400-5. PubMed PMID: 10962035; PubMed Central PMCID: PMC27036.

Palade G. Intracellular aspects of the process of protein synthesis. Science. 1975 Aug 1;189(4200):347-58. Review. PubMed PMID: 1096303.

Pasqualato S, Renault L, Cherfils J. Arf, Arl, Arp and Sar proteins: a family of GTP-binding proteins with a structural device for 'front-back' communication. EMBO Rep. 2002 Nov;3(11):1035-41. PubMed PMID: 12429613; PubMed Central PMCID: PMC1307594.

Pazour GJ, Baker SA, Deane JA, Cole DG, Dickert BL, Rosenbaum JL, Witman GB, Besharse JC. The intraflagellar transport protein, IFT88, is essential for vertebrate photoreceptor assembly and maintenance. J Cell Biol. 2002 Apr 1;157(1):103-13. Epub 2002 Mar 26. PubMed PMID: 11916979; PubMed Central PMCID: PMC2173265.

Peters PJ, Hsu VW, Ooi CE, Finazzi D, Teal SB, Oorschot V, Donaldson JG, Klausner RD. Overexpression of wild-type and mutant ARF1 and ARF6: distinct perturbations of nonoverlapping membrane compartments. J Cell Biol. 1995 Mar;128(6):1003-17. PubMed PMID: 7896867; PubMed Central PMCID: PMC2120412.

Poon PP, Cassel D, Spang A, Rotman M, Pick E, Singer RA, Johnston GC. Retrograde transport from the yeast Golgi is mediated by two ARF GAP

proteins with overlapping function. EMBO J. 1999 Feb 1;18(3):555-64. PubMed PMID: 9927415; PubMed Central PMCID: PMC1171148.

Powers J, Barlowe C. Erv14p directs a transmembrane secretory protein into COPII-coated transport vesicles. Mol Biol Cell. 2002 Mar;13(3):880-91. PubMed PMID: 11907269; PubMed Central PMCID: PMC99606.

Presley JF, Cole NB, Schroer TA, Hirschberg K, Zaal KJ, Lippincott-Schwartz J. ER-to-Golgi transport visualized in living cells. Nature. 1997 Sep 4;389(6646):81-5. PubMed PMID: 9288971.

Pretorius PR, Baye LM, Nishimura DY, Searby CC, Bugge K, Yang B, Mullins RF, Stone EM, Sheffield VC, Slusarski DC. Identification and functional analysis of the vision-specific BBS3 (ARL6) long isoform. PLoS Genet. 2010 Mar 19;6(3):e1000884. doi: 10.1371/journal.pgen.1000884. PubMed PMID: 20333246; PubMed Central PMCID: PMC2841623.

Pretorius PR, Aldahmesh MA, Alkuraya FS, Sheffield VC, Slusarski DC. Functional analysis of BBS3 A89V that results in non-syndromic retinal degeneration. Hum Mol Genet. 2011 Apr 15;20(8):1625-32. doi: 10.1093/hmg/ddr039. Epub 2011 Jan 31. PubMed PMID: 21282186; PubMed Central PMCID: PMC3063988.

Randazzo PA, Kahn RA. GTP hydrolysis by ADP-ribosylation factor is dependent on both an ADP-ribosylation factor GTPase-activating protein and acid phospholipids. J Biol Chem. 1994 Apr 8;269(14):10758-63. Erratum in: J Biol Chem 1994 Jun 10;269(23):16519. PubMed PMID: 8144664.

Rastogi S, Liberles DA. Subfunctionalization of duplicated genes as a transition state to neofunctionalization. BMC Evol Biol. 2005 Apr 14;5:28. PubMed PMID: 15831095; PubMed Central PMCID: PMC1112588.

Raymond PA, Barthel LK. A moving wave patterns the cone photoreceptor mosaic array in the zebrafish retina. Int J Dev Biol. 2004;48(8-9):935-45. Review. PubMed PMID: 15558484.

Raymond PA, Barthel LK, Curran GA. Developmental patterning of rod and cone photoreceptors in embryonic zebrafish. J Comp Neurol. 1995 Sep 4;359(4):537-50. PubMed PMID: 7499546.

Rémillard-Labrosse G, Lippé R. Meeting of conventional and unconventional pathways at the TGN. Commun Integr Biol. 2009 Sep;2(5):434-6. PubMed PMID: 19907711; PubMed Central PMCID: PMC2775244.

Renault L, Guibert B, Cherfils J. Structural snapshots of the mechanism and inhibition of a guanine nucleotide exchange factor. Nature. 2003 Dec 4;426(6966):525-30. PubMed PMID: 14654833.

Renninger SL, Schonthaler HB, Neuhauss SC, Dahm R. Investigating the genetics of visual processing, function and behaviour in zebrafish.

Neurogenetics. 2011 May;12(2):97-116. doi: 10.1007/s10048-011-0273-x. Epub 2011 Jan 26. Review. PubMed PMID: 21267617.

Ronquist, F., Huelsenbeck, J. P. 2003. MrBayes 3: Bayesian phylogenetic inference under mixed models. *Bioinformatics* 19:1572-1574.

Rothman JE, Wieland FT. Protein sorting by transport vesicles. Science. 1996 Apr 12;272(5259):227-34. Review. PubMed PMID: 8602507.

Sadakata T, Shinoda Y, Sekine Y, Saruta C, Itakura M, Takahashi M, Furuichi T. Interaction of calcium-dependent activator protein for secretion 1 (CAPS1) with the class II ADP-ribosylation factor small GTPases is required for dense-core vesicle trafficking in the trans-Golgi network. J Biol Chem. 2010 Dec 3;285(49):38710-9. doi: 10.1074/jbc.M110.137414. Epub 2010 Oct 4. PubMed PMID: 20921225; PubMed Central PMCID: PMC2992304.

Saraste J, Palade GE, Farquhar MG. Antibodies to rat pancreas Golgi subfractions: identification of a 58-kD cis-Golgi protein. J Cell Biol. 1987 Nov;105(5):2021-9. PubMed PMID: 3316245; PubMed Central PMCID: PMC2114852.

Saraste J, Kuismanen E. Pre- and post-Golgi vacuoles operate in the transport of Semliki Forest virus membrane glycoproteins to the cell surface. Cell. 1984 Sep;38(2):535-49. PubMed PMID: 6432345.

Schlacht A, Mowbrey K, Elias M, Kahn RA, Dacks JB. Ancient complexity, opisthokont plasticity, and discovery of the 11th subfamily of Arf GAP proteins.Traffic. 2013 Jun;14(6):636-49. doi: 10.1111/tra.12063. Epub 2013 Mar 20. PubMed PMID: 23433073; PubMed Central PMCID: PMC3660519.

Schweizer A, Fransen JA, Bächi T, Ginsel L, Hauri HP. Identification, by a monoclonal antibody, of a 53-kD protein associated with a tubulo-vesicular compartment at the cis-side of the Golgi apparatus. J Cell Biol. 1988 Nov;107(5):1643-53. PubMed PMID: 3182932; PubMed Central PMCID: PMC2115344.

Schweizer A, Fransen JA, Matter K, Kreis TE, Ginsel L, Hauri HP. Identification of an intermediate compartment involved in protein transport from endoplasmic reticulum to Golgi apparatus. Eur J Cell Biol. 1990 Dec;53(2):185-96. PubMed PMID: 1964413.

Shu X, Zeng Z, Gautier P, Lennon A, Gakovic M, Cheetham ME, Patton EE, Wright AF. Knockdown of the zebrafish ortholog of the retinitis pigmentosa 2 (RP2) gene results in retinal degeneration. Invest Ophthalmol Vis Sci. 2011 May 5;52(6):2960-6. doi: 10.1167/iovs.10-6800. PubMed PMID: 21282572.

Sitia R, Meldolesi J. Endoplasmic reticulum: a dynamic patchwork of specialized subregions. Mol Biol Cell. 1992 Oct;3(10):1067-72. Review. PubMed PMID: 1421566; PubMed Central PMCID: PMC275671.

Spang A, Matsuoka K, Hamamoto S, Schekman R, Orci L. Coatomer, Arf1p, and nucleotide are required to bud coat protein complex I-coated vesicles from large synthetic liposomes. Proc Natl Acad Sci U S A. 1998 Sep 15;95(19):11199-204. PubMed PMID: 9736713; PubMed Central PMCID: PMC21619.

Spang A, Shiba Y, Randazzo PA. Arf GAPs: gatekeepers of vesicle generation. FEBS Lett. 2010 Jun 18;584(12):2646-51. doi: 10.1016/j.febslet.2010.04.005. Epub 2010 Apr 13. Review. PubMed PMID: 20394747; PubMed Central PMCID: PMC2878913.

Stamatakis, A. 2006. RAxML-VI-HPC: maximum likelihood-based phylogenetic analyes with thousands of taxa and mixed models. *Bioinformatics* 22:2688-2690.

Stephens DJ, Lin-Marq N, Pagano A, Pepperkok R, Paccaud JP. COPI-coated ER-to-Golgi transport complexes segregate from COPII in close proximity to ER exit sites. J Cell Sci. 2000 Jun;113 (Pt 12):2177-85. PubMed PMID: 10825291.

Stoorvogel W, Oorschot V, Geuze HJ. A novel class of clathrin-coated vesicles budding from endosomes. J Cell Biol. 1996 Jan;132(1-2):21-33. PubMed PMID: 8567724; PubMed Central PMCID: PMC2120710.

Strating JR, Martens GJ. The p24 family and selective transport processes at the ER-Golgi interface. Biol Cell. 2009 Sep;101(9):495-509. doi: 10.1042/BC20080233. Review. PubMed PMID: 19566487.

Suyama M, Torrents D, Bork P. PAL2NAL: robust conversion of protein sequence alignments into the corresponding codon alignments. Nucleic Acids Res. 2006 Jul 1;34(Web Server issue):W609-12. PubMed PMID: 16845082; PubMed Central PMCID: PMC1538804.

Suzuki T, Kanai Y, Hara T, Sasaki J, Sasaki T, Kohara M, Maehama T, Taya C, Shitara H, Yonekawa H, Frohman MA, Yokozeki T, Kanaho Y. Crucial role of the small GTPase ARF6 in hepatic cord formation during liver development. Mol Cell Biol. 2006 Aug;26(16):6149-56. PubMed PMID: 16880525; PubMed Central PMCID: PMC1592812.

Tanabe K, Torii T, Natsume W, Braesch-Andersen S, Watanabe T, Satake M. A novel GTPase-activating protein for ARF6 directly interacts with clathrin and regulates clathrin-dependent endocytosis. Mol Biol Cell. 2005 Apr;16(4):1617-28. Epub 2005 Jan 19. PubMed PMID: 15659652; PubMed Central PMCID: PMC1073646.

Taylor TC, Kahn RA, Melançon P. Two distinct members of the ADP-ribosylation factor family of GTP-binding proteins regulate cell-free intra-Golgi transport. Cell. 1992 Jul 10;70(1):69-79. PubMed PMID: 1623523.

Vihtelic TS, Doro CJ, Hyde DR. Cloning and characterization of six zebrafish photoreceptor opsin cDNAs and immunolocalization of their corresponding proteins. Vis Neurosci. 1999 May-Jun;16(3):571-85. PubMed PMID: 10349976.

Volpicelli-Daley LA, Li Y, Zhang CJ, Kahn RA. Isoform-selective effects of the depletion of ADP-ribosylation factors 1-5 on membrane traffic. Mol Biol Cell. 2005 Oct;16(10):4495-508. Epub 2005 Jul 19. PubMed PMID: 16030262; PubMed Central PMCID: PMC1237059.

Ward HH, Brown-Glaberman U, Wang J, Morita Y, Alper SL, Bedrick EJ, Gattone VH 2nd, Deretic D, Wandinger-Ness A. A conserved signal and GTPase complex are required for the ciliary transport of polycystin-1. Mol Biol Cell. 2011 Sep;22(18):3289-305. doi: 10.1091/mbc.E11-01-0082. Epub 2011 Jul 20. PubMed PMID: 21775626; PubMed Central PMCID: PMC3172256.

Watanabe K, Nishimura Y, Oka T, Nomoto T, Kon T, Shintou T, Hirano M, Shimada Y, Umemoto N, Kuroyanagi J, Wang Z, Zhang Z, Nishimura N, Miyazaki T, Imamura T, Tanaka T. In vivo imaging of zebrafish retinal cells using fluorescent coumarin derivatives. BMC Neurosci. 2010 Sep 15;11:116. doi: 10.1186/1471-2202-11-116. PubMed PMID: 20843315; PubMed Central PMCID: PMC2945357.

Waters MG, Griff IC, Rothman JE. Proteins involved in vesicular transport and membrane fusion. Curr Opin Cell Biol. 1991 Aug;3(4):615-20. Review. PubMed PMID: 1772655.

Wennerberg K, Rossman KL, Der CJ. The Ras superfamily at a glance. J Cell Sci. 2005 Mar 1;118(Pt 5):843-6. Review. PubMed PMID: 15731001.

Westerfield M, (2000) The Zebrafish Book. A Guide for the Laboratory Use of Zebrafish (Danio rerio). Eugene, Oregon, USA: University of Oregon Press.

Yano H, Kobayashi I, Onodera Y, Luton F, Franco M, Mazaki Y, Hashimoto S, Iwai K, Ronai Z, Sabe H. Fbx8 makes Arf6 refractory to function via ubiquitination. Mol Biol Cell. 2008 Mar;19(3):822-32. Epub 2007 Dec 19. PubMed PMID: 18094045; PubMed Central PMCID: PMC2262996.

Young RW. The renewal of photoreceptor cell outer segments. J Cell Biol. 1967 Apr;33(1):61-72. PubMed PMID: 6033942; PubMed Central PMCID: PMC2107286.

Zhao X, Claude A, Chun J, Shields DJ, Presley JF, Melançon P. GBF1, a cis-Golgi and VTCs-localized ARF-GEF, is implicated in ER-to-Golgi protein traffic. J Cell Sci. 2006 Sep 15;119(Pt 18):3743-53. Epub 2006 Aug 22. PubMed PMID: 16926190.

Zhao X, Lasell TK, Melançon P. Localization of large ADP-ribosylation factor-guanine nucleotide exchange factors to different Golgi compartments:

evidence for distinct functions in protein traffic. Mol Biol Cell. 2002 Jan;13(1):119-33. PubMed PMID: 11809827; PubMed Central PMCID: PMC65077.

Zuo Z, Cai J, Wang X, Li B, Wang C, Chen Y. Acute administration of tributyltin and trimethyltin modulate glutamate and N-methyl-D-aspartate receptor signaling pathway in Sebastiscus marmoratus. Aquat Toxicol. 2009 Apr 2;92(1):44-9. doi: 10.1016/j.aquatox.2009.01.008. Epub 2009 Feb 15. PubMed PMID: 19223082.